Title
RELAXATION AND REACTION OF HCO AND CHL(1A1)

Author
Langford, A.O.

Publication Date
1983-10-01

Lawrence Berkeley Laboratory
UNIVERSITY OF CALIFORNIA

Materials & Molecular Research Division

RELAXATION AND REACTION OF HCO AND $CH_2(^1A_1)$

A.O. Langford
(Ph.D. Thesis)

October 1983

Prepared for the U.S. Department of Energy under Contract DE-AC03-76SF00098

DISCLAIMER

LBL-17025

RELAXATION AND REACTION OF HCO AND $CH_2(^1A_1)$

Andrew O'Neil Langford
(Ph.D. Thesis)

Department of Chemistry
University of California, Berkeley
and
Materials and Molecular Research Division
Lawrence Berkeley Laboratory
Berkeley, California 94720

October 1983

This work was supported by the Director, Office of Energy Research, Office of Basic Energy Sciences, Chemical Sciences Division of the U.S. Department of Energy under Contract No. DE-AC03-76SF00098.

RELAXATION AND REACTION OF HCO AND CH_2 ($^1A_1$)

Andrew O'Neil Langford

Abstract

The laser photolysis/resonance absorption technique has been used to measure absolute rate constants for collisional removal of ground state and vibrationally excited HCO, DCO, and CH_2 ($^1A_1$). For HCO(0,1,0), rate constants for collisions with He, N_2, H_2CO, $(HCO)_2$, NO and O_2 were determined. The number of collisions required to deactivte HCO(0,1,0) ranges from 10 for NO to 10^3 for N_2. Upper limits for the rate of reaction between HCO(0,1,0) and NO or O_2 were established and found to be slower than the corresponding HCO(0,0,0) reaction rate. These interesting results are attributed to the formation of strongly bound collision complexes. This hypothesis is corroborated by inverse kinetic isotope effects which were observed for the ground state reactions. Simple RRKM calculatons based on the collision complex mechanism semiquantitatively reproduce the experimental isotope effects as well as the experimentally observed decreases in rate constant which result from vibrational excitation of the HCO or from an increase in temperature.

The rate constants for removal of CH_2 ($^1A_1$) in collisions with He, Ar, Kr, N_2, CO, O_2, CH_4, C_2H_6, C_3H_8, C_2H_4, i-C_4H_8, and CH_2CO were also measured. The number of collisions required to remove CH_2 ($^1A_1$) ranges from 1 for higher hydrocarbons and CH_2CO to 10^2 for He. The relative contributions of reaction and deactivation were not determined.

Identical results were found for the (0,1,0) vibrational level which indicates that the collision-induced intersystem crossing rate is independent of the initial vibrational level. Equilibration of the CH_2 ($^1A_1$) rotational levels in collisions with CH_2CO and He also found to be very fast with rates factors of 2.7 and 17, respectively, faster than the corresponding removal rates.

ACKNOWLEDGEMENTS

The work described in the following chapters would not have been possible without the support and encouragement of Brad Moore. I particularly appreciate his willingness to let me pursue my own ideas, without letting me stray into water too far over my head. I hope that I manage to keep some of his enthusiasm and philosophy towards science when I leave Berkeley. I would also like to take this opportunity to thank my friend and mentor, A. R. Ravishankara. Ravi receives credit for kindling my interest in chemical physics and convincing me to come to Berkeley in the first place.

Many other peole have contributed technical assistance along the way, and helped to make my graduate career more pleasure than work. Andy Kung, now of the San Fransisco Laser Center (SFLC) was always helpful with technical advice, laser assistance, and the occasional use of his PET. My collaboration with Hrvoje Petek of the Facility for Laser Absorption Spectroscopy and Kinetics (FLASK) on the methylene experiments was both enjoyable and fruitful. Good company (and pinball) makes those long nights grinding out data much more bearable. We'll look for you in Boulder soon. Linda Young acquainted me with the hardware, and provided much of the software used to take the data. Joe Jasinski, Mike Berman, and Hai-lung Dai deserve thanks for introducing me to collision complexes and RRKM theory.

Many other members of the Moore group, past and present, have contributed something along the way which deserves special mention. The same can be said for my non-chemistry friends, particularly those associated with the "Pick of the Litter" (POTL), for reminding me that

there is more to life than chemistry. Space and modesty prevents me from elaborating. Alison gets special credit (and then some) for trying to show me that there is more to graduate school than getting a Ph.D.

Jackie Denney gets a gold star for special favors; I think Muhammad Zughul said it all.

Last but not least, an entire paragraph is devoted to Kennan, my faithful secretary, who cheerfully battled with the NBI to turn this thesis into reality.

This work was supported by the Director, Office of Energy Research, Office of Basic Energy Sciences, Chemical Sciences Division of the U. S. Department of Energy under contract No. DE-AC03-76SF00098.

TABLE OF CONTENTS

CHAPTER I. INTRODUCTION

Many everyday phenomena are macroscopic manifestations of molecular collisions. A seemingly simple process like hydrocarbon combustion may actually be composed of hundreds of coupled reaction and energy transfer processes. Information about each microscopic process is required before the macroscopic process can be completely understood. Fortunately, experimental methods for obtaining this information are rapidly improving. Lasers in particular have had an emormous impact on the study of bimolecular reacton dynamics. A variety of laser techniques have been used to generate and monitor short-lived species as they participate in hundreds of collisional processes, many of practical importance in atmospheric chemistry[1] or combustion systems[2]. The improved sensitivity and temporal resolution compared to conventional photochemical techniques make it possible to study reactive events which occur within a few collisions. The state specificity of laser excitation can be used to prepare reagents in specific quantum states. Unravelling the dependence of chemical reactivity on reagent quantum state may ultimately improve our understanding of the reaction dynamics on a microscopic level.

Comprehensive reviews of optical techniques for studying bimolecular reactions are numerous (Ref. 3 for example). One possible criterion for classifying laser techniques is: those which exploit the unique properties of laser light and were not possible before the advent of the necessary lasers, and those which are improved versions of standard methods developed for conventional light sources. Examples of the former include multiphoton dissociation (MPD) and coherent anti-Stoke's Raman scattering (CARS). Examples of the latter include the techniques of

pulsed laser photolysis and cw laser resonance absorption which are used for the kinetic studies in the following chapters.

Pulsed ultraviolet lasers are now routinely used as photolysis sources in place of the flashlamps introduced by Norrish and Porter in 1949.[4] laser photolysis improves the technique in several ways. The timescale for transient production is reduced from several milliseconds (10 μs for modern flashlamps) to less than 10 ns. Kinetic studies of highly reactive species such as CH_2 ($^1A_1$) become possible on these timescales. With narrow band tunable lasers, specific rovibronic levels of the parent molecule can often be excited. Flashlamps emit light over a wide range of wavelengths which may result in unwanted (and possibly unknown) dissociation channels and products with a wide spread of internal energies. Absorption at many different wavelengths can also lead to sample heating and unwanted temperature excursions.

Resonance absorption was first used in conjunction with flash photolysis by Davidson et al.[5] to follow the recombination of iodine atoms. The filtered output of a broadband lamp was used in those early experiments. In subsequent studies, the broadband lamp was replaced by nearly monochromatic resonance lamps,[6] and later by cw lasers.[7,8] Several distinct advantages are gained by using cw lasers as absorption probes. The high degree of collimation means that much longer absorption pathlengths are possible, particularly with the use of multipass techniques. Tunable dye lasers with linewidths much narrower than Doppler (or lifetime) broadened absorption lines can be used to probe different rovibrational levels and reduce background absorption from other species. As kinetic probes, cw lasers also offer several advantages over pulsed lasers. The most obvious advantage is that of

continuos temporal resolution; a time-resolved absorption signal can in principle be obtained following a single pulse from the photolysis laser. Another important advantage is that of wavelength resolution; the narrower linewidths of cw lasers (0.0005 vs. 0.03 cm^{-1}) simplify the selection of a specific rotational state and may be used to obtain high resolution spectra of transient species.[9] These advantges apply to cw laser-induced fluorescence as well as absorption. Absorption has an obvious advantage when the species of interest fluoresces only weakly or not at all.

In this thesis, the results of several experiments based on these techniques are described. A XeCl excimer laser (308 nm) with a 12 ns pulse is used to produce ground state and vibrationally excited HCO and CH_2 ($^1A_1$) through photodissociation of the appropriate parent compound. Subsequent reactions and relaxation processes are monitored through resonance absorption with a cw dye laser. The experimental details are described in Chapter II. In Chapter III, rate constants for relaxation of HCO (0,1,0) by several collision partners are reported and the role of attractive forces in these collisions is discussed. Contrary to expectations, vibrational excitation was found to decrease the rate of reaction with NO and O_2. Experimental results for the reaction of ground state HCO (and DCO) with NO and O_2 are described in Chapter IV, and a theoretical model is developed to explain the unusual behavior of these interesting reactions. Finally, analogous experiments on reaction and deactivation of CH_2 ($^1A_1$) are described in Chapter V.

References

1. See for example, articles by Pitts et al. and Johnston in Tunable Lasers and Applications (Springer-Verlag, New York, 1976).
2. D. R. Crosley, Laser Probes for Combustion Chemistry, ACS Symp. Ser. No. 134, Washington D. C., 1980.
3. M. C. Lin and J. R. McDonald, in Reactive Intermediates in the Gas Phase (Academic, New York, 1979).
4. R. G. W. Norrish and G. Porter, Nature 164, 658 (1949).
5. N. Davidson, R. Marshall, A. E. Larsh Jr., and T. Carrington, J. Chem. Phys. 19, 1311 (1951).
6. D. D. Davis and W. Braun, Appl. Opt. 7, 2071 (1968).
7. R. Lesclaux, P. V. Khe, P. Dezauzier, and J. C. Soulignac, Chem. Phys. Lett. 35, 493 (1975).
8. P. L. Houston and C. B. Moore, J. Chem. Phys. 65, 757 (1976).
9. H. Petek, D. J Nesbitt, P. R. Ogilby, and C. B. Moore, J. Phys. Chem. (submitted).

CHAPTER II. GENERAL EXPERIMENTAL

The essential features of the laser photolysis/laser resonance absorption apparatus are illustrated in Figure II-1. A gas mixture containing the HCO or $^1CH_2$ precursor is placed in the all quartz reaction cell and irradiated by pulses from the XeCl excimer laser (308 nm). A small fraction of the parent molecules are dissociated to produce the transient species of interest, and the temporal evolution of specific rovibrational levels of the transient is monitored through absorption of the resonant cw laser beam which passes colinearly through the cell. The time-dependent absorption is detected by a fast photodiode, the dye laser noise subtracted, and the resulting signal digitized, computer averaged, and stored for analysis. Rate constants for various processes are then determined from the dependence of the absorption on the partial pressures of reactants in the mixture. In the following sections, the individual components of the apparatus and general experimental procedures are described in detail. Additional details relevant to specific experiments are included in the appropriate chapter.

A. Photolysis Laser

The photolysis source in all of the experiments is a rare gas-halide TEA laser operated with XeCl. This laser produces 12 ns (FWHM) pulses at 308 nm of up to 35 mJ at repetition rates of 1-5 Hz. The laser is constructed from a Lumonics K-261 TEA discharge head mounted in an aluminum cabinet fabricated at LBL. The laser cavity is formed by the 50 mm diameter flat quartz windows of the discharge head. The rear window

is Al coated (on the back surface for protection from the HCl in the gas mixture) while the front window is uncoated (>70% T). The simple optical alignment procedure is described in the Lumonics manual. Realignment is necessary only if the windows are removed or the gas mixture is changed. Alignment of the output coupler is not very critical since the laser is superradiant and most of the output energy comes from the first pass through the head.

The energy for the discharge is provided by a 50 kV, 5 mA power supply from Hippotronics (50-B). Operating voltages ranged from 20 to 32 kV with 25 kV typical. The charging circuit is similar to that used in the TEA CO_2 lasers described in the theses of Hovis[1] and Berman.[2] A +20 V pulse triggers the breakdown of a spark gap which discharges a storage capacitor across the laser head. The variable repetition rate trigger circuit was designed by Andy Kung and fabricated by Eliot Specht. This circuit provides +20 V pulses with 10 ns risetimes (1 μs duration) at repetition rates of 10 mHz to 1kHz. The laser repetition rate is limited to about 5 Hz by the charging circuit and power supply; the output energy and pulse stability decrease dramatically when operation at higher rates is attempted. In later experiments the laser was triggered externally at 5 Hz by the (20 ms/div) + gate out from a Tektronix 555 or similar oscilloscope.

Gas mixtures were made in a stainless steel manifold built into the aluminum cabinet. A schematic diagram of the manifold is shown is Figure II-2. For rare gas-halides, the laser was always operated with static fills of 15 psig (two atmospheres). The gas mixture for XeCl and minimum purities recommended by Lumonics is 6.5% Xe (C.P. grade >99.9%), 0.2% HCl (Electronic grade >99.9%), and 94.7% He (99.995%). Following exposure to

air, the laser head must first be passivated by filling to 15 psig with 10% HCl in He and leaving overnight. The procedure for making a XeCl mixture is as follows:

i) pump out the head and manifold to 28 in. Hg vac.

ii) close valves (1) - (4) and fill the manifold to 0 psig (one atmosphere) with HCl.

iii) open valve (2) and expand the HCl into the laser head.

iv) add Xe until the pressure in the head reaches 26 in. Hg vac.

v) add He to a total pressure of 15 psig.

To facilitate mixing, the He should be added in rapid bursts. If this procedure is followed, lasing should occur immediately although several minutes may be required for the pulse energy to stabilize. A new fill typically produces 30 mJ per pulse if the optics are clean. After 5000-10,000 laser shots, the output energy begins to decrease and lasing eventually stops. This is usually due to depletion of the HCl. When the output energies become too low to be useful, the mixture can usually be resurrected for several thousand additional shots just by replenishing the HCl. This is done by reducing the pressure in the head to ~13 psig, closing valve (2) and evacuating the manifold to 28 in. Hg vac., and repeating steps ii), iii), and v). For best results, the manifold should be filled with 15 psig HCl in step ii). This procedure can usually be repeated several times to prolong the mixture lifetime. When it becomes ineffective, a new mixture is required. Since Xe is very expensive ($600 per lecture bottle on the open market), replenishing the HCl as many times as possible is recommended.

After ~100,000 shots, the output power is significantly reduced by the formation of deposits on the optics. The optics are removed

following the procedure described in the Lumonics manual. They are easily cleaned by acetone, methanol or even water and a fine detergent. The latter is not recommended since any water in the laser head will lead to formation of liquid HCl which attacks the electrodes. Complete disassembly and painstaking cleaning may be required if this occurs. To prevent water vapor from entering the laser head while the optics are being cleaned, it should be filled with a positive pressure of N_2 and the optics removed one at a time.

Operation with nitrogen (337 nm) or other rare gas-halide systems is also possible. Up to 3.5 mJ per pulse have been obtained with N_2 (P = 24 in Hg vac.). The laser was also operated briefly with ArF. This is not recommended; although output energies between 50 and 100 mJ were obtained, the mixture was good for less than 100 laser shots.

B. Probe Laser

The initial absorption probe for HCO experiments was an Ar^+ pumped linear cavity dye laser (Spectra-Physics UV-171/375) capable of producing up to 800 mW of power near the peak of Rhodamine 6G (590 nm) with a 4 W pump. The spacing between longitudinal modes is 200 MHz and the width of a single mode 40 MHz. Rotation of a three-plate birefringent filter in the laser cavity selects the laser wavelength by suppressing the gain on those longitudinal modes outside a 30 GHz linewidth. The frequency profile is narrowed to 7 GHz (0.23 cm^{-1}) by the addition of a fine tuning etalon. The result is a 7 GHz FWHM envelope of 40 MHz wide modes separated by 200 MHz. The laser wavelength was measured with a 1 m Spex or 1.5 m Jobin-Yvon monochromator calibrated to a Ne line standard. Since the HCO linewidths are intrinsically broad ($\gtrsim$0.3 cm^{-1}), the laser

linewidth was narrow enough to probe individual unblended rotational lines.

The 375 was replaced at a very early stage in the experiments by a Spectra-Physics 380C ring dye laser, also pumped by a Spectra-Physics UV-171 Ar^+ laser. The 380C produces up to 1 W of tunable radiation between 570 and 630 nm with Rhodamine 6G at pump powers of 4 W (514.5 nm). The ring configuration results in lasing on a single cavity mode with a linewidth of 20 MHz. During the course of the experimental work, the laser was upgraded from a 380C to a 380A. This upgrade improved the single frequency scanning capabilities of the laser by introducing additional tuning elements, and has little bearing on the present experiments which use fixed frequencies. Details of the single frequency scanning capabilities of the laser will be found in Petek's thesis.[3]

Two laser dyes were used; the proper concentrations and appropriate optics are given in the operator's manual. Most of the wavelengths of interest (570-630 nm) were accessible with Rhodamine 6G, the preferred dye because of its longterm stability (several months of daily use) and high output powers. This dye was used in all of the methylene experiments described in Chapter V and most of the ground state HCO and DCO experiments in Chapters III and IV. For experiments with HCO(0,1,0), it was necessary to use Rhodamine 110 which is slightly less stable (noticable power decreases after several hundred hours of use) to reach transitions near 550 nm. The laser wavelengths were measured by a Burleigh WA-20 wavemeter accurate to 1 part in 106 or 0.02 cm^{-1} in the visible.

C. Optical Layout

The final optical configuration is that of in Fig. II-1. The photolysis beam is coupled into the cell by two uv high reflectors oriented at 45°. A circular spot from the rectangular beam is defined by two adjustable apertures, one between the two uv mirrors, and another 20 cm from the cell. A third mirror placed after the cell reflects most of the unabsorbed uv into a beam stop. The uv mirrors are 1/4" x 2" x 2" quartz plates coated (Uvira Inc.) for a reflectance of >98% (45° incidence) at 312 nm, and >90% at wavelengths between 300 and 325 nm. Higher quality substrates are unnecessary since the excimer beam is not well defined. A glass interference filter (Schott UG11 with 70% transmission at 308 nm and 0% between 400 and 600 nm) is placed between the cell and the excimer laser to remove short-lived emission between 400 and 500 nm which may be due to Xe_2.[4] This emission is a potentially serious source of scattered light since it is difficult to separate from the probe beam after the cell. Reflected light from the filter is used to trigger the transient digitizer through a fast photodiode (HP 5082-4200) biased at -30 V.

The probe beam is reflected across the room from the dye laser, collimated to a diameter of 2 mm by a 4 m f.l. lens (2 meters from the cell) and an adjustable aperture (1 meter from the cell), and divided into signal (40%) and reference (60%) beams by a beamsplitter (Rolyn). The reference beam passes through another aperture before being reflected by an Al mirror through a draft tube parallel to the photolysis cell. The draft tube reduces thermal currents from cold traps on the vacuum line. After the draft tube, the reference beam passes through another aperture and a rotatable polarizer which serves as a variable neutral

density filter. The signal beam passes through the second uv high reflector, the adjustable aperture, and down the center of the cell. After exiting the cell, the signal beam passes through another aperture, the uv mirror, and two colored glass interference filters (Schott GG395 and OG590) to remove any remaining uv. Both beams are then focussed onto the photodiodes by 15 cm f.l. lenses.

The signal beam was originally passed more than once through the cell to increase the absorption pathlength. Multiple passes were used for all of the experiments described in Chapter V, and some of those described in Chapter IV. The basic multipass configuration is shown in Fig. II-3. The photolysis beam was defined by rectangular (7mm x 20mm) rather than circular apertures. The first "aperture" is actually a piece of rectangular glass tubing roughly six inches long. The probe beam was confined to the region of the cell swept out by the photolysis beam. One inch diameter dielectric mirrors which are flattened on one edge are placed at either end of the cell, one meter apart. Both mirrors are mounted in 2" diameter aluminum collars held in mirror mounts with fine micrometer adjustments (Lansing or Burleigh). The mirror on the laser side of the cell is a flat dichroic (F-2 output coupler from a Chromatix CMX-4 dye laser) which transmits 70% of the 308 nm light while reflecting >98% of the visible. The photolysis beam passes through the uncoated side of this mirror and into the cell. The visible beam passes through an opening on one side of the collar, just missing the flattened edge of the dichroic as it enters the cell. After passing through the cell, the beam strikes the second mirror (CVI) which is curved (1 m f.l.) and coated for >98% reflectivity in the visible. The visible beam passes seven times between the two mirrors before grazing the flattened edge of

the second mirror and passing through an adjustable aperture. The one meter separation and focal length of the curved mirror keeps the beam collimated over the seven passes.

The glass interference filter (Schott OG590) in Fig. II-3 prevents uv light from passing through the visible beam opening. This is undesirable since the intensity of this light will be significantly greater than that which passes through the dichroic. This also means that the probe beam does not completely overlap with the photolysis beam on the first and last passes. To improve the overlap, a slightly different configuration was adopted. The only difference is that the uv mirror is placed between the multipass mirrors. The effective pathlength is increased since the probe beam can overlap with the photolysis beam on all nine passes. After nine passes through the 1/4" thick uv mirror and eighteen passes through the cell windows, the intensity and quality of the probe beam is substantially reduced. This configuration was not envisioned when the uv mirrors were designed; much thinner substrates and visible AR coatings would work better.

Since the excimer beam is somewhat irregular and has considerable divergence, the overlap between the two beams and hence the effective pathlength was always somewhat ambiguous. The photolysis laser energy density was also uncertain since as much as 30% of the uv was reflected back into the photolysis cell by the high reflector. In order to make the experiment more quantitative, both multipass configurations were ultimately dropped in favor of the single pass arrangement described above. This leads to better definition of both beams, and complete control over the overlap. Surprisingly, the reduction in signal-to-noise was considerably less than the factor of nine expected from the decrease

in pathlength. This is primarily due to reduced noise levels in the single pass arrangement. Over the course of nine passes, mechanical vibrations and scattering losses lead to very different noise spectra for the signal and reference beams. As a result, much of the dye laser noise is not subtracted out, and additional noise (particularly low frequencies) is introduced. The 8 meter difference in pathlength also results in a 25 ns phase shift between the signal and reference beams which exacerbates the imperfect subtraction of dye laser noise at frequencies above 4 MHz. A further reduction in noise due to imperfect subtraction may be possible if both signal and reference beams pass through the photolysis cell. Low laser fluence and a larger diameter cell (to prevent heating effects) are recommended for such an experiment.

Several factors should be considered when selecting the relative sizes of the photolysis and probe beams. One of the advantages of laser vs. flashlamp photolysis is that only a well defined region of the cell is irradiated. Irradiation of a large volume is undesirable since any events which are not sampled by the dye laser are wasted. Uncertainties due to wall reactions are also minimized. If the cell is much larger in diameter than the photolysis beam, only a small fraction of the reactant molecules are consumed in each laser shot and many shots can be used to signal average and improve the signal-to-noise. In practice, the probe beam should be somewhat smaller than the photolysis beam to prevent diffusion of the species being probed on the time scale of the ensuing reactions.

D. Detectors, Electronics, and Signal Processing

The detection system in these experiments must convert small ($<1\%$)

transient changes in a large dc background to time-dependent voltages for the digitizer. High saturation thresholds, fast response times, and high spectral sensitivity are obvious detector requirements. Silicon photodiodes are ideal for this purpose. Many commercial photodiodes with subnanosecond response times and 0.3 mA/mW (at 600 nm) responsivities are readily available and quite inexpensive. The initial experiments were performed with Hewlett-Packard 5082-4200 photodiodes which have a responsivity of 0.35 mA/mW at 600 nm and a risetime of < 1 ns (-20 V bias). One additional consideration quickly became apparent from these experiments. Mechanical vibrations (particularly for multiple pass experiments) and gas heating effects (when the photolysis beam is strongly absorbed) can produce "signals" by deflecting the probe beam from the photodiode's active area. The probe and reference beams were therefore focussed tightly on the photodiodes to eliminate the effects of beam wander. This proved insufficient for the small active area of the HP photodiodes (0.20 mm^2) and SGD 100A photodiodes from EG&G with larger active areas (5.1 mm^2) were obtained. Since the photodiode risetime scales with the surface area, the larger photodiodes have a risetime of 5 ns (-90 V bias).

The SGD 100 A photodiodes have a responsivity of 0.30 mA/mW at 600 nm. Since a linear response is specified only for photocurrents below 1 mA, the maximum power striking the photodiode must be less than 3.3 mW. The system was always operated with 3 mW or less incident power or a maximum photocurrent of 0.9 mA. The dc light levels on the photodiodes were matched by rotating a polarizer placed in the reference beam. The photocurrents from the photodiodes were converted to voltages at the 50 ohm inputs of a 150 MHz wideband amplifier (Keithley 104), amplified 10x,

and subtracted by a Tektronix 7704 oscilloscope with a 7A24 differential plug-in (10:1 common mode rejection ratio, dc to 50 MHz). The time response of the detection system was limited by the photodiode risetime. The vertical signal output from the oscilloscope was digitized (Tektronix 7912AD), averaged over (typically) 64-256 laser shots by an LSI-11/03 microcomputer, and stored for analysis.

A photocurrent of 0.9 mA results in 450 mV at the input of the differential amplifier. The output voltage from the 7704 is 25 mV per division of CRT deflection. On the most sensitive scales of the 7A24 plug-in (5 mV/div), a 450 mV input therefore results in an output voltage of 2.25 V (450/5 x 25 mV) when the signal beam is completely blocked. Before subtraction, fluctuations in the dye laser intensity are the limiting source of noise. After subtraction, the high frequency (>1 MHz) noise on long timescales was usually amplifier limited at 3-5 mV (peak-to-peak). On 10-100 microsecond timescales, the minimum detectable single shot absorbance (signal-to-noise of one) in a single pass of 85 cm was therefore 0.15% under optimum conditions, with 0.5-1.0% typical. When submicrosecond time response was unnecessary, the high frequency noise was usually reduced by a 3.2 MHz low pass filter at the 7912AD input. Subtraction of low frequency noise was always less than ideal. On the timescales of most experiments (<100 μs), the result was fluctuations in the entire baseline which were eliminated by a high pass (1.2 kHz) filter. It should be noted that this set up is far from optimum for experiments on millisecond timescales. The Keithley has a low frequency cut off of 10 Hz and must be replaced by an amplifier which goes to dc. A system based on the (National Semiconductor) LH0032 and LH0033 operational amplifiers such as that used by Marinelli[5] is

recommended.

On short timescales, an additional source of noise is RF pick-up from the excimer laser. This continues for several microseconds following the laser pulse. All of the electronic components are susceptible to pick-up, and even the strongest signals can be completely obscured if no precautions are taken. Fortunately, most of the pick-up in an averaged waveform can be eliminated by subtracting an equal number of shots with the photolysis laser blocked or the probe laser tuned off resonance. It is important, however, to eliminate as much of the pick-up as possible since any which is not subtracted may distort weak signals. Significant reductions are possible in just a few simple steps. The most important step is to make sure that none of the electronics are grounded to the excimer laser. The usual procedure is to float the digitizer, amplifier, and oscillocope, and 2-prong plug them into outlets in an adjacent room. This somewhat dangerous practice may not be necessary if a line filter (e.g. Corcom 3K5 EMI) is placed on the 110 V AC input to the laser. Scattered light striking a photodiode should always be used to trigger the digitizer since the "sync out" grounds the digitizer to the laser. Even with ground loops eliminated, a large amount of RF is transmitted to the electronics through the air. Two approaches are possible: shielding the laser or shielding the electronics. The best solution is to completely enclose one or the other (preferably the former) in a screen cage with isolated connections. If a screen room is not available, liberal use of aluminum foil may be helpful. A good procedure for reducing the overall RF pick-up is to start with the digitizer and add one component (or cable) at a time while minimizing the pick-up at each step. It is very important to actually monitor the pick-

up, while applying the foil since seemingly insignificant changes can have a dramatic effect.

Pick-up by the 7912AD is significantly reduced by placing the digitizer in the adjacent room. Also, most of the RF does not enter the digitizer through the BNC input connector. This means that the peak-to-peak RF noise displayed on the TV monitor (and added to the waveform) is independent of the amplifier setting. The most sensitive amplifier setting compatible with keeping the signal on scale should therefore be used. Similar considerations apply to the differential amplifier (osilloscope). Relatively little RF enters the system through the cables which connect the various components. These should be checked anyway and wrapped in foil if necessary. The Keithley 104 is enclosed on five sides by an aluminum covered wooden box. The face of the amplifier where the connections are made is partially covered by copper screen. This box substantially reduces the RF pick-up and should always be used. Covering the face of the amplifier with foil is also recommended. The 110 V AC power cords should not be ignored in the search for gremlins. Wrapping foil on connections between these and extension cords sometimes eliminates a lot of pick-up. The photodiodes and three the 30 V batteries which provide the -90 V bias are mounted in aluminum boxes which are relatively impervious to RF. Unfortunately, the various holes which must be added to make the boxes useful introduce a lot of RF leaks. RF pick-up at this stage is most critical since it is amplified (along with the signals) in the next stage. The RF leaks can be reduced by wrapping the boxes in aluminum foil. For best results, the photodiode elements should not be covered.

Two data acquisition systems were used. Some of the early data

described in Chapter IV was acquired using a Biomation 8100 transient digitizer in conjunction with a Northern NS-575 Signal Analyzer (10 ns-10 s/channel with up to 2048 channels, and a sensitivity of 100 mv in 8 bits). The acquired data is stored on magnetic tape and transferred to the LSI-11 and floppy diskette for analysis. The transfer program is described in Young's thesis.[6] The remaining data was acquired using a Tektronix 7912AD transient digitizer (9.8 ps-19.5 μs/channel with 512 channels and a sensitivity of 100 mv in 9 bits) in conjunction with the LSI-11. The timescale was periodically calibrated with an external timebase. The 7912AD has a built-in microprocessor which averages 64 waveforms and dumps them to the LSI-11 through an IEEE-488 buss. The computer can then be used to average and store the 7912AD waveforms. The entire process is regulated through a Basic program called "7912AD" which was written by Linda Young.

The 7912AD has several advantages over the 8100 such as faster time response and greater sensitivity. The direct interface to the computer is particularly useful and saves a great deal of time (and a potential for lost data) otherwise wasted in transferring the data from signal analyzer to cassette and from cassette to diskette. This also makes it possible to spot check the data within minutes which can prevent the accumulation of many hours of data with some systematic error. The 8100 has distinct advantages over the LSI-11, however, when the signals of interest are on timescales greater than about 100 us. The greater temporal resolution (128 to 2048 horizontal channel vs 512 channels) and dual timebases are particularly useful. A direct interface between the 8100 and a microcomputer such as the LSI-11 is recommended if extensive work on these timescales is contemplated.

The LSI-11 was used to analyze the absorption data through least squares fitting programs based on Gauss' algorithm. A sample program which can be used to fit a signal which rises and decays exponentially is given in Ref. 6. The method is quite general and can be adapted for any combination of analytic functions. Details can be found in Young's thesis and in the notebook of computer programs by Michael Diegelmann.

E. Photolysis Cell and Gas Handling.

A standard glass and grease vacuum manifold (mercury diffusion pump) with a background pressure of 10^{-6} Torr (Phillips gauge) was used to evacuate and fill the photolysis cell. An 8 mm stopcock divides the manifold into two sections, each of which is connected to one end of the photolysis cell. A schematic drawing of the vacuum line is shown in Fig. II-4. Pressures were measured with either 0-10 Torr (Baratron 145-AH) or 0-1000 Torr (Baratron 310-BH) capacitance manometers accurate to within 0.3% of the fullscale reading. The calibration was checked with an oil manometer. The reference sides of the Baratrons were attached directly to the manifold or to the tubing which connects the manifold to the cell. The sample sides were also attached to this tubing. A mercury manometer attached to the manifold was used to monitor the line pressure when up to 1000 Torr N_2 was added to the photolysis cell.

The photolysis cell itself is as 85 cm long, 5 cm i.d. quartz cylinder with quartz windows sealed on at Brewster's angle by glass transfer tape (Vitta Corp. G-105). Two small sample fingers are attached to one end of the cell by 8 mm teflon stopcocks. The all quartz construction allowed the entire cell (including the windows) to be heated with a gas-oxygen flame to remove polymerized formaldehyde, glyoxal,

ketene or reaction products. The cell is usually wrapped in heating tapes for periodic baking. Since the cell temperature is not regulated during the experiments, all of the measurements were made at an ambient temperature of 295±2 K.

The typical procedure for making mixtures is as follows. The cell is first filled to the desired pressure of precursor from a supply (~5 fills) frozen into one of the two sidearms. This sample is then frozen into the other sidearm, the stopcock closed, and the cell filled to the desired lower pressure of the reactant gas. The precursor is then allowed to thaw and the gases mix for several minutes. If buffer gases are used, these are then bled slowly into the cell from the right side of the manifold which contains the buffer gas at high pressure to prevent diffusion of the reactants from the cell. The gases are then allowed to mix for 5 to 30 minutes, depending on the total pressure.

References

1. F. E. Hovis, Ph. D. Disseration, University of California, Berkeley, 1979.
2. M. R. Berman, Ph. D. Dissertation, University of California, Berkeley, 1981.
3. H. Petek, Ph. D. Dissertation, University of California, Berkeley, 1985?
4. L. L. Nichols and W. Vali, J. Chem. Phys. 49, 814 1968.
5. W. J. Marinelli, Ph. D. Dissertation, University of California, Berkeley, 1981.
6. L. Young, Ph. D. Dissertation, University of California, Berkeley, 1981.

Figure II-1. Schematic diagram of the laser photolysis/laser resonance absorption apparatus. See text for details.

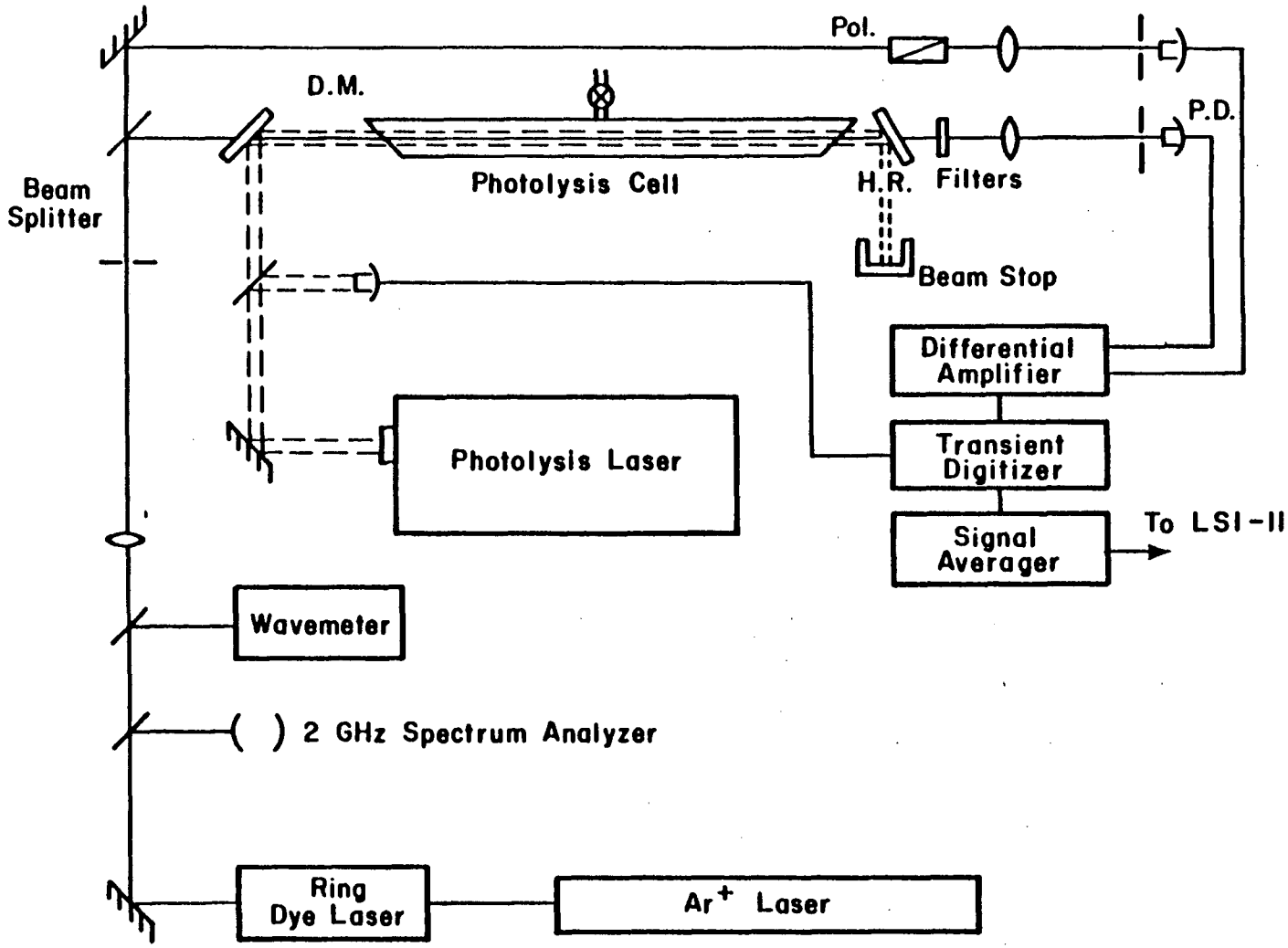
Pol.
D.M.
P.D.
Photolysis Cell
H.R.
Filters
Beam
Splitter
Beam Stop
Differential
Amplifier
Photolysis Laser
Transient
Digitizer
Signal
Averager
To LSI-II
Wavemeter
( ) 2 GHz Spectrum Analyzer
Ring
Dye Laser
Ar+ Laser

Fig. II-1

Figure II-2. Manifold for preparing excimer laser gas mixtures.

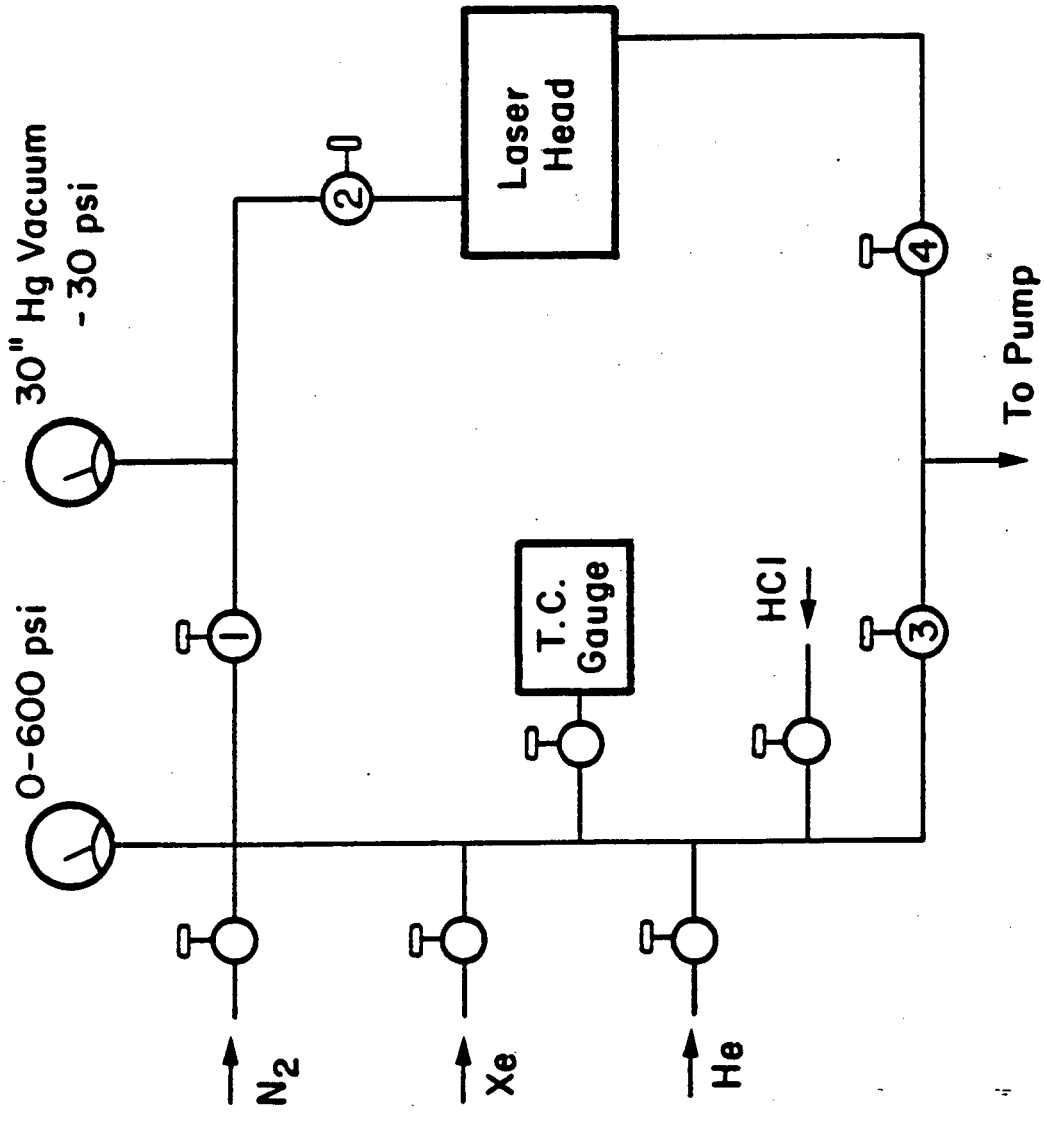
30" Hg Vacuum
- 30 psi
0-600 psi
Laser Head
T.C. Gauge
HCl
To Pump
N2
Xe
He
1
2
3
4

Fig. II-2

Figure II-3 Set up for multiple passes of the probe beam (not to scale). HR-high reflector, DM-dichroic mirror, F-colored glass filter. The photolysis cell is not shown for clarity. See text for other details.

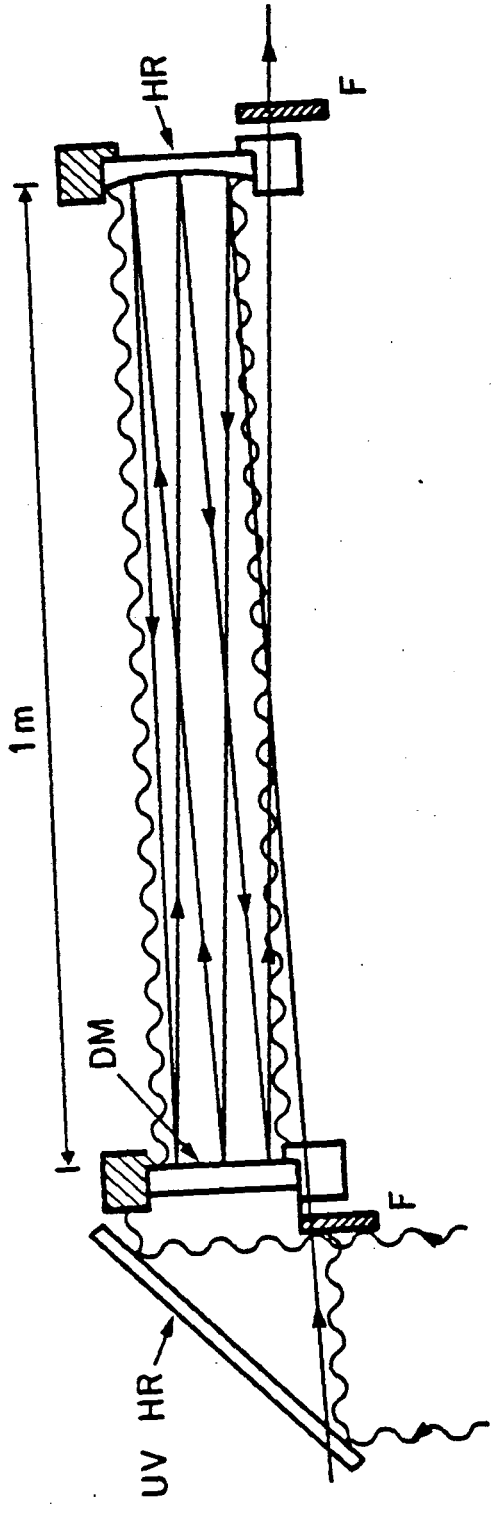

Fig. II-3

Figure II-4. Vacuum line (and photolysis cell) for sample preparation.

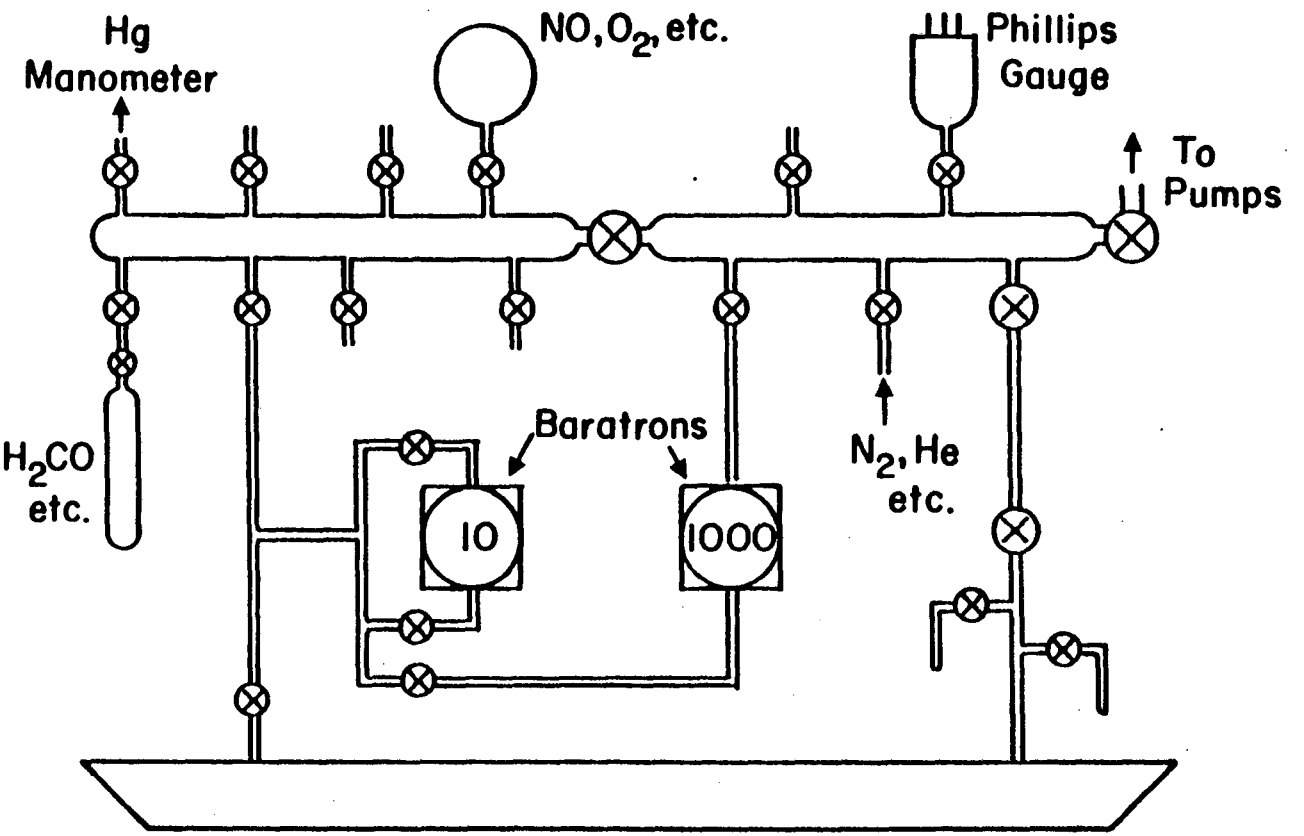
Hg
Manometer
NO, O_2, etc.
Phillips
Gauge
To
Pumps
H_2CO
etc.
Baratrons
10
1000
N_2, He
etc.

Fig. II-4

CHAPTER III. REACTION AND RELAXATION OF VIBRATIONALLY EXCITED FORMYL RADICALS

A. INTRODUCTION

Strong attractive forces between molecules are known to facilitate vibration-to-rotation and translation (V - R, T) energy transfer.[1] Vibrational relaxation in pure gaseous H_2O or NH_3 which form strong hydrogen bonds occurs with nearly every collision.[2] For H_2S which forms weaker hydrogen bonds fewer than 10^2 collisions are required[2] while relaxation of CH_4 with similar vibrational frequencies but no hydrogen bonding requires ~ 10^4 collisions.[3]

The unpaired electrons of free radicals form weak bonds with many collision partners and strong bonds with other free radicals. Efficient deactivation of hydrogen halides has been attributed to orbiting collisions.[4] Complex formation may account for the effectiveness of NO and O_2 deactivation by H, F, Cl, Br, I, and O atoms.[5] Complex formation may be particularly important for polyatomic free radicals since the complexes which are formed will have more degrees of freedom into which the translational energy and subsequently the vibrational energy may be dissipated.

Experimental data on vibrational deactivation of polyatomic free radicals is scarce. One of the few direct measurements of vibrational deactivation of an unstable triatomic radical was reported by Reilly et al.,[6] who measured a rate constant for deactivation of HCO(0,1,0) by H_2CO. More recently, Nadtochenko and co-workers[7] have reported rate constants for deactivation of unidentified NH_2 vibrational levels. In

the present paper, rate constants for deactivation of vibrationally excited formyl radicals by several collision partners are reported. Collision numbers for deactivation of HCO(0,1,0) range from approximately 10^3 for He and N_2 to 50 - 100 for $(HCO)_2$ and H_2CO and 10 - 30 for NO and O_2. Deuteration decreases the rate with formaldehyde, DCO (0,1,0) by (D_2CO), by a factor of four and the rate with NO by less than 25%. Excitation of the HCO bending mode was also found to decrease the rate of reaction with NO and O_2. This result, as well as the efficient deactivation of HCO(0,1,0) by NO and O_2 is attributed to formation of strongly bound collision complexes.

B. EXPERIMENTAL

1. Apparatus

Ground state and vibrationally excited formyl radicals were produced by photodissociation of formaldehyde and glyoxal with the XeCl excimer laser. A 5 mm diameter spot from the unfocussed 7 mm x 25 mm photolysis beam was selected by apertures (at the laser and in front of the cell) and directed down the center of the 5 cm i.d. x 85 cm long cylindrical quartz cell. The energy fluence entering the cell in this configuration was 6 - 15 mJ/cm^2.

The formyl radicals were detected through absorption of the 2 mm diameter beam from a 20 MHz linewidth Ar^+-pumped ring dye laser (Spectra-Physics UV-171/380A). The laser was operated with R6G or R110 to obtain 200 - 800 mW of tunable radiation between 5400 and 6200 Å. The visible beam was directed down the center of the photolysis cell, collinear with the 0.20 cm^2 photolysis beam. After the cell, a uv mirror oriented at 45° to the incident beams reflected most of the unabsorbed uv light into

a beam stop. Two interference filters (Schott GG395 and OG590) were used to remove residual uv and the probe beam was focused by a 15 cm f.l. lens onto a silicon photodiode (EG & G SGD 100A biased at - 90 V). The large active area (5.1 mm^2) of the SGD 100A facilitated alignment and ensured that signals due to deflection of the probe beam through thermal lensing were unimportant. Approximately 40% of the probe beam was split off before the reaction cell and focussed onto an identical reference photodiode. The dc light levels on the photodiodes were matched by rotating a polarizer placed in the reference beam. The dye laser intensity on the photodiodes was 1 - 3 mW. The photocurrents from the detectors were converted to voltages at the 50 ohm inputs of a 150 MHz wideband amplifier (Keithley 104), amplified 10 x, and subtracted by a Tektronix 7704 oscilloscope with a 7A24 differential amplifier plug-in (10:1 common-mode rejection ratio, dc to 50 MHz). The minimum detectable single shot absorbance (signal-to-noise of one) was 0.15% under optimum conditions, with 0.5-1.0% typical in most experiments. The time response of the detection system was limited by the 5 ns photodiode risetime. The vertical signal output from the oscilloscope was digitized (Tektronix 7912AD), averaged over (typically) 64 - 256 laser shots by an LSI-11/03 microcomputer, and stored for analysis.

When 10.1 Torr of H_2CO was irradiated with (2.5 ± 1.0) x 10^{16} photons/cm^2, the peak signal at 16,263.56 cm^{-1} (blended Q(9) and P(2) lines of the (0,9,0) ← (0,0,0) band) corresponded to an absorbance of 1.3% 10 to 20 μs after the laser pulse. The absorption coefficient of H_2CO at 308 nm was determined to be (3.2 ± 0.4) x 10^{-4} cm^{-1} $Torr^{-1}$ by direct measurement with the excimer laser. The uv absorbance is therefore 24 ± 4% and (7 ± 3) x 10^{13} cm^{-3} formaldehyde molecules are

excited. The HCO quantum yield is 0.6 ± 0.1;[9] thus (4 ± 2) x 10^{13} cm^{-3} HCO are formed and the HCO absorption cross-section is (3.6 ± 1.6) x 10^{18} cm^2. This implies a minimum detectable (S/N = 1) of 2 x 10^{11} cm^{-3} under optimum conditions with 512 laser shots.

2. Spectroscopy

The visible absorption spectrum of HCO ($\tilde{A}\ ^2A'' \leftarrow \tilde{X}\ ^2A'$) has been studied extensively by Herzberg and Ramsay[10] and later by Johns, Priddle, and Ramsay.[11] The spectrum is primarily a long progression of bands between 4500 and 7000 Å with the bending mode (ν_2) excited in the upper state. Alternate bands are sharp and diffuse; the sharp bands ($\Delta\nu > 0.3$ cm^{-1}) involve K" = 1 rotational levels in the ground state and K' = 0 levels in the upper state, while most of the diffuse bands ($\Delta\nu \simeq 20$ cm^{-1}) originate in the K" = 0 or K" = 2 levels of the ground state. An unstructured absorption continuum underlies the entire spectrum. Several hot bands originating from the (0,1,0) vibrational level were reported in these studies. Rotational line positions for transitions originating in both the (0,0,0) and (0,1,0) vibrational levels observed in the latter study were obtained from the Canadian National Research Council Depository for Unpublished Data. Ground state HCO was monitored primarily through the $Q_{0-1}(10)$ line of the (0,9,0) ← (0,0,0) band at 16,262.25 cm^{-1}. Ground state DCO was monitored in the Q-branch of the (0,11,0) ← (0,0,0) band near 15,923 cm^{-1}, and HCO(0,1,0) was monitored at 18,138.4 cm^{-1} which corresponds to the $Q_{0-1}(1)$ line of the (0,13,0) ← (0,1,0) band. Wavelengths for hot bands originating in the (0,0,1) level of HCO were taken from Reilly et al..[6,12] Since all rotational lines in the $\tilde{A} \leftarrow \tilde{X}$ transition have a linewidth of at least 0.3 cm^{-1},[11,13] kinetic studies with much broader laser linewidths than 20 MHz are possible.

Initial experiments were performed with the 0.25 cm^{-1} line from a Spectra-Physics 375 dye laser.

3. Materials

HCO radicals were produced by photolysis of H_2CO or $(HCO)_2$ while DCO was produced by photolysis of D_2CO. Similar HCO signals were observed following photolysis of the same pressure of H_2CO or $(HCO)_2$ with a given laser fluence. Both formaldehydes were prepared as before[14] and stored at 77 K to prevent polymerization. Glyoxal, prepared by heating the trimer (Matheson, Coleman, and Bell) in the presence of phosphorous pentoxide, was also stored at 77 K. O_2 (Baker UHP 99.995%) and was used without further purification while N_2 (LBL 99.999%) was passed through a copper loop in liquid nitrogen. NO (Matheson 99.0%) was purified by distillation through a silica gel trap kept at 195 K to remove NO_x impurities. All gases were kept in vessels with teflon stopcocks and transferred to the photolysis cell using a standard glass vacuum line with a base pressure of 10^{-6} Torr. Pressure measurements were made with either a 10 Torr (Baratron 145-AH) or a 1000 Torr (Baratron 310-BH) capacitance manometer accurate to within 0.3%. All measurements were made at an ambient temperature of 295 ± 2 K.

C. RESULTS AND ANALYSIS

1. Relaxation Rates

The transient absorbance due to HCO(0,1,0) following excitation of 4.02 Torr glyoxal is shown in Fig. 1. 256 laser shots were averaged with the dye laser tuned to the $Q_{0-1}(1)$ rotational line of the (0,13,0) ← (0,1,0) band at 18,138.40 cm^{-1}. RF pick-up and the weak background signal due to the underlying HCO(0,0,0) absorption continuum[11] were

reduced by subtracting 256 shots with the dye laser tuned +1 cm^{-1} off resonance into the region between the Q and R branches. The background absorption was approximately 10% of the HCO(0,1,0) absorption at this wavelength. The signal does not appear promptly following the photolysis pulse, but rises exponentially at a rate of 3.3×10^6 s^{-1}. HCO(0,1,0) risetimes at other pressures can also be fit reasonably well as single exponentials with rates proportional to the glyoxal pressure, although the signal-to-noise was inadequate to completely rule out the possibility of a multiple exponential rise. The HCO(0,i,0) signal also decays exponentially with a rate proportional to the glyoxal pressure (8.6×10^5 s^{-1} at 4.02 Torr).

The absorbance due to HCO(0,0,0) following excitation of 4.05 Torr $(HCO)_2$ is shown in Fig. III-2. Sixty-four laser shots were averaged with the dye laser tuned to the $Q_{0-1}(10)$ rotational line of the (0,9,0) ← (0,0,0) band at 16,262.25 cm^{-1}. Sixty-four shots were then subtracted with the photolysis laser blocked to reduce RF pick-up. Identical results were obtained when the photolysis laser was unblocked and the probe laser tuned between rotational lines during the subtraction. The HCO(0,0,0) signal rises biexponentially, levels off after about 5 μs, and decays through the second-order recombination reaction[9]

$$HCO + HCO \rightarrow H_2CO + CO$$

on much longer time scales ($K < 450$ s^{-1} for $[HCO]_o = 10^{13}$ cm^{-3}).[15] The fast initial rise (5×10^7 s^{-1}) is followed by a much slower rise (8.0×10^5 s^{-1}) which accounts for two-thirds of the total amplitude. The relative amplitudes are independent of pressure over the range of the measurements (1 to 6 Torr for pure glyoxal). The initial risetime (~20 ns) is comparable to the laser pulse duration. Although the fast rise

exhibits some pressure dependence, its amplitude does not vanish when extrapolated to zero pressure. A reliable detailed analysis of the initial rise was not possible; the rates of glyoxal dissociation and HCO rotational relaxation are probably convoluted with the laser pulse at these pressures.

The rate of the slow HCO(0,0,0) rise is proportional to the glyoxal pressure and is essentially the same as the HCO(0,1,0) decay rate, suggesting the pseudo-first-order vibrational relaxation process

$$HCO(0,1,0) + (HCO)_2 \rightarrow HCO(0,0,0) + (HCO)_2. \qquad (1)$$

Identical results were obtained for the $Q_{0-1}(2)$ line at 16,268.77 cm^{-1} which demonstrates that equilibration of the J rotational levels occurs on much shorter timescales. The pseudo-first-order rates obtained from photolysis of pure glyoxal are shown in Fig. III-3. The uncertainties of the individual rates are estimated as 10% for the ground state rises, and 20% for the excited state rises and decays. Absolute rate constants of $(2.4 \pm 0.4) \times 10^{-11}$ and $(6.7 \pm 1.1) \times 10^{-12}$ cm^3 $molec^{-1}$ s^{-1} for HCO (0,1,0) production and removal, respectively, were obtained from a linear least-squares fit of the HCO(0,1,0) rates, constrained to zero at zero pressure. The HCO(0,0,0) data give a similar rate constant of $(6.3 \pm 0.9) \times 10^{-12}$ cm^3 $molec^{-1}$ s^{-1} for HCO(0,1,0) relaxation. The quoted uncertainties correspond to two standard deviations in the least-squares rate constants. The combined data give $k_1 = (6.4 \pm 1.0) \times 10^{-12}$ cm^3 $molec^{-1}$ s^{-1}.

When mixtures of glyoxal and He, N_2, NO or O_2 were irradiated, the slow HCO (0,0,0) appearance rate increased linearly with added gas pressure (Figs. III-4 and 5) while the relative amplitudes of the fast and slow rises were unchanged. The factor of 250 difference in

relaxation efficiency between $(HCO)_2$ and N_2 underscores the unimportance of rotational relaxation processes on these timescales. For He and N_2, the signals were again analyzed as biexponential rises. For O_2 and NO, a fixed single exponential decay based on the known rate constant for the appropriate HCO (0,0,0) reaction was added. The rate constants are summarized in Table III-1. Uncertainties in the individual pseudo-first-order rates are again estimated to be 10%, and quoted uncertainties for the bimolecular rate constants obtained in the least-squares fit are two standard deviations.

The HCO(0,0,0) absorbance produced by irradiation of equal pressures H_2CO or $(HCO)_2$ at 308 nm was similar. Weak absorption due to HCO(0,1,0) was also observed following H_2CO photolysis. Decay rates of 0.95 ± 0.15 and $2.0 \pm 0.2\ \mu s^{-1}$ were obtained at formaldehyde pressures of 10 and 20 Torr, respectively. The experimental conditions (> 2048 laser shots for 10 - 20 Torr H_2CO) necessary to obtain reasonable signal-to-noise made extensive kinetic measurements using formaldehyde as the radical precursor impractical. The increase in HCO(0,0,0) absorbance due to vibrational relaxation (Fig. 1 of Chapter IV) indicates that approximately 20% of the HCO photoproduct is vibrationally excited. This increase was too small to permit reliable measurements of relaxation rates through ground state analysis. Since photolysis of H_2CO at 294.1 nm (~11 kcal mol^{-1} excess energy) produces approximately 30% of the HCO product in the (0,1,0) vibrational level and only 1 - 10% in the (0,0,1) vibrational level,[6] the low yield of HCO(0,1,0) at 308 nm is not particularly surprising.

A larger fraction (~30%) of vibrationally excited radicals was produced in the photolysis of D_2CO at 308 nm. No attempt was made to

observe DCO(0,1,0) directly. The rate constants for deactivation of DCO(0,1,0) by D_2CO and NO given in Table III-1 were obtained from DCO(0,0,0) risetime measurements in D_2CO/NO mixtures. The larger uncertainties in these rates reflect the smaller signal-to-noise and limited data base.

2. Reaction Rates

For He and N_2, the increase in ground state absorbance can only be due to energy transfer processes, most likely

$$HCO(0,1,0) + M \rightarrow HCO(0,0,0) + M \; . \qquad (2)$$

For NO and O_2, reaction as well as deactivation is possible

$$HCO(0,1,0) + NO \rightarrow HCO(0,0,0) + NO \qquad (3a)$$

$$\rightarrow HNO + CO \qquad (3b)$$

$$HCO(0,1,0) + O_2 \rightarrow HCO(0,0,0) + O_2 \qquad (4a)$$

$$\rightarrow HO_2 + CO \; . \qquad (4b)$$

The concentrations of HCO and $HCO^\dagger$ in $(HCO)_2$/NO mixtures therefore follow the rate equations

$$-\frac{d[HCO^\dagger]}{dt} = \{(k_{3a} + k_{3b})\,[NO] + k_1\,[(HCO)_2]\}\,[HCO^\dagger] \qquad (5)$$

$$\frac{d[HCO]}{dt} = \{k_{3b}[NO] + k_1\,[(HCO)_2]\}\,[HCO^\dagger] - k_R[HCO]\,[NO] \qquad (6)$$

where k_R is the rate constant for the reaction of HCO (0,0,0) with NO and $HCO^\dagger$ refers to vibrationally excited HCO. The effect of vibrational cascading is considered below. These expressions lead to the following rate equations:

$$[HCO^\dagger] = [HCO^\dagger]_o e^{-K' t} \qquad (7)$$

$$[HCO] = [HCO]_o e^{-K_R t}$$

$$+ \left\{ \frac{k_{3b}\,[NO] + k_1\,[(HCO)_2]}{k_R[NO] - (k_{3a} + k_{3b})\,[NO] - k_1\,[(HCO)_2]} \right\} [HCO^\dagger]_o \left(e^{-K' t} - e^{-K_R t}\right) \quad (8)$$

where $K' = (k_{3a} + k_{3b})\,[NO] + k_1\,[(HCO)_2]$ and $K_R = k_R[NO]$. The analogous expressions are obtained for O_2. The HCO(0,0,0) signals were fit by least-squares to a biexponential rise and a fixed single exponential decay corresponding to the appropriate HCO(0,0,0) reaction using the rate constant from Chap. IV.

According to Eq. (8), the extrapolatd ($K_R = 0$) maximum in the HCO(0,0,0) absorbance will given by

$$A_{max} = A_f + A_s \quad (9)$$

where

$$A_f = [HCO]_o \quad (10)$$

$$A_s = \left\{ \frac{k_{3b}\,[NO] + k_1\,[(HCO)_2]}{(k_{3a} + k_{3b})\,[NO] + k_1\,[(HCO)_2]} \right\} [HCO^\dagger]_o. \quad (11)$$

From these equations, it can be seen that

$$\frac{A_s}{A_f} = \left(1 - \frac{K_{3a}}{K'}\right) \frac{[HCO^\dagger]_o}{[HCO]_o} \quad (12)$$

If the dissociation of glyoxal with 92.8 kcal mol^{-1} internal energy is collision free as suggested by the fast rise of Fig. 2, the yield of nascent HCO and $HCO^\dagger$ will be unchanged by the addition of NO or O_2. This assumption is supported by the absence of a pressure dependence in the relative amplitudes of the two rises for pure glyoxal. Equation (12)

then becomes

$$(A_s/A_f) = \left(1 - \frac{K_{3a}}{K'}\right) (A_s/A_f)_o \qquad (13)$$

which can be rearranged to obtain

$$\left(1 - \frac{(A_s/A_f)}{(A_s/A_f)_o}\right) K' = K_{3a} \qquad (14)$$

From this expression it follows that a nonzero reaction rate will cause the amplitude ratio A_s/A_f to decrease from the value obtained with pure glyoxal. This ratio is shown as a function of added NO and O_2 pressure in Fig. III-6. No systematic change is apparent over the pressure range 0.0 to 0.9 Torr which suggests that the reaction rates are small compared to vibrational deactivation. The pure glyoxal results give $(A_s/A_f)_o = 1.95 \pm 0.13$. For 4.05 Torr glyoxal with 0.8 Torr NO ($K' = 1.72 \times 10^6$ s^{-1}) or 0.9 Torr O_2 ($K' = 1.06 \times 10^6$ s^{-1}), the measured amplitude ratios were 1.94 ± 0.19. From these quantities and Eq. (14), upper limits of 8.0×10^{-12} and 4.4×10^{-12} cm^3 $molec^{-1}$ s^{-1} are obtained for (3b) and (4b), respectively.

D. DISCUSSION

Formyl radicals are produced in at least two vibrationally excited states following $(HCO)_2$ excitation at 308 nm. The (0,1,0) level does not appear to be a direct product. The exponential rise of the (0,1,0) signal is indicative of relaxation from at least one higher vibrational level. Although only one HCO (0,1,0) rotational level was monitored, attributing the exponential rise to rotational relaxation would imply a rate at least one order of magnitude slower than that for HCO(0,0,0).

The identity of the levels involved was not directly determined although (1,0,0), (0,0,1), and (0,2,0) are obvious candidates. The vibrational levels which are energetically accessible in the 308 nm (92.8 kcal mol^{-1}) photolysis are shown in Fig. III-7. The available excitation energy is estimated as 20 kcal mol^{-1}, assuming ΔH_f^o = - 58 kcal mol^{-1} for $(HCO)_2$[16] and 8 kcal mol^{-1} for HCO.[6]

The absence of (0,1,0) as a direct photoproduct suggests that higher vibrational levels in the ν_2 manifold are probably also unpopulated initially. A dissociation process that populates v_2=0 and v_2=2, but not v_2=1 would be very unusual. This implies that one or both of the stretching modes are preferentially excited in the dissociation process. This does not necessarily imply that (0,2,0) → (0,1,0) relaxation is unimportant since the stretching modes may be coupled to the bending manifold at higher levels. The rate constant for v_2=1 production in collisions with $(HCO)_2$ is approximately 4 times the rate constant for deactivation of v_2=1. This result is consistent with the formation of (0,1,0) by deactivation of (0,2,0). Efficient coupling of the (0,0,1) and (0,1,0) levels can not be ruled out, however, since the process HCO(0,0,1) + $(HCO)_2$ → HCO(0,1,0) + $(HCO)_2(v_6=1)$ + 16 cm^{-1} is nearly resonant. Attempts to monitor the (0,0,1) level directly were unsuccessful because of diffuse background absorption from the Q_{2-1} and R_{2-1} branches of the (0,9,0) ← (0,0,0) band.[11]

The population of HCO(0,1,0) through vibrational cascading implies that the simple exponential analysis of the slow HCO(0,0,0) rise is not quite correct. For a sequential process in which

$$HCO(v') + (HCO)_2 \rightarrow HCO(0,1,0) + (HCO)_2 \qquad (15)$$

is followed by (1), [HCO(0,1,0)] and [HCO(0,0,0)] are given by

$$[HCO(0,1,0)] = \frac{[HCO(v')]_o K_{15}}{K_1 - K_{15}} [e^{-K_{15}t} - e^{-K_1 t}] \qquad (16)$$

$$[HCO(0,0,0)] = [HCO(0,0,0)]_o + [HCO(v')] \times$$
$$\{1 + (\frac{K_1}{K_{15} - K_1}) e^{-K_{15}t} - (\frac{K_{15}}{K_{15} - K_1}) e^{-K_1 t}\} \qquad (17)$$

where K_{15} and K_1 are the pseudo-first order rates k_{15} $[(HCO)_2]$ and k_1 $[(HCO)_2]$. From Eq. (17) it can be seen that the slow rise will deviate from a single exponential with rate $k_1[(HCO)_2]$ if the second term in the parentheses is important. For 4.0 Torr $(HCO)_2$, the second term is 8% of the third term 0.5 μs after the laser pulse and <3% after 1.0 μs. This suggests that vibrational cascading will not significantly alter the rate constants based on the simplified analysis.

1. HCO(0,1,0) + He, N_2

The rate constants for HCO(0,1,0) deactivation by He and N_2 are (2.5 ± 0.3) and (2.5 ± 0.8) x 10^{-13} cm^3 $molec^{-1}$ s^{-1}. These values are based on measurements at 5 different pressures between 0 and 400 Torr. Only V - T, R transfer can occur in these collisions since the vibrational frequency of N_2 is more than twice the HCO bending frequency of 1083 cm^{-1}. The similar rates for He and N_2 suggest that V - R transfer into HCO rotation is the dominant process; V - T transfer should have an

appreciable mass dependence. Similar results have been found for deactivation of other vibrationally excited hydrides (e.g. CH_4) by inert gases.[3] Efficient transfer of vibrational energy into rotation of the excited molecule is possible because of the rapid rotational motion associated with hydrogen atoms.[17] Rate constants for DCO and several rare gases are necessary to test this hypothesis.

2. HCO(0,1,0) + $(HCO)_2$, H_2CO

The value of $(3.0 \pm 0.5) \times 10^{-12}$ cm^3 $molec^{-1}$ s^{-1} found for the H_2CO deactivation rate constant is in good agreement with the value of $(4.3 \pm 1) \times 10^{-12}$ cm^3 $molec^{-1}$ s^{-1} reported by Reilly et al.[6] Although rates for only two H_2CO pressures were obtained in either study, the laser resonance absorption result is expected to be more accurate since the temporal resolution is greatly improved. Deactivation of the HCO bending mode by $(HCO)_2$ occurs with comparable efficiency and is more than an order of magnitude faster than deactivation by He and N_2. The similar rate constants suggest that the same processes are involved. V - V (vibration-to-vibration) as well as V - R, T processes may be important in these collisions. Energy transfer to the H_2CO out-of-plane bending mode (ν_4 = 1167 cm^{-1}) is endothermic by approximately 84 cm^{-1} while the energy gaps for V - V transfer to the ν_{11} and ν_6 ir-active modes of glyoxal are larger (- 229 and + 282 cm^{-1}, respectively). These energy gaps are too large for efficient dipole-dipole V - V transfer. Quadrupole-dipole allowed V - V transfer to the nearly resonant ν_4 (a_g) and ν_8 (b_g) modes (ΔE = - 18 and - 35 cm^{-1}, respectively) may be important, as could transfers involving shorter range interactions.

The factor of four decrease in relaxation rate following formaldehyde deuteration is consistent with vibrational energy being

transferred primarily into rotation. For V-V transfer caused by perturbations linear in the vibrational co-ordinates a smaller isotope effect is expected. The energy gap for transfer from DCO(ν_2 = 850 cm^{-1}) to D_2CO(ν_6 = 938) is + 88 cm^{-1}, essentially unchanged by deuteration. Deuterium substitution decreases the V-R efficiency by reducing the rotational velocity. More efficient V-R transfer in these collisions (relative to inert gases) could be indicative of energy transfer into the rotational motion of the collision partner. The very dissimilar moments of inertia for formaldehyde and glyoxal, however, suggest that vibrational energy is once again transferred into rotation of the radical. Efficient V - R, T transfer in collisions between HCO and H_2CO or $(HCO)_2$ may result from interactions between the half-filled valence orbital of HCO and the non-bonding lone pairs on the oxygen atoms of H_2CO and $(HCO)_2$. Hydrogen bonding may also be important. The HCO(0,1,0) deactivation efficiencies of H_2CO and $(HCO)_2$ are intermediate (40-90 collisions) between those of H_2O/H_2O or NH_3/NH_3 (strong hydrogen bonds) and H_2S/H_2S or CH_4/CH_4 (weak or nonexistent hydrogen bonds).[2]

3. HCO(0,1,0) + NO, O_2

V - V transfer from the HCO bend (1083 cm^{-1}) to the NO (1904 cm^{-1}) or O_2 (1580 cm^{-1}) stretches is highly endothermic. The total rate constants for destruction (reaction + deactivation) of HCO(0,1,0) by NO and O_2 were determined to be (3.4 ± 0.4) x 10^{-11} and (9.4 ± 1.1) x 10^{-12} cm^3 $molec^{-1}$ s^{-1}, respectively. The upper limits to the rate constants for reaction of HCO(0,1,0) with NO and O_2 therefore imply lower limits of 2.6 x 10^{-11} and 5.0 x 10^{-12} cm^3 $molec^{-1}$ s^{-1} for the corresponding vibrational deactivation rate constants. The two order of magnitude difference in V - R, T transfer rates for NO and N_2 underscores the

strong chemical interaction which takes place in these collisions.

Ground state HCO reacts efficiently with either NO or O_2 to form HNO or HO_2 and CO. The rate constants for these reactions are 1.26×10^{-11} and 4.65×10^{-12} cm^3 $molec^{-1}$ s^{-1}, respectively. Vibrational excitation of the HCO decreases the reaction rates. The indicated products have been observed experimentally and are consistent with a simple hydrogen transfer mechanism. It is not immediately obvious, however, that excitation of the HCO bend should decrease the rate of hydrogen transfer.

These results may be explained if a strongly bound complex is formed in collisions between HCO and NO (or O_2). Nitrosoformaldehyde (HCONO) should be a stable molecule with a singlet ground state. Gas phase absorptions attributed to this species have been reported by Napier and Norrish.[18] The hydroperoxy radical ($HCOO_2$) should also be relatively stable and has been reported following photolysis of formaldehyde in oxygen matrices.[19] Decreased reaction rates following vibrational excitation of CO [20] have been reported for the reaction

$$OH + CO \rightarrow H + CO_2$$

which is also believed to proceed through a collision complex.[21]

If complex formation occurs, equations (5) and (6) become

$$-\frac{d[HCO^\dagger]}{dt} = \left\{\left(\frac{k_a(f_0 k_{-a} + k_b)}{k_{-a} + k_b}\right)[NO] + k_1\,[(HCO)_2]\right\}[HCO^\dagger] \qquad (18)$$

$$\frac{d[HCO]}{dt} = \left\{\left(\frac{k_a f_0 k_{-a}}{k_{-a} + k_b}\right)[NO] + k_1[(HCO)_2]\right\}[HCO^\dagger] - k_R[HCO]\,[NO] \qquad (19)$$

where k_a is the bimolecular rate constant for complex formation, k_{-a} and k_b are unimolecular rate constants for dissociation of the complexes to

reactants and products, respectively, f_0 is the fraction of complexes which form HCO(0,0,0) upon redissociation, and f_1 is the fraction which form HCO(0,1,0). levels, $f_0 + f_1 = 1$. The additional energy brought into the complex by vibrationally excited reagents increases k_{-a} more than k_b since this process is nearer threshold. It should be noted that these expressions result in rate equations which have the same form as Eqs. (7) and (8) and do not change the relative rate constants for reaction and deactivation.

From these equations it can be seen that $f_0 = 1$ implies that the rate of $HCO^\dagger$ removal is equal to the rate of complex formation. For a sufficiently long-lived complex, this assumption is reasonable since the energy from the relatively high frequency radical vibrations will end up in the lower frequency bending and torsional modes before the complex dissociates. This argument also implies that all HCO vibrational levels should be removed with very nearly the same rate and that vibrationally excited DCO should be deactivated with comparable efficiency since isotopic substitution changes the collision rate by less than 2%. Unfortunately, the present experimental data does not give reliable information on the production of HCO(0,1,0) in collisions with NO. The DCO(0,0,0) production rate does support this conclusion.

In the following chapter additional experimental evidence which support complex formation between HCO(DCO) and NO or O_2 is presented. A simple RRKM model based on complex formation is also developed which quantitatively reproduces the experimental dependences of the reaction rate constants on isotope, pressure, temperature, and vibrational excitation.

References

1. R.J. Gordon, J. Chem. Phys. 74, 1676 (1981) and J.D. Lambert, Vibrational Relaxation in Gases (Clarendon, Oxford, 1977).
2. S.S. Miljanic, E. Specht, and C.B. Moore, J. Chem. Phys. 77, 4949 (1982), F.E. Hovis and C.B. Moore, J. Chem. Phys. 72, 2397 (1980), and T.G. Winter and H.E. Bass, J. Acoust. Soc. Am. 48, 1119 (1970).
3. P. Hess and C.B. Moore, J. Chem. Phys. 65, 2339 (1976).
4. G.D. Billing and L.L. Poulson, J. Chem. Phys. 68, 5128 (1978) and C.B. Moore and P.F. Zittel, Science 182, 541 (1973).
5. M. Kneba and J. Wolfrum, Ann. Rev. Phys. Chem. 31, 47 (1980) and references therein.
6. J.P. Reilly, J.H. Clark, C.B. Moore, G.C. Pimentel, J. Chem. Phys. 69, 4381 (1978).
7. V.A. Nadtochenko, O.M. Sarkisov, M.P. Frolov, R.A. R.A. Tsanava, and S.G. Cheskis, Kinet. Catal. USSR 22, 670 (1981).
8. A.O. Langford, H. Petek, and C.B. Moore, J. Chem. Phys. 78, 6650 (1983).
9. J.H. Clark, N.S. Nogar, and C.B. Moore, J. Chem. Phys. 68, 1264 (1978).
10. G. Herzberg and D.A. Ramsay, Proc. Roy. Soc. A 233, 34 (1955).
11. J.W.C. Johns, S.H. Priddle, and D.A. Ramsay, Disc. Far. Soc. 35, 90 (1963).
12. J.P. Reilly, J.H. Clark, C.B. Moore, and G.C. Pimentel, Advances in Laser Chemistry (Springer- Verlag, New York, 1978).

13. R. B. Vasudev and R.N. Zare, J. Chem. Phys. 76, 5267 (1982).

14. E.S. Yeung and C.B. Moore, J. Chem. Phys. 58, 3988 (1973).

15. C. J. Hochanadel, T. J. Sworski, and P. J. Ogren, J. Phys. Chem. 84, 231 (1980).

16. Estimated from group additivity rules. S.W. Benson, Thermochemical Kinetics, 2nd ed., (Wiley, New York, 1976).

17. C.B. Moore, J. Chem. Phys. 43, 2979 (1965).

18. I.M. Napier and R.G.W. Norrish, Proc. Roy. Soc. A 229, 337 (1967).

19. T.-L. Tso, M. Diem, and E.K.C. Lee, Chem. Phys. Lett. 91, 339 (1982).

20. T. Drier and J. Wolfrum, Eighteenth Symposium (International) on Combustion, The Combustion Institute, Pittsburgh, 1981, p. 801.

21. I.W.M. Smith, Chem. Phys. Lett. 49, 112 (1977).

TABLE III-1. Rate constants and cross-sections for vibrational relaxation of formyl radicals

Excited Molecule	Collision Partner	k (cm^3 $molec^{-1}$ s^{-1})	σ^a ($Å^2$)
HCO	$(HCO)_2$[b,c]	$(6.4 \pm 1.0) \times 10^{-12}$	1.2
	H_2CO[c]	$(3.0 \pm 0.5) \times 10^{-12}$	0.5
	He[c]	$(2.5 \pm 0.3) \times 10^{-13}$	0.018
	N_2[c]	$(2.5 \pm 0.8) \times 10^{-13}$	0.038
	NO[c,d]	$(3.4 \pm 0.4) \times 10^{-11}$	5.2
	O_2[c,d]	$(9.4 \pm 1.1) \times 10^{-12}$	1.5
DCO	D_2CO[c]	$(7.1 \pm 1.8) \times 10^{-13}$	0.11
	NO[c,d]	$(2.6 \pm 0.6) \times 10^{-11}$	3.9

[a] $\sigma = k/\bar{v}$, $\bar{v} = (8kT/\pi\mu)^{1/2}$.

[b] Data from HCO(0,1,0) decay.

[c] Data from HCO(0,0,0) formation.

[d] May include contribution from reactive removal.

FIG. III-1. Time dependence of HCO(0,1,0) absorbance at 18,138.4 cm^{-1} following excitation of 4.02 Torr $(HCO)_2$. 256 laser shots (~ 10 mJ/cm^2) were averaged. The solid line corresponds to an appearance rate of 3.32 x 10^6 s^{-1}, and a decay rate of 8.61 x 10^5 s^{-1}.

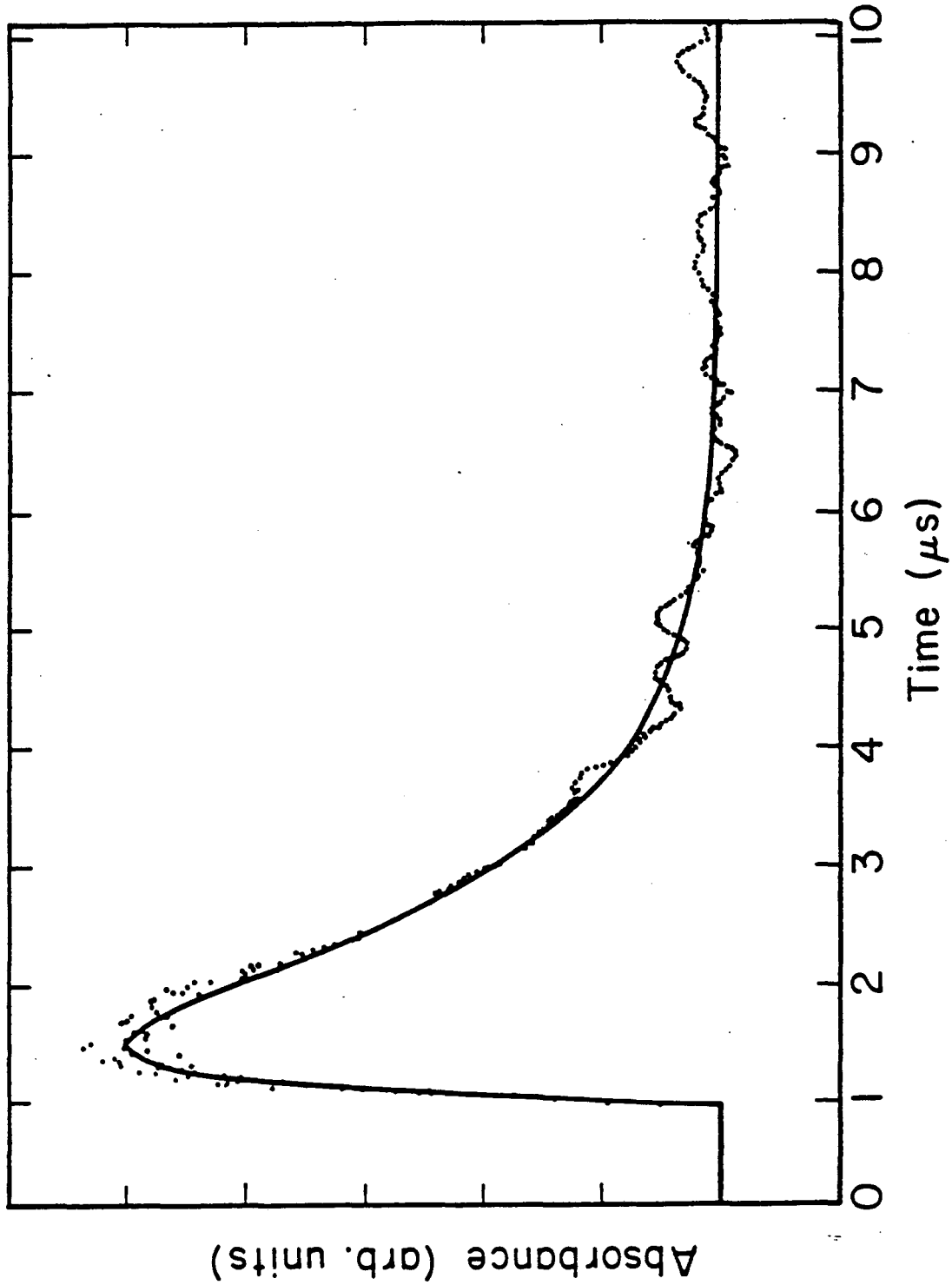

Fig. III-1

FIG. III-2. Time dependence of HCO(0,0,0) absorbance at 16,262.25 cm^{-1} following excitation of 4.05 Torr $(HCO)_2$. 64 laser shots (~ 10 mJ/cm^2) were averaged. The solid line corresponds to $K_f = 5.0 \times 10^7\ s^{-1}$ and $K_s = 8.05 \times 10^5\ s^{-1}$.

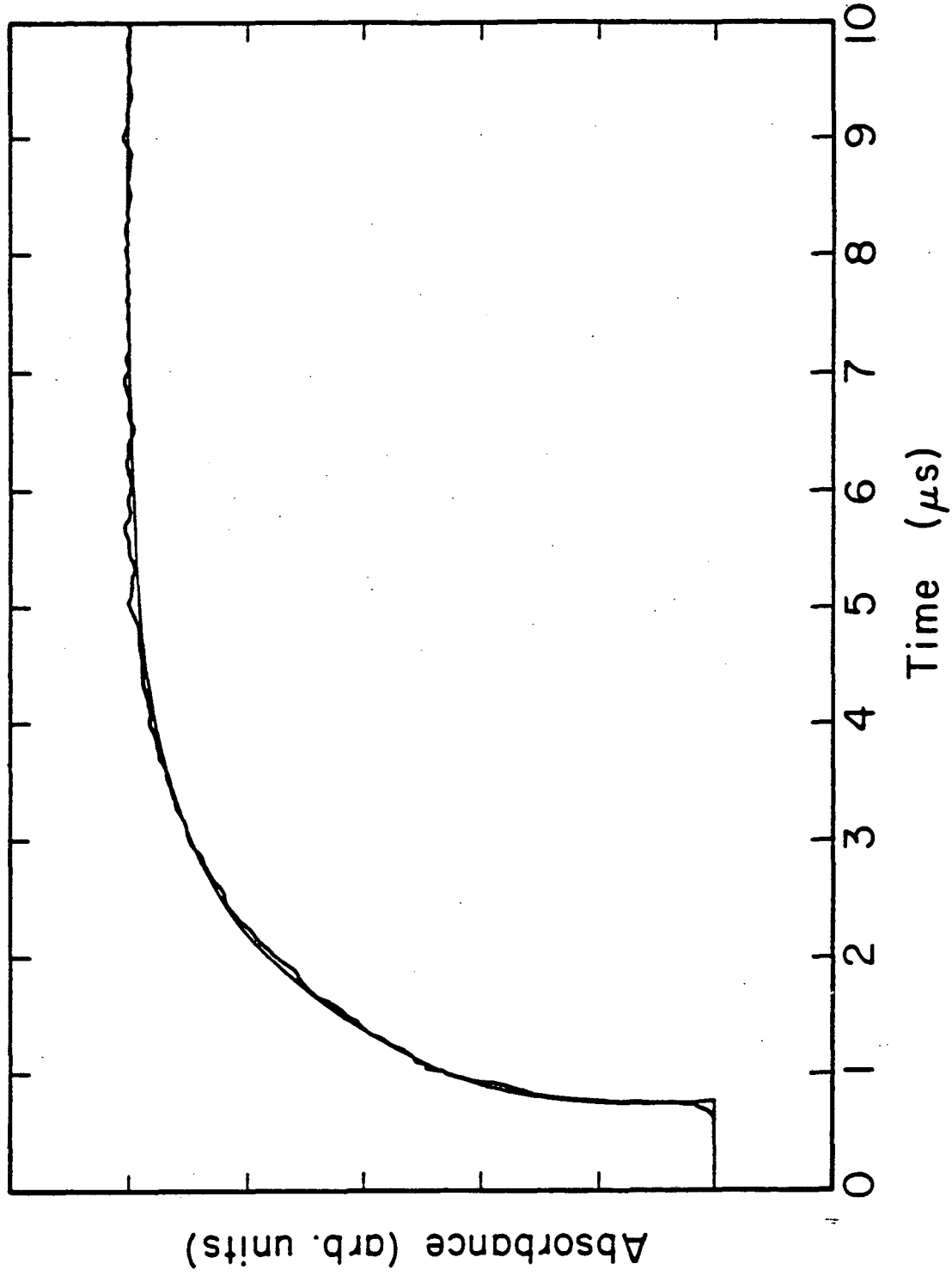

Fig. III-2

FIG. III-3. Pseudo-first-order appearance (□) and decay (●) rates for HCO(0,1,0), and appearance rates for HCO(0,0,0) (10,1 (△) and 2,1 (○) rotational levels) as a function of glyoxal pressure. The solid lines correspond to the rate constants given in Table III-1 and the text.

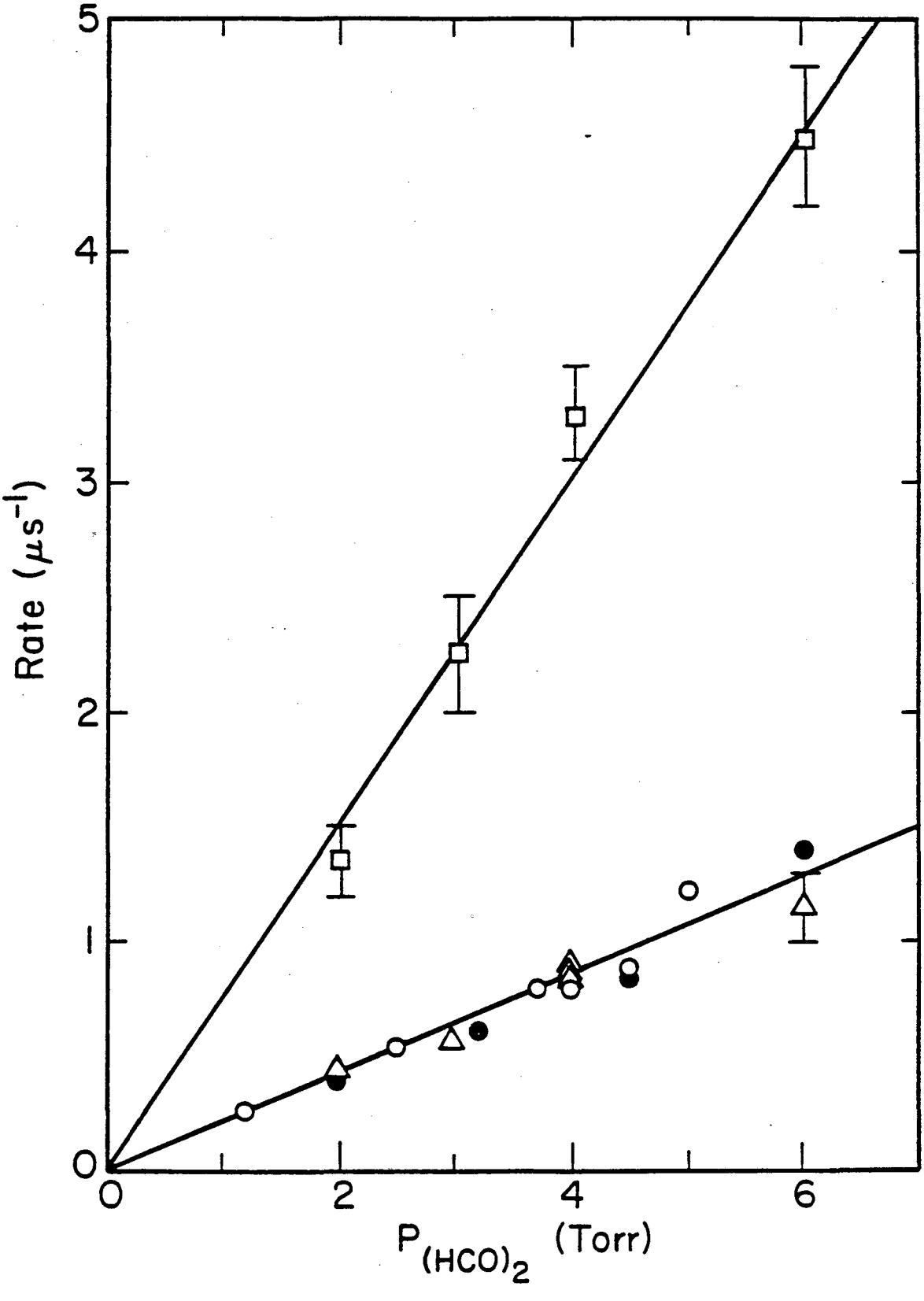

Fig. III-3

FIG. III-4. Pseudo-first-order HCO(0,0,0) appearance rates as a function of He (O) and N_2 (△) pressure. The glyoxal pressure is 4.0 Torr. The solid lines correspond to the rate constants given in the text and Table III-1.

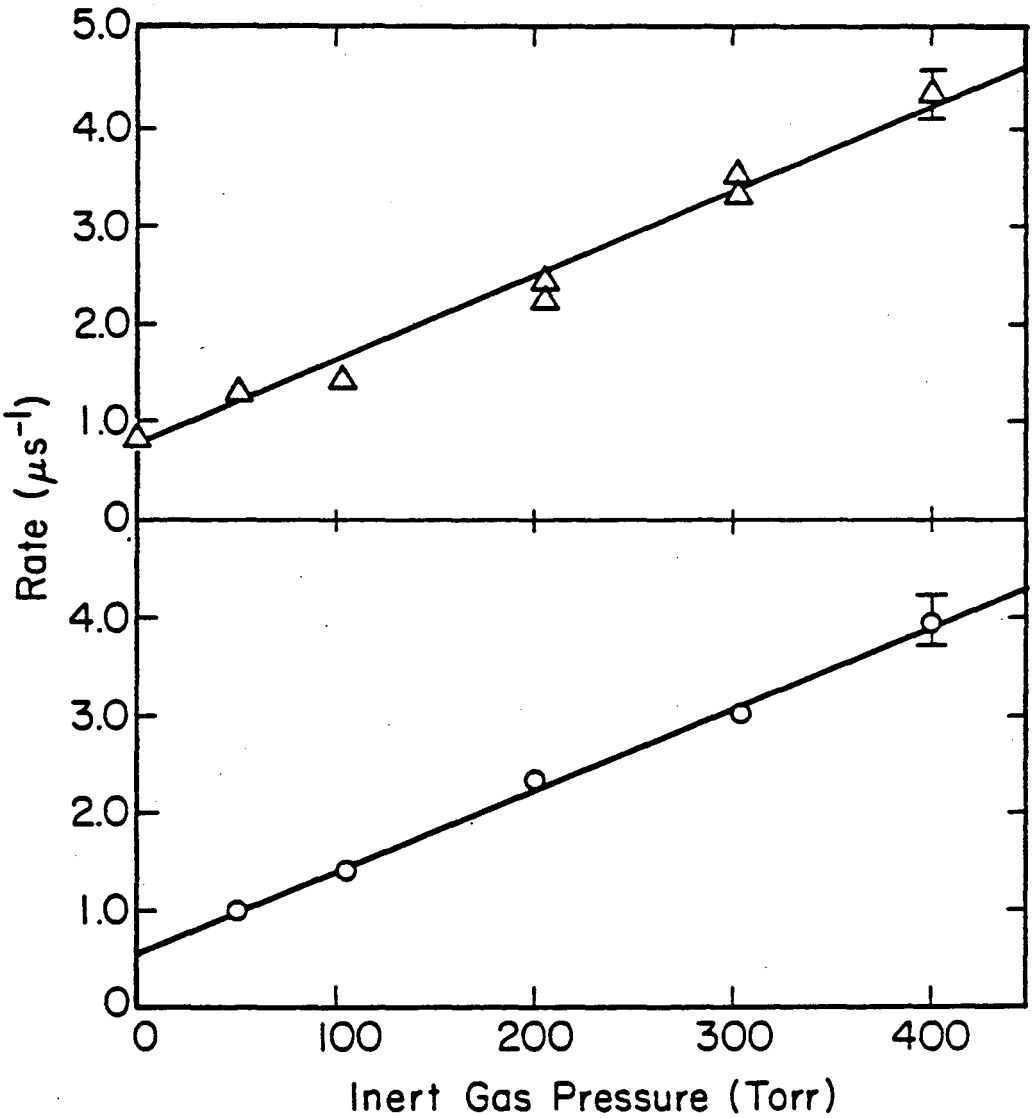
5.0
4.0
3.0
2.0
1.0
0
Rate (μs^{-1})
4.0
3.0
2.0
1.0
0
0
100
200
300
400
Inert Gas Pressure (Torr)

Fig. III-4

FIG. III-5. Pseudo-first-order HCO(0,0,0) appearance rates as a function of NO (△) and O_2 (○) pressure. The glyoxal pressure is 4.0 Torr. The solid lines correspond to the rate constants given in Table III-1 and the text.

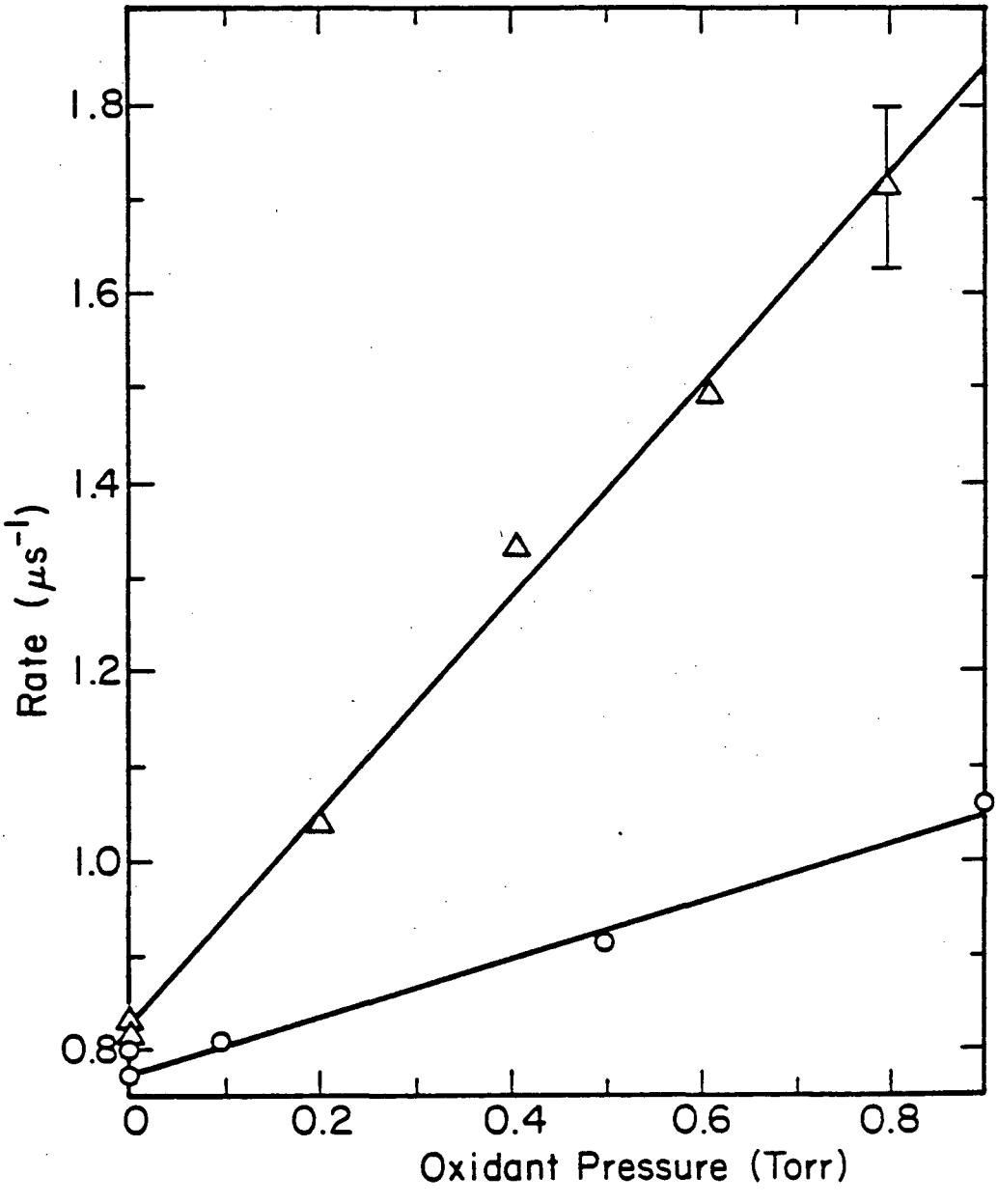

Fig. III-5

FIG. III-6. Relative amplitudes of the slow and fast HCO(0,0,0) rises as a function of NO (△) and O_2 (○) pressure. See text for details.

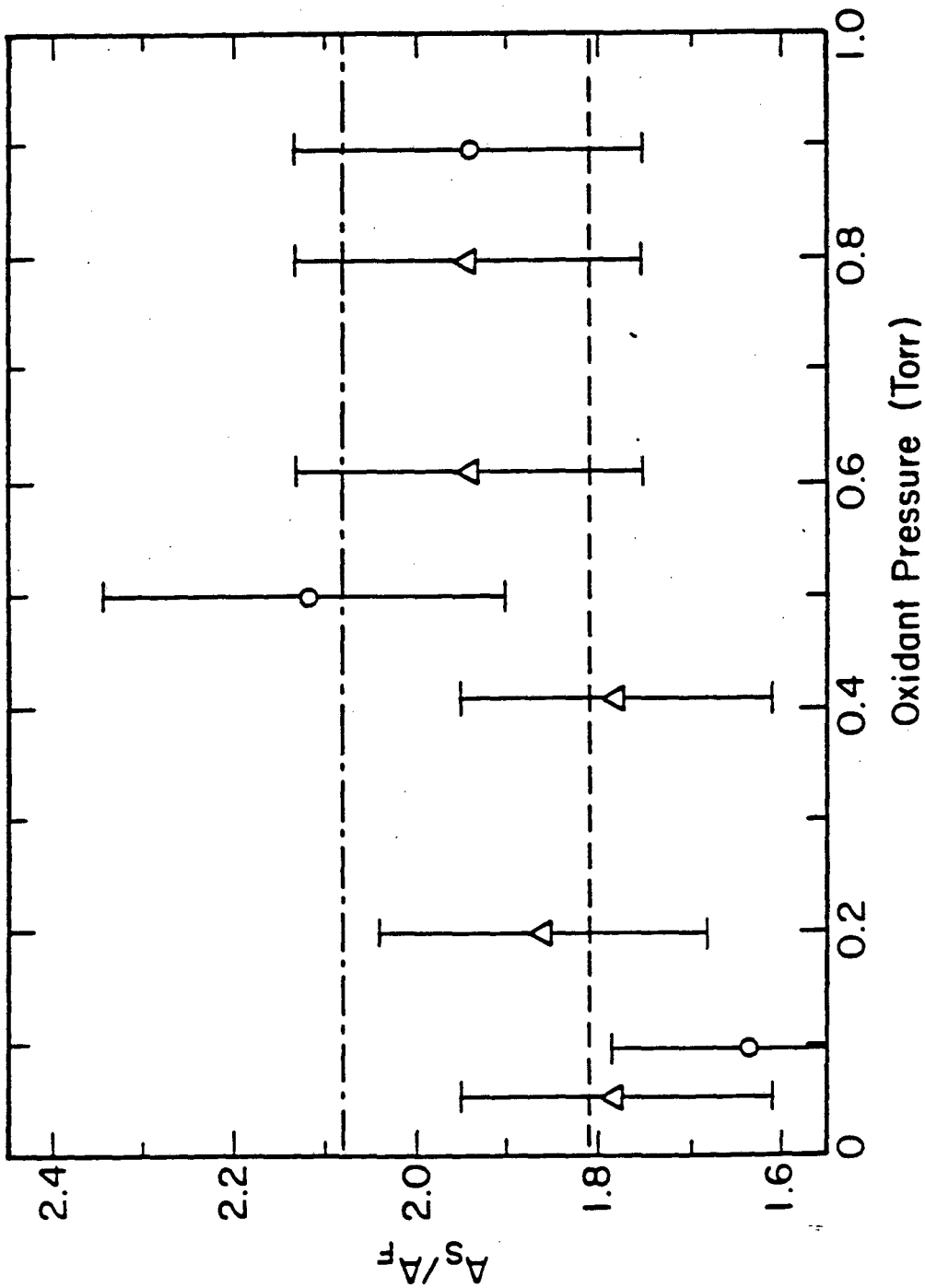

Fig. III-6

FIG. III-7. HCO vibrational levels energetically accessible following $(HCO)_2$ photolysis at 308 nm (92.8 kcal mol^{-1}). The heats of formation for $(HCO)_2$ and HCO are assumed to be - 58 and 8 kcal mol^{-1}, respectively.

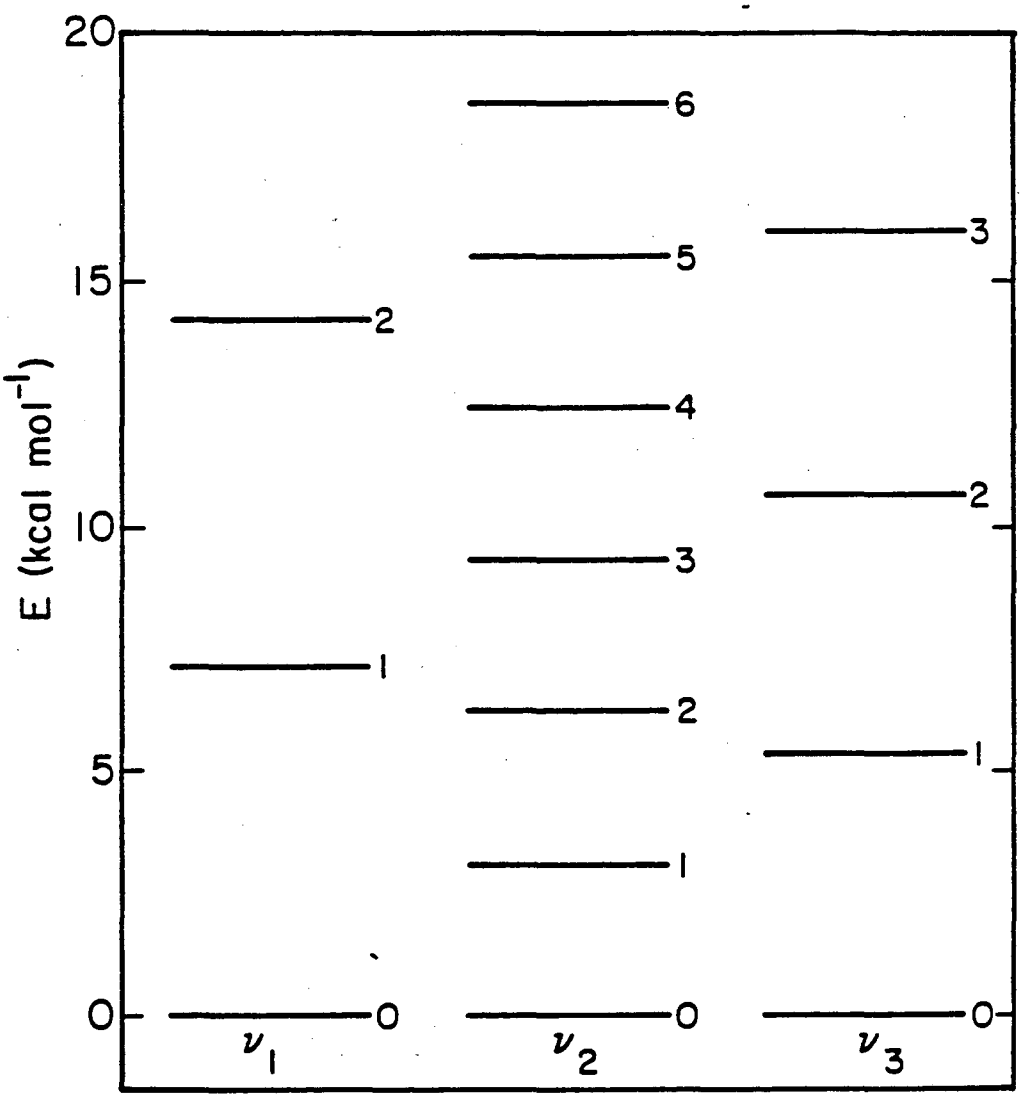

Fig. III-7

CHAPTER IV. COLLISION COMPLEX FORMATION IN THE REACTIONS OF FORMYL RADICALS WITH NITRIC OXIDE AND OXYGEN

A. INTRODUCTION

The oxidation of formyl radicals is an important process in hydrocarbon combustion systems.[1] In the atmosphere, reaction (1) is also a major source of hydroperoxy radicals which contribute to the formation of photochemical smog.[2]

$$HCO + O_2 \rightarrow HO_2 + CO \ . \qquad (1)$$

Absolute rate constants for HCO removal by O_2 have been measured[4-8], and the production of HO_2 has been verified spectroscopically.[9] It is generally agreed that HO_2 and CO are the only significant products. The most straightforward reaction mechanism is a direct hydrogen abstraction. The reaction

$$HCO + NO \rightarrow HNO + CO. \qquad (2)$$

behaves in a similar way.[4-7]

In the preceding chapter the formation of collision complexes between HCO and O_2 or NO was proposed to explain the rapid deactivation of vibrationally excited HCO and DCO by these species. The possibility of adduct formation in reaction (1) has been debated for many years. The pressure independence of the rate constant between 5 and 500 Torr[4,7] has been cited as evidence that adduct formation is unimportant in both reactions. The pressure independence of rate constants implies only that most of the adducts which are formed dissociate to products or to the original reactants before being stabilized. Evidence for complex formation in (1) is supplied by recent reports of absorption features

assigned to $HCOO_2$ following the photolysis of H_2CO in a solid low-temperature O_2 matrix.[10,11] HCONO formation in the gas phase has also been reported.[12] Adduct formation in both reactions is consistent with the decrease in reaction rate constants with increasing temperature between 300 and 500 K.[7]

In this paper, absolute rate constants for the removal of ground state HCO and DCO through collisions with NO and O_2 have been measured at 295 K. Deuteration was found to increase the reaction rates, contrary to predictions based on hydrogen abstraction.[13] RRKM calculations[14] based on a collision complex model semi-quantitatively reproduce the reaction rate constants, the vibrational relaxation rates, the decrease in rate constant with HCO vibrational excitation, and the kinetic isotope effects suggesting that collision complexes are formed in both reactions. The calculations also reproduce the experimental temperature dependences of Ref. 7 and are used to estimate rate constants for these reactions in the temperature ranges 228-300 K and 500-1500 K where experimental results are unavailable.

B. EXPERIMENTAL

Most of the details relevant to the present experiments are in the preceding chapters.Two optical configurations were used. In the experiments with formaldehyde as the radical precursor, the multipass configuration described in Chap. II and Ref. 15 was used. The 2 mm diameter probe beam was passed 9 times through the 7 mm x 25 mm area swept out by the photolysis beam. The typical excimer laser fluence entering the sample in these experiments was 10 mJ/cm^2. In later

experiments with glyoxal as the radical precursor, the probe beam made a single pass through the cylindrical photolysis volume defined by 5 mm diameter apertures. Typical laser fluences in these experiments were 10-15 mJ/cm^2. All measurements were made at an ambient temperature of 295 ± 2K.

C. RESULTS AND ANALYSIS

1. Formaldehyde Photolysis

Since photodissociation of H_2CO at 308 nm produces hydrogen atoms as well as ground state and vibrationally excited formyl, a complete kinetic analysis must consider the following processes:[5]

$H_2CO + h\nu$	→	$H_2 + CO$		(3a)
	→	$H + HCO$		(3b)
	→	$H + HCO^\dagger$		(3c)
$HCO^\dagger + H_2CO$	→	$HCO + H_2CO$	3.0×10^{-12} [10]	(4)
$HCO^\dagger + NO$	→	$HCO + NO$	3.4×10^{-11} [10]	(5)
$HCO^\dagger + O_2$	→	$HCO + O_2$	9.4×10^{-12} [10]	(6)
$H + H_2CO$	→	$H_2 + HCO$	4.4×10^{-14} [16]	(7)
$H + HCO$	→	$H_2 + CO$	1.2×10^{-10} [17]	(8)
$HCO + HCO$	→	$H_2CO + CO$	2.3×10^{-11} [17]	(9)
$H + NO + M$	→	$HNO + M$	4.5×10^{-31} [5,18,19]	(10)
$H + O_2 + M$	→	$HO_2 + M$	4.5×10^{-31} [5,18,19]	(11)
$H + HNO$	→	$H_2 + NO$	1×10^{-11} [20]	(12)
$H + HO_2$	→	$OH + OH$		
	→	$H_2 + O_2$	3×10^{-11} [21] .	(13)
	→	$H_2O + O$		

The rate constants for reactions (10) and (11) are in cm^6 $molec^{-2}$ s^{-1}; others are in cm^3 $molec^{-1}$ s^{-1}; references are noted in brackets. $HCO^\dagger$ refers to all vibrationally excited formyl, approximately 20% of the radicals formed by photolysis of H_2CO at 308 nm.[10] Vibrational relaxation will be 95% complete within 5 μs for 3.20 Torr H_2CO and 0.30 Torr NO.

The experimental conditions were chosen to minimize the effects of reactions (7)-(13). Of these reactions, only (8) and (9) compete with (1) or (2) for the removal of HCO. The rectangular photolysis configuration was used in the H_2CO (and D_2CO) experiments. From the typical laser fluence of 10 mJ/cm^2, the radical quantum yield of 0.6,[22] and the absorption coefficient of $(3.2 \pm 0.4) \times 10^{-4}$ cm^{-1} $Torr^{-1}$ at 308 nm (based on measured attenuation of the excimer beam), the initial HCO concentration from 3.20 Torr H_2CO is estimated as 9×10^{12} cm^{-3}. At the lowest oxidant concentrations (0.3 Torr NO and 1.0 Torr O_2), reactions (8) and (9), respectively, will be 100 and 250 times slower than (1) or (2), immediately after the photolysis pulse, and negligible after 5 μs. This is illustrated by the single exponential decay of HCO following irradiation of 3.20 Torr H_2CO and 0.30 Torr NO shown in Fig. IV-1.

In the absence of other channels, reaction (7) will slowly convert the hydrogen atoms to HCO and the radical decay will deviate from a single exponential on long timescales. Fig. IV-1 demonstrates that this process is not important under the experimental conditions. The resolvable rise of HCO on short timescales in Fig. IV-1 is clearly too fast for reaction (7) and is attributed to the relaxation processess (4)

and (5). Reactions (8) and (10)-(13) will compete with (7) for the hydrogen atoms, but the combined rates of these reactions will be less than 35% of the rate of (7) (4450 s^{-1} at 3.2 Torr H_2CO). A more important loss mechanism for hydrogen atoms is diffusion from the photolysis region.

In the rectangular photolysis geometry, the center of the probe beam is only 3.0 mm from the edge of the photolysis volume. At a total pressure of 3.5 Torr, HCO radicals will diffuse this distance in approximately 2 ms while hydrogen atoms require only 75 μs. Approximate pseudo-first-order rate constants for loss of HCO and H by diffusion are calculated to be 450 s^{-1} and 1.3×10^4 s^{-1}. Diffusion will clearly be the primary mechanism for hydrogen removal (>65%), but a negligible (<0.5%) source of HCO loss.

2. Glyoxal Photolysis

As a check on the validity of neglecting reactions (7)-(9), additional experiments were performed with glyoxal as the radical precursor. The cylindrical photolysis geometry was used in these experiments. The decay of HCO produced in the photolysis of 4.05 Torr $(HCO)_2$ with 0.052 Torr and NO and 1,000 Torr N_2 is shown in Fig. IV-2. The vibrational relaxation time is too short to resolve on this timescale. The decay is fit quite well as a single exponential.

Estimating the glyoxal heat of formation as -58 kcal mol^{-1} [23], the following processes are energetically possible at 308 nm:

$$(HCO)_2 + h\nu \rightarrow H_2 + CO + CO + 88 \text{ kcal mol}^{-1} \quad (14a)$$

$$\rightarrow H_2CO + CO + 88 \text{ kcal mol}^{-1} \quad (14b)$$

$$\rightarrow HCO + HCO + 19 \text{ kcal mol}^{-1}. \quad (14c)$$

Dissociation to H + CO + HCO is thermoneutral at this wavelength and

should be negligible. End product analysis studies by Calvert and Layne[24] indicate that all of the excited glyoxal molecules dissociate following near uv excitation. These workers found quantum yields of 0.13 and 1.2 for H_2 and CO, respectively, at 313 nm. The negligible temperature dependence of these quantum yields led to the erroneous conclusion that no HCO radicals were produced in the photolysis since these were presumed to lead to the (temperature dependent) chain process

$$\begin{aligned} HCO &\rightarrow H + CO \\ H + (HCO)_2 &\rightarrow H_2 + HCOCO \\ HCOCO &\rightarrow HCO + CO \ . \end{aligned}$$

HCO may be removed through reaction (9) instead,[22] and thus (14b) and (14c) yield the same final products. The present experiments suggest that HCO is a direct photoproduct, a reasonable expectation considering the excess energy.

Neglecting (14c) implies quantum yields of 0.15 and 0.85 for (14a) and (14b), respectively. If the HCO products recombine to form H_2CO and CO instead of dissociating, it can then be inferred that $\Phi(14b) + \Phi(14c) = 0.85$. An approximate value for $\Phi(14c)$ can be obtained by comparing the radical signals following H_2CO and $(HCO)_2$ photolysis. The absorption coefficient of glyoxal at 308 nm was determined to be $(1.0 \pm 0.1) \times 10^{-3}$ cm^{-1} $Torr^{-1}$ by direct measurement with the excimer laser. The absorption coefficient at 308 nm should be very similar to that at 313 nm since the absorption is only weakly structured. When 5.00 Torr $(HCO)_2$ was irradiated with 11 mJ/cm^2 of 308 nm, the single shot HCO absorbance at 16,263.50 cm^{-1} (85 cm pathlength) was 1.76%. The excited glyoxal density is calculated to be 6.9×10^{13} cm^{-3}. Using $\sigma_{HCO} = (3.6 \pm 1.6) \times 10^{-18}$ cm^2 from Ref. 10, the radical quantum yield is 0.8 ± 0.4 and $\Phi(14c) = 0.4$

± 0.2 which implies a typical radical density of 4.5×10^{13} cm^{-3} from 4.0 Torr $(HCO)_2$.

3. Rate Constants

The pseudo-first-order rate constants obtained from exponential analysis of the formaldehyde and glyoxal data are given in Figs. IV-3 and 4. The uncertainties for individual decay rates are ± 10%. The bimolecular rate constants corresponding to these rates are shown as a function of oxidant pressure in Figs. IV-5 and 6. Similar rate constants were obtained with glyoxal and formaldehyde precursors supporting the validity of neglecting reactions (7) and (8) in the analysis of H_2CO data. The assumptions given above for H_2CO are extended to D_2CO photolysis. Rate constant measurements were made at total pressures up to 1000 Torr (N_2) in the quartz reaction cell. High pressure measurements were made only with the glyoxal precursor. The rates for both reactions were found to be independent of pressure to within ±15% over this range. The average rate constants obtained from these data are $(4.65 \pm 0.6) \times 10^{-12}$ and $(1.26 \pm 0.2) \times 10^{-11}$ cm^3 $molec^{-1}$ s^{-1} for reactions (1) and (2), respectively, and $(5.1 \pm 0.7) \times 10^{-12}$ and $(1.56 \pm 0.2) \times 10^{-11}$ cm^3 $molec^{-1}$ s^{-1} for the corresponding DCO reactions.

4. Error Estimates

The quoted uncertainties (±15%) correspond to two standard deviations in the averages of the bimolecular rate constants. The kinetic isotope effects (k_H/k_D) for reactions (1) and (2) are 0.91 ± 0.17 and 0.81 ± 0.14, respectively. Possible errors from the data analysis or pressure uncertainties should lie well within these limits. The potential sources of error in the data analysis arise from the validity of assuming pseudo-first-order decays. Although the pressure

measurements are accurate to within < 1%, potential uncertainties due to reactant depletion or product buildup during the photolyses must be considered. The photolysis volume was approximately 5% of the total cell volume; if one oxidant molecule is removed for each HCO produced, less than 3% of the NO or O_2 molecules in the cell is converted to products over the course of 512 laser shots. Although at low O_2 pressures (<0.3 Torr) the pseudo-first-order rate constant did decrease in formaldehyde mixtures (approximately 20%) when the mixture was irradiated for several hundred laser shots, no decrease was observed for oxygen pressures in excess of 1.0 Torr.

Photodissociation of H_2CO/O_2 mixtures results in the formation of a white particulate which diffuses out of the probe beam between laser shots at low pressure and eventually forms a powdery deposit on the cell walls. At pressures greater than 100 Torr, these particles are confined to the photolysis region where they scatter the probe beam and raise the baseline to as much as 50% of the absorption maximum. Baseline changes did not occur during the experimental runs with 1000 Torr N_2 when glyoxal was used as the radical precursor. Wall deposits were formed with $(HCO)_2$ when CH_4 was used as the buffer gas.

5. Comparison to Previous Experiments

The absolute rate constants obtained for reactions (1) and (2) in the present study are compared to literature values in Table IV-1. The values of k_2 obtained in three previous studies are in excellent agreement with the present result. Although Shibuya et al.[4] reported a value approximately 30% lower, four independent studies indicate that $k_2 \approx (1.2 \pm 0.2) \times 10^{-11}$ cm^3 molec^{-1} s^{-1}. Such good agreement is expected since these results were obtained using similar techniques which

monitored photolytically generated HCO via the visible $\tilde{A} \leftarrow \tilde{X}$ absorption. It is surprising that the values of k_1 obtained by the same methods range from 3.7 to 5.6 x 10^{-12} $cm^3 molec^{-1} s^{-1}$. Uncertainties in the radical-radical rate constants used for kinetic modelling in the intracavity experiments should affect rate constants for both reactions. The wide variation in k_1 may be due to the complicated nature of formaldehyde photooxidation.[26] When static mixtures were repeatedly photolyzed (irradiating the entire vessel with a broadband flashlamp) by Veyret and Lesclaux,[7] a shot-to-shot decrease in the first-order rate constant, k_1 $[O_2]$ was observed and attributed to depletion of oxygen through chain reactions initiated by HO_2 addition to H_2CO.[26] The particulate observed in the H_2CO/O_2 photolyses is presumed to be a product of this chain. The formaldehyde-to-oxygen ratios were kept small in the present experiments to minimize chain reactions. The absence of the particulate in $(HCO)_2$ photolyses suggests that similar chain reactions are not important in that system. The source of the 20% discrepancy between the values of k_1 determined in the present study and those reported by Shibuya et al. and by Veyret and Lesclaux remains unclear.

D. MECHANISM

The inverse kinetic isotope effects provide another indication that reactions (1) and (2) are not simple hydrogen abstractions. The formation of HCONO or $HCOO_2$ adducts in (1) and (2) can explain much of the unusual behavior which has been observed for these reactions. A similar mechanism has been proposed for the reaction

$$OH + CO \rightarrow H + CO_2$$

where potentially stable HOCO radicals may be formed.[27] As in this reaction[28], collision complex formation in (1) and (2) satisfies adiabatic correlation requirements. Simple bonding pictures[29,30] indicate that the ground states of HCONO and $HCOO_2$ are $^1A'$ and $^2A''$ respectively (C_s symmetry group). The $^2A''$ ground state of $HCOO_2$ is verified by ab initio calculations of Winter et al.[30] These states correlate with the appropriate reactants HCO ($^2A'$) + NO ($^2\pi_u$) or HCO ($^2A'$) + O_2 ($^3\Sigma_g^-$), and products HNO ($^1A'$) + CO ($^1\Sigma_g^+$) or HO_2 ($^2A''$) + CO ($^1\Sigma_g^+$).

1. Kinetic Scheme

The basic features of the collision complex mechanism are illustrated schematically for reaction (2) in Fig. IV-7. Here k_a and k_c are the bimolecular rate constants for complex formation and stabilization respectively, while k_{-a} and k_b are the unimolecular rate contants for dissociation of the complexes to reagents and products. The following treatment assumes that randomization of the internal energy of the complex is much faster than any of the other processes. If the complex dissociation rates are much faster than the formation rate (k_b, $k_{-a} >> k_a[NO] \cong 10^6\ s^{-1}$), the excited adduct concentration will reach steady state and the following expression for the rate of HCO removal is obtained:

$$\frac{d[HCO]}{dt} = -k_a \left(\frac{k_b + k_c[M]}{k_{-a} + k_b + k_c[M]}\right) [HCO]\ [AB] \qquad (15)$$

$$= -k_{exp}[HCO]\ [AB] \qquad AB = NO,\ O_2\ .$$

This implies that the experimentally observed rate constant is the

product of two terms: the rate constant for complex formation, k_a, and that fraction of complexes which do not redissociate to reagents.

At low pressures, Eq. (15) gives

$$k_{exp} = k_a\left(\frac{k_b}{k_{-a} + k_b}\right) \qquad (16)$$

The quantity in parentheses will be referred to below as the forward reaction efficiency (FRE). If the transfer of vibrational energy among the vibrational modes of the complex is fast, then k_a is equal to the rate constant for removal of vibrationally excited HCO. The forward reaction efficiency is therefore simply the ratio of the experimental rate constants for reaction and vibrational relaxation. The rate constants for removal of HCO(0,1,0) by NO and O_2 were determined to be $(3.4 \pm 0.4) \times 10^{-11}$ and $(9.4 \pm 1.1) \times 10^{-12}$ cm^3 $molec^{-1}$ s^{-1}, respectively.[11] The corresponding HCO(0,0,0) reaction rate constants of $(1.26 \pm 0.2) \times 10^{-11}$ and $(4.65 \pm 0.6) \times 10^{12}$ therefore imply reaction efficiencies of 0.37 ± 0.07 and 0.49 ± 0.09 for reactions (2) and (1), respectively.

Randomization of the internal energy of the complex implies that k_b and k_{-a} (and hence the forward reaction efficiency) can also be calculated through RRKM or other statistical theories. RRKM calculations based on a similar kinetic model were used by Olmstead and Brauman[14] to successfully treat complex formation in ion-molecule reactions. The RRKM expressions for the rate constants k_{-a} and k_b at a given energy E are:[31]

$$k_{-a}(E) = G_A\,(E-E_o) \,/\, hN(E) \qquad (17)$$

$$k_b(E) = G_B\,(E-E_o')\,/\,hN(E) \qquad (18)$$

$G_A(E-E_o)$ and $G_B(E-E_o')$ are the sums of internal vibrational and rotational states for transition states A and B respectively, while N(E) is the density of states for the collision complex. The forward reaction efficiency at a fixed energy E is

$$\frac{k_b(E)}{k_{-a}(E) + k_b(E)} = \frac{G_B(E-E_o'-\Delta E_{rot})}{G_A(E-E_o) + G_B(E-E_o'-\Delta E_{rot})} \qquad (19)$$

where ΔE_{rot} is a correction to the energy available for internal excitation required by the conservation of angular momentum, since the moments of inertia will be different for the complex and the two transition states. This correction is given by[32]

$$\Delta E_{rot} = (1 - I_B/I_A)\,kT \qquad (20)$$

where I_A and I_B are the moments of inertia ($I = (I_b I_c)^{1/2}$) for the adiabatic rotations corresponding to orbital motion of transition states A and B, respectively. The rotations corresponding to torsional motion (I_a) are treated as active. It can be seen from Eq. (20) that less energy will be constrained to overall rotations in the passage through the loose transition state to reactants than through the tight transition state to products.

Eq. (19) assumes that all complexes have the same internal energy. Since the complexes are formed by chemical activation, the internal energy will actually be characterized by a distribution function[31]

$$\frac{G_A(E-E_o)\ e^{-E/kT}}{\int_{E_o}^{\infty} G_A(E-E_o)e^{-E/kT}dE} \tag{21}$$

Combining (17), (18), (19), and (21), a final expression for the forward reaction efficiency is obtained

$$\frac{\int_{E_0}^{\infty} \frac{G_B(E-E_o'-\Delta E_{rot})\ G_A(E-E_o)e^{-E/kT}}{G_A(E-E_o) + G_B(E-E_o'-\Delta E_{rot})}\,dE}{\int_{E_o}^{\infty} G_A(E-E_o)\ e^{-E/kT}dE} \tag{22}$$

This equation can be evaluated only if the vibrational frequencies and moments of inertia for the two transition states, and the difference in barrier heights, $\Delta E_o = E_o - E_o'$, are known. In the following section, the estimation of transition state vibrational frequencies is described.

2. Transition States

Since reactions (1) and (2) have negative temperature dependences, there is no significant activation barrier in the entrance channel for complex formation. The transition state is therefore located at the centrifugal barrier which results from the relative orbital motion of the reagents. Only those collision pairs which approach sufficiently closely for the long-range dipole-induced dipole attractive force to overcome this barrier will form complexes.[32,23] The average separation of the collision pairs in the transition state is estimated as the distance at which the centrifugal and attractive forces are equal.

$$\frac{\partial}{\partial\rho}\left(\frac{E_{rot}}{\rho^2}\right) = \frac{\partial}{\partial\rho}\left(-\frac{2}{\rho^6}\right) \qquad \rho = r/r_o \tag{23}$$

$$\rho_{TSA} = \left(\frac{r_{TSA}}{r_o}\right) = \left(\frac{6D_o}{RT}\right)^{1/6}$$

In these expressions, D_o is the dissociation energy (at 0 K) and r_o is the average length of the new bond which is formed.[23] D_o differs from E_o only by the zero-point energy of the complex. E_{rot} is the average rotational energy of the transition state, assumed to be 0.6 kcal mol^{-1} (RT) at 300 K. The C-N and C-O covalent bond lengths are assumed to be 1.47 and 1.43 Å,[23,33] respectively. The potential well depths for $HCOO_2$ and HCONO are estimated by analogy to known species such as CH_3NO and CH_3O_2 using thermochemical data from the appendices of Ref. 23.

$$CH_3 + NO \rightarrow CH_3NO \qquad \Delta H = -40 \text{ kcal mol}^{-1}$$
$$CH_3 + O_2 \rightarrow CH_3O_2 \qquad \Delta H = -28 \text{ kcal mol}^{-1}.$$

Estimating the relative strengths of bonds formed by HCO and CH_3 from

$$CH_3 + CH_3 \rightarrow C_2H_6 \qquad \Delta H = -89 \text{ kcal mol}^{-1}$$
$$CH_3 + HCO \rightarrow CH_3HCO \qquad \Delta H = -82 \text{ kcal mol}^{-1},$$

leads to the following estimated enthalpy changes for HCONO and $HCOO_2$:

$$HCO + NO \rightarrow HCONO \qquad \Delta H = -33 \text{ kcal mol}^{-1}$$
$$HCO + O_2 \rightarrow HCOO_2 \qquad \Delta H = -21 \text{ kcal mol}^{-1}.$$

The bond dissociation energies at 0 K are taken to be 37 and 25 kcal mol^{-1} for HCONO and $HCOO_2$, respectively. The calculated transition state

bond lengths are very insensitive to these energies because of the one-sixth power dependence in Eq. (23). The average center of mass separation calculated from these quantities is 4.0 Å for HCO-NO and 3.6 Å for $HCO-O_2$. The transition state A geometries were then obtained from the collision complex geometries (described below) by stretching the C-N or C-O bonds to the lengths proscribed by the calculated center of mass separations.

At 3 to 4 Å, the coupled reagents will interact only weakly and the new internal modes will be very low frequency vibrations or internal rotations. The four high frequency vibrations of transition state A were taken to be those of the separated reagents. The four remaining low frequency modes were chosen such that the transition state theory expression for the complex formation rate constant (= the vibrational relaxation rate constant)

$$k_a(T) = \left(\frac{kT}{h}\right)\left(\frac{g_p}{g_r}\right)\frac{Q^{\neq}_{HCOAB}}{Q_{HCO}\,Q_{AB}}\,e^{-\Delta\varepsilon^{\neq}_o/kT} \qquad (24)$$

reproduced the experimental value. The electronic degeneracy factor (g_p/g_r) is required since not all of the collisions form stable complexes. The reactants in (1) correlate with $^4A''$ states in addition of the $^2A''$ ground state of $HCOO_2$. The degeneracy factor for this reaction is therefore one-third. The reactants in (2) correlate with $^1A''$, $^3A''$, and $^3A'$ states as well as the $^1A'$ ground state of the complex which leads to a factor of one-eigth. For reaction (2), Eq. (24) reproduced the experimental value of k_a when free rotations were used for the four remaining internal modes. For reaction (1), better agreement was obtained when the free internal rotations were replaced by very low

frequency vibrations. These frequencies are shown in Table IV-2.

The dissociation of $HCOO_2$ and HCONO to products is analogous to the process:

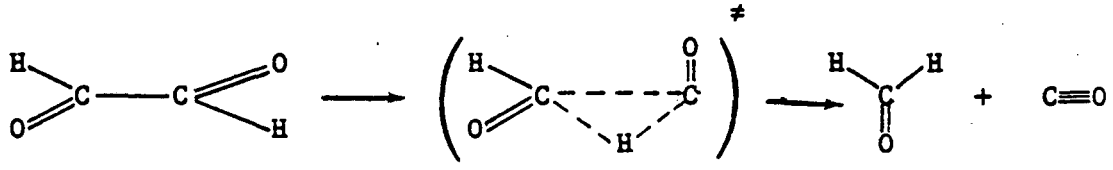

Vibrational frequencies and geometries for the transition state in this reaction have recently been calculated by Osamura et al.[34] These were used to model transition state B for reactions (1) and (2). Vibrational frequencies for the deuterated transition state were estimated from comparison to $(DCO)_2$ and by use of the Teller-Redlich product rule.[35] The parameters for transition state B are given in Table IV-3.

3. Calculations

The sums and densities of states in Eq. (22) were calculated semiclassically[31] and the integrals were evaluated numerically using a program based on that of Hase and Bunker.[14,36] The calculated reaction efficiencies for various barrier height differences are shown in Table IV-4. The best agreement with the experimental HCO reaction efficiencies was found for ΔE_o = 9.0 and 8.0 kcal mol^{-1} for reactions (1) and (2), respectively. At a given barrier height, the calculated reaction efficiencies are relatively insensitive to the high frequency vibrations of the transition states. The most critical parameters are the low frequency vibrations (and free rotations) of transition state A. For example, changing the low frequency vibrational modes of transition state A (reaction (1)) from 200, 105, 65, and 25 cm^{-1} to 250, 135, 80, and 40 cm^{-1} increases the reaction efficiency for ΔE_o = 9.0 kcal mol^{-1} by 40% (0.49 to 0.69). The experimental reaction efficiency is reproduced for

ΔE_o = 7.0 kcal mol^{-1} with these parameters.

For DCO reactions, the relative heights of the barriers to products and reactants were corrected for the differences in zero-point energies between transition states. The inverse isotope effect is largely due to the difference in available energy that results from this correction. The complex formation rate constants were assumed to be identical for HCO and DCO since the difference in masses changes the collision rate by only 2%. The unusual direction of the experimental isotope effects is reproduced in the calculations.

The calculated reaction rates for vibrationally excited HCO are less than the ground state reaction rates, also in agreement with experiment. The addition of 1083 cm^{-1} of vibrational energy to the complex decreased the calculated reaction efficiencies for (1) and (2) from 0.49 and 0.37 to 0.21 and 0.14, respectively. The corresponding rate constants of 2 x 10^{-12} and 4.8 x 10^{-12} cm^3 $molec^{-1}$ s^{-1} for reaction of HCO(0,1,0) with O_2 and NO, respectively are consistent with the experimental upper limits of 4.4 x 10^{-12} and 8.0 x 10^{-12} cm^3 $molec^{-1}$ s^{-1} for these reactions. This result is qualitatively obvious from the model; the addition of energy to the complex will increase k_{-a} relative to k_b since k_{-a} is at threshold and k_b is nearly 10 kcal mol^{-1} above threshold.

4. Pressure Dependences

The calculated reaction efficiencies, isotope effects, and vibrational energy dependences are independent of the complex frequencies and potential well depths. These parameters are required, however, to estimate the complex lifetimes and collisional stabilizaton probabilities. The collision complex vibrational frequencies were

estimated primarily by analogy to related species such as glyoxal, nitrosomethane, and methoxy. The C-N and C-O bond lengths are given above. The C-O-O and C-N-O bond angles of 103° and 121° were taken from CH_3O_2 and CH_3NO as were the N-O and O-O bond lengths. The remaining bond lengths and angles were taken from glyoxal. The assumed vibrational frequencies and moments of inertia are given in Table IV-5 along with those of glyoxal for comparison. The previously assumed transition state vibrational frequencies and moments of inertia are used in conjunction with these parameters to calculate the complex lifetimes and dissociation rates. These are shown as a function of the assumed well depths in Table VI-4.

The experiments indicate that the rate constants for reactions (1) and (2) are pressure independent between 5 and 1000 Torr. Given the calculated values of k_{-a} and k_b in Table VI, this result can be compared with the model through Eq. (15). Using the potential well depths of 21 and 32 kcal mol^{-1} for $HCOO_2$ and HCONO, respectively, and assuming that one collision decreases the complex vibrational energy by the ~1 kcal mol^{-1} necessary to prevent redissociation to reactants, $k_c = 9.8 \times 10^6$ s^{-1} $Torr^{-1}$ and the calculated rate constants for reactions (1) and (2) are 4.7×10^{-12} and 1.6×10^{-11} cm^3 $molec^{-1}$ s^{-1}, respectively, at 1000 Torr. The calculated increase of 1% for reaction (1) would not be detected in the experiments; a 28% increase as predicted for reaction (2), however, should be observable. This suggests that the HCONO well depth is less than 32 kcal mol^{-1}. Decreasing the well depth to 24 kcal mol^{-1} results in a lifetime of 4.6 ps and a rate constant of 1.35×10^{-11} cm^3 $molec^{-1}$ s^{-1} at 1000 Torr, an increase of only 7% over the low pressure rate constant. This result demonstrates that the pressure

independence of the rate constants is consistent with the collision complex model, although uncertainties in the well depths limit the accuracy of predicted high pressure rate constants.

The fate of $HCCO_2$ and HCONO adducts in the atmosphere is even more difficult to evaluate. Whereas one collision with an N_2 molecule almost certainly removes enough energy to prevent redissociation to reagents, several collisions may be required to decrease the vibrational energy by the 8-9 kcal mol^{-1} necessary to prevent dissociation to products. Setser et al. have reported average energy transfers of 6 kcal mol^{-1} from chemically activated 1,2-dichloroethane[37] or cyclopropane[38] to molecular nitrogen. Assuming that two collisions are required to deactivate the $HCOO_2$ adducts ($k_c = 4.9 \times 10^6$ s^{-1} $Torr^{-1}$), a well depth of 21 kcal mol^{-1} implies that less than 1% will be stabilized at 760 Torr, while 49% dissociate to products and 50% redissociate to reactants. If reaction (1) is the only important mechanism for HCO removal, the 50% which redissociate to reactants will form new complexes and 1% of these will be stabilized. the conversion of HCO to stable $HCOO_2$ will thus be 1-2%, with the remaining 98% converted to HO_2 + CO. An HCONO well depth of 24 $kcal^{-1}$ mol^{-1} implies 2% stabilization, 50% redissociation to reactants, and 48% dissociation to products for HCONO adducts at 760 Torr. The conversion of HCO to HCONO when reaction (2) dominates will thus be $\lesssim$4%.

Although these results depend on the assumed potential well depths, it appears likely that stable $HCOO_2$ (or HCONO) production in the atmosphere will be insignificant. It appears equally likely, however, that $HCOO_2$ and HCONO concentrations in excess of 1×10^{12} cm^{-3} can be readily generated in the laboratory for spectroscopic studies. A detailed examination of the gas phase ultraviolet spectrum attributed to

HCONO by Napier and Norrish[12] should prove interesting.

5. Temperature Dependences

The reaction efficiencies were calculated for temperatures ranging from 200 to 1500 K. Using a simple hard sphere collision model which includes the temperature dependent cross section from Eq. 23 to calculate the temperature dependence of the complex formation rates, the temperature dependent rate constants shown in Fig. IV-8 were obtained. The overall temperature dependence is dominated by the decrease in reaction efficiency with increasing temperature. This results from the much faster increase in $k_{-a}(E)$ (relative to $k_b(E)$) with energy, and the barrier height correction required by adiabatic rotations. The temperature dependence calculated for reacton (2) is in good agreement with the experimental results (300-500 K) of Veyret and Lesclaux[7]. The temperature dependence for reaction (1) is also in good qualitative agreement although better quantitative agreement is obtained for a barrier height difference of 10.5 kcal mol^{-1}.

Experimental results at higher and lower temperatures are not available for comparison. Rate constants for reaction (1) below 300 K and above 500 K are of practical interest for stratospheric and combustion models. At 228 K, the predicted rate constant for reaction (1) is 4.4×10^{-12} cm^3 $molec^{-1}$ s^{-1} for ΔE_o = 9.0 kcal mol^{-1} and 5.1×10^{-12} cm^3 $molec^{-1}$ s^{-1} for ΔE_o = 10.5 kcal mol^{-1}. A temperature independent rate constant of $(5.0 \pm \frac{2.0}{1.5}) \times 10^{-12}$ cm^3 $molec^{-1}$ s^{-1} (E_a = 0.0 ± 0.25 kcal mol^{-1}) is given in a recent compilation of recommended rate constants for stratospheric modelling.[39] This rate constant is an average of the room temperature values of k_1 from Refs. 4-6. At high temperatures, Peeters and Mahnen[40] have suggested a rate constant of 5 x

10^{-11} cm^3 $molec^{-1}$ s^{-1} (1400 to 1800 K) for reaction (1) based on their mass spectrometric measurements of species in a methane–oxygen flame, while Westbrook et al.[41] have proposed a much smaller value of 2.2 x 10^{-13} (1100 K) cm^3 $molec^{-1}$ s^{-1}, in their model of chemical kinetics in a turbulent flow reactor. A 1500 K rate constant of 2.6 x 10^{-13} cm^3 $molec^{-1}$ s^{-1} is also obtained from the Arrhenius expression recommended in the recent compilation by Westley,[42] although the 3.5 kcal mol^{-1} activation energy in this expression predicts a 300 K rate constant of 2 x 10^{-17} cm^3 $molec^{-1}$ s^{-1}. Reaction (2) is also of interest for combustion systems containing nitrogen oxides.[43] The calculated value of k_2 at 1500 K (~4 x 10^{-12} cm^3 $molec^{-1}$ s^{-1}) is in reasonable agreement with the value of 6.6 x 10^{-12} cm^3 $molec^{-1}$ s^{-1} obtained from the modified Arrhenius expression in Ref. 42, although this expression gives a room temperature rate constant of 2 x 10^{-13} cm^3 $molec^{-1}$ s^{-1}.

D. CONCLUSIONS

The RRKM calculations described above are admittedly simplistic. The accuracy of the results is limited more by uncertainties in the input parameters, however, (particularly the vibrational frequencies) than by the actual calculations. The calculated reaction efficiencies are particularly sensitive to the low frequency modes of transition state A. The complex lifetimes and stabilization probabilities are also limited by uncertainties in the potential well depths. *Ab initio* calculations of the complex and transition state vibrational frequencies might provide a basis for more sophisticated calculations.

Nevertheless, the above discussion demonstrates that with a reasonable choice of transition state and collision complex

parameters, RRKM calculatons can reproduce the inverse isotope effect, the decrease in reaction rate with reagent vibrational excitation, the negative "activation energy", and the pressure independences of the bimolecular rate constants of these interesting reactions. Complex formation must be the dominant channel for both reactions. The calculated rate constants at high and low temperatures should prove useful in combustion and atmospheric models. Although an insignificant fraction of the HCO produced in the atmosphere will be converted to stable $HCOO_2$ and HCONO, it should be possible to produce adequate concentrations of these species for spectroscopic studies in the laboratory.

References

1. C. K. Westbrook and F. L. Dryer, Eighteenth Symposium (International) on Combustion, The Combustion Institute, Pittsburgh, 1981, p. 749.
2. H. Okabe, Photochemistry of Small Molecules (Wiley, New York 1978).
3. N. Washida, R. I. Martinez, and K. D. Bayes, Z. Naturforsch. A 29, 251 (1974).
4. K. Shibuya, T. Ebata, K. Obi, and I. Tanaka, J. Phys. Chem. 81, 2292 (1977).
5. J. P. Reilly, J. H. Clark, C. B. Moore, and G. C. Pimentel, J. Chem. Phys. 69, 4381 (1978).
6. V. A. Nadtochenko, O. M. Sarkisov, and V. I. Vedeneev, Dokl. Akad. Nauk SSSR 244, 152 (1979).
7. B. Veyret and R. Lesclaux, J. Phys. Chem. 85, 1918 (1981).
8. R. J. Gill, W. D. Johnson, and G. H. Atkinson, Chem. Phys. 58, 29 (1981).
9. H. E. Radford, K. M. Evenson, and C. J. Howard, J. Chem. Phys. 60, 3178 (1974).
10. M. Diem and E. K. C. Lee, J. Phys. Chem. 86, 4507 (1982).
11. T. -L. Tso, M. Diem, and E. K. C. Lee, Chem. Phys. Lett. 91, 339 (1982).
12. I. M. Napier and R. G. W. Norrish, Proc. R. Soc. London A 229, 337 (1967).
13. J. Bigeleisen and M. Wolfsberg, Adv. Chem. Phys. 1, 15 (1958); M. M. R. Berman, Ph. D. Dissertation, University of California,

Berkeley, 1981.

14. W. N. Olmstead and J. I. Brauman, J. Am. Chem. Soc. 99, 4219 (1977).

15. A. O. Langford, H. Petek, and C. B. Moore, J. Chem. Phys. 78, 6650 (1983).

16. A. A. Westenberg and N. de Haas, J. Phys. Chem. 76, 2213 (1972).

17. C. J. Hochanadel, T. J. Sworski, and P. J. Ogren, J. Phys. Chem. 84, 231 (1980).

18. J. J. Ahumada, J. V. Michael, and D. T. Osborne, J. Chem. Phys. 57, 3736 (1972).

19. W. Wong and D. D. Davis, Int. J. Chem. Kinet. 6, 401 (1974).

20. E. M. Bulewicz and T. M. Sugden, Proc. R. Soc. London A 277, 143 (1964).

21. E. A. Albers, K. Hoyermann, H. G. Wagner, and J. Wolfrum, Thirteenth Symposium (International) on Combustion, The Combustion Institute, Pittsburgh, 1971, p. 81.

22. J. H. Clark, N. S. Nogar, and C. B. Moore, J. Chem. Phys. 68, 1264 (1978).

23. S. W. Benson, Thermochemical Kinetics, 2nd ed. (Wiley, New York, 1976).

24. J. G. Calvert and G. S. Layne, J. Am. Chem. Soc. 75, 856 (1953).

25. R. Vasudev and R. N. Zare, J. Chem. Phys. 76, 5267 (1982).

26. F. Su, J. G. Calvert, J. H. Shaw, H. Niki, P. D. Maker, C. M. Savage, and L. D. Breitenbach, Chem. Phys. Lett. 49, 112 (1977).

27. I. W. M. Smith and R. Zellner, J. Chem. Soc. Faraday II 69, 1617 (1973).

28. I. W. M. Smith, Chem. Phys. Lett. 49, 112 (1977).

29. W. A. Goddard III, T. H. Dunning Jr., W. J. Hunt, and P. J. Hay, Accounts Chem. Res. 6, 368 (1973).

30. N. W. Winter, W. A. Goddard III, and C. F. Bender, Chem. Phys. Lett. 33, 25 (1975).

31. W. Forst, Theory of Unimolecular Reactions (Academic, New York, 1973).

32. E. V. Waage and B. S. Rabinovitch, Chem. Rev. 70, 377 (1970).

33. R. C. Weast, Handbook of Chemistry and Physics, 53th ed. (Chemical Rubber Co., Cleveland, 1972).

34. Y. Osamura, H. F. Schaefer III, M. Dupuis, and W. A. Lester, Jr., J. Chem. Phys. 75, 5828 (1981).

35. G. Herzberg, Molecular Spectra and Molecular Structure, v. III, (Van Nostrand, New York, 1966).

36. W. L. Hase and D. L. Bunker, Quantum Chemistry Program Exchange Cat. No. QCPE-2234.

37. D. W. Setser and J. C. Hassler, J. Phys. Chem. 71, 1364 (1967).

38. J. W. Simons, B. S. Rabinovitch, and D. W. Setser, J. Chem. Phys. 41, 800 (1964).

39. W. B. DeMore et al., Chemical Kinetic and Photochemical Data for Use in Stratospheric Modelling Evaluation Number 4 JPL Publicaton 81-3, 1981.

40. J. Peeters and G. Mahnen, Fourteenth Symposium (International) on Combustion, The Combustion Institute, Pittsburgh, 1973, p. 13.

41. C. K. Westbrook, J. Creighton, C. Lund, and F. L. Dryer, J. Phys. Chem. 81, 2542 (1977).

42. F. Westley, Table of Recommended Rate Constants for Chemical Rections Occuring in Combustion NSRDS-NBS-67 (U. S. GPO,

Washington, D. C., 1980).

43. R. A. Fifer, Seventeenth Symposium (International) on Combustion, The Combustion Institute, Pittsburgh, 1978, p. 587.

44. T. Shimanouchi, J. Phys. Chem. Ref. Data 3, 293 (1974).

TABLE IV-1. Summary of reported rate constants (cm^3 $molec^{-1}$ s^{-1}) at room temperature.

k_1	k_2	Method[a]	Reference
$(5.7 \pm 1.2) \times 10^{-12}$		DF/MS	3
$(5.6 \pm 0.9) \times 10^{-12}$	$(0.85 \pm 0.1) \times 10^{-11}$	FP/FS	4
$(4.0 \pm 0.8) \times 10^{-12}$	$(1.4 \pm 0.2) \times 10^{-11}$	LF/IDLS	5
$(3.7 \pm 0.8) \times 10^{-12}$	1.2×10^{-11}	FP/IDLS	6
$(5.6 \pm 0.6) \times 10^{-12}$	$(1.23 \pm 0.12) \times 10^{-11}$	FP/LRA	7
$(4.2 \pm 0.7) \times 10^{-12}$		FP/IDLS	8
$(4.65 \pm 0.6) \times 10^{-12}$	$(1.26 \pm 0.2) \times 10^{-11}$	LP/LRA	This Work

[a]DF/MS - discharge flow with mass spectrometry detection.

FP/FS - flash photolysis with flash spectroscopy detection.

LP/IDLS - laser photolysis with intra-cavity dye laser detection.

LP/LRA - laser photolysis with laser resonance absorption detection.

TABLE IV-2. Transition state A: Vibrational frequencies and moments of inertia for adiabatic rotations.

	$HCOO_2$	$DCOO_2$	HCONO	DCONO
$\nu(cm^{-1})$	2488	1910	2488	1910
	1083	850	1083	850
	1868	1800	1868	1800
	1555	1555	1875	1875
	200	170		
	105	103	9.88[a]	9.88[a]
	65	63	0.69[a]	1.13[a]
	25	24	11.44[b]	13.45[b]
I_b (amu-Å^2)	161	161	173	173
I_c	227	231	259	263

[a]one-dimensional internal rotor (amu-Å^2).

[b]two-dimensional internal rotor (amu-Å^2).

TABLE IV-3. Transition state B: Vibrational frequencies and moments of inertia for adiabatic rotations.

	$HCOO_2$	$DCOO_2$	HCONO	DCONO
ν (cm^{-1})				
a'	3450	2600	3450	2600
	2050	2000	2050	2000
	1100	1080	1525	1500
	1150	1000	1100	950
	1740i	1500i	1740i	1500i
	650	610	600	550
a"	1370	1160	1340	1150
	600	560	600	560
	125	115	125	105
I_b (amu-$Å^2$)	100	101	110	110
I_c	106	107	116	117

TABLE IV-4. Calculated reaction efficiencies.

$E_o-E'_o$ (kcal/mole)	FRE (H)	FRE (D)	FRE (H)/FRE (D)
		$HCO + O_2$	
5.0	0.19	0.23	0.81
6.0	0.26	0.31	0.83
7.0	0.33	0.39	0.84
8.0	0.41	0.48	0.87
9.0	0.49	0.55	0.89
10.0	0.56	0.62	0.90
		HCO + NO	
5.0	0.14	0.18	0.75
6.0	0.20	0.26	0.79
7.0	0.28	0.35	0.82
8.0	0.37	0.44	0.85
9.0	0.46	0.52	0.88
10.0	0.54	0.61	0.90

TABLE IV-5. Collision complex: Vibrational frequencies and moments of inertia for adiabatic rotations.

	$(HCO)_2$[a]	$(DCO)_2$[a]	$HCO-O_2$	$DCO-O_2$	HCO-NO	DCO-NO
ν (cm^{-1})						
a'	2843	2138	2840	2100	2840	2100
	1745	1722	1725	1715	1725	1715
			1200	1150	1800	1800
	1065	915	1100	945	1000	950
	1338	1130	1390	1170	1300	1130
	551	537	625	560	540	530
a"	1048	911	1035	870	1000	860
	339	311	320	310	320	310
	127	118	110	110	120	120
I_b (amu-$Å^2$)	105	106	93	93	107	107
I_c	114	120	102	104	114	117

[a]Ref. 44.

TABLE IV-6. RRKM lifetimes and dissociation rates for $HCOO_2$ and HCONO complexes.

E^a	$E_o'^a$	k_b (s^{-1})	k_{-a}(s^{-1})	τ (ps)	FRE[b]
		$HCOO_2$			
33	24	2.1×10^{10}	2.2×10^{10}	23	0.58
29	20	4.4×10^{10}	4.6×10^{10}	11	0.54
25	16	9.9×10^{10}	1.0×10^{11}	5.0	0.52
21	12	2.4×10^{11}	2.5×10^{11}	2.0	0.50
17	8	6.8×10^{11}	7.1×10^{11}	0.7	0.49
		HCONO			
40	32	4.6×10^{9}	7.8×10^{9}	80	0.64
36	28	8.6×10^{9}	1.5×10^{10}	43	0.55
32	24	1.7×10^{10}	2.9×10^{10}	22	0.48
28	20	3.5×10^{10}	6.0×10^{10}	10	0.43
24	16	8.0×10^{10}	1.4×10^{11}	4.5	0.40

[a] kcal mol^{-1}.

[b] at 1000 Torr with $k_c = 9.8 \times 10^6$ s^{-1} $Torr^{-1}$.

FIG. IV-1. Decay of ground state HCO in 3.20 Torr H_2CO and 0.300 Torr NO (total pressure = 3.50 Torr). The decay is an average of 128 laser shots (10 mJ/cm^2). The solid line corresponds to $k_2 = 1.30 \times 10^{-11}$ cm^3 $molec^{-1}$ s^{-1}.

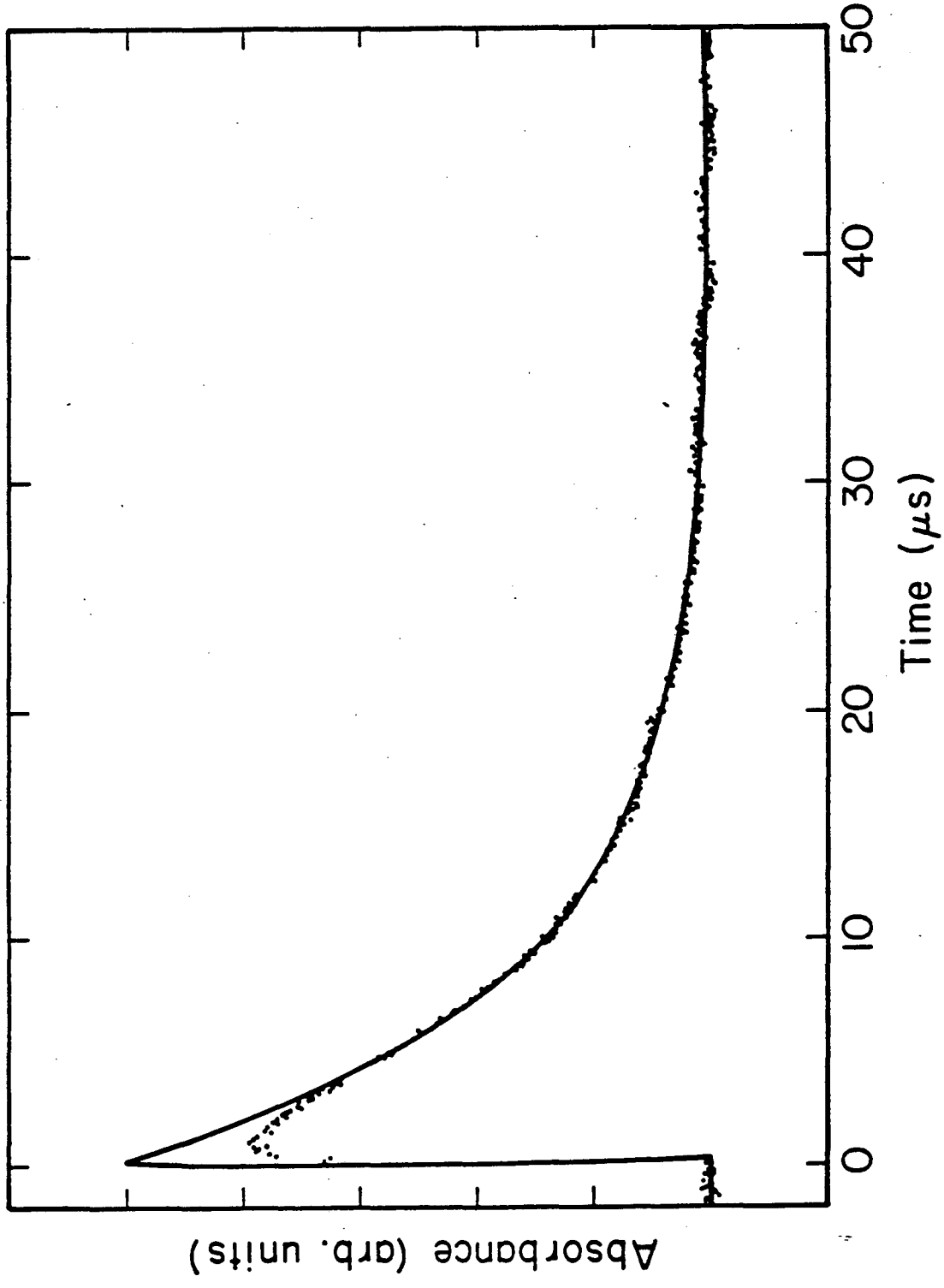

Fig. IV-1

FIG. IV-2. Decay of ground state HCO in 4.05 Torr $(HCO)_2$, 0.052 Torr NO, and 1000 Torr N_2. The decay is an average of 128 laser shots. The solid line corresponds to $k_1 = 1.15 \times 10^{-11}$ cm^3 $molec^{-1}$ s^{-1}.

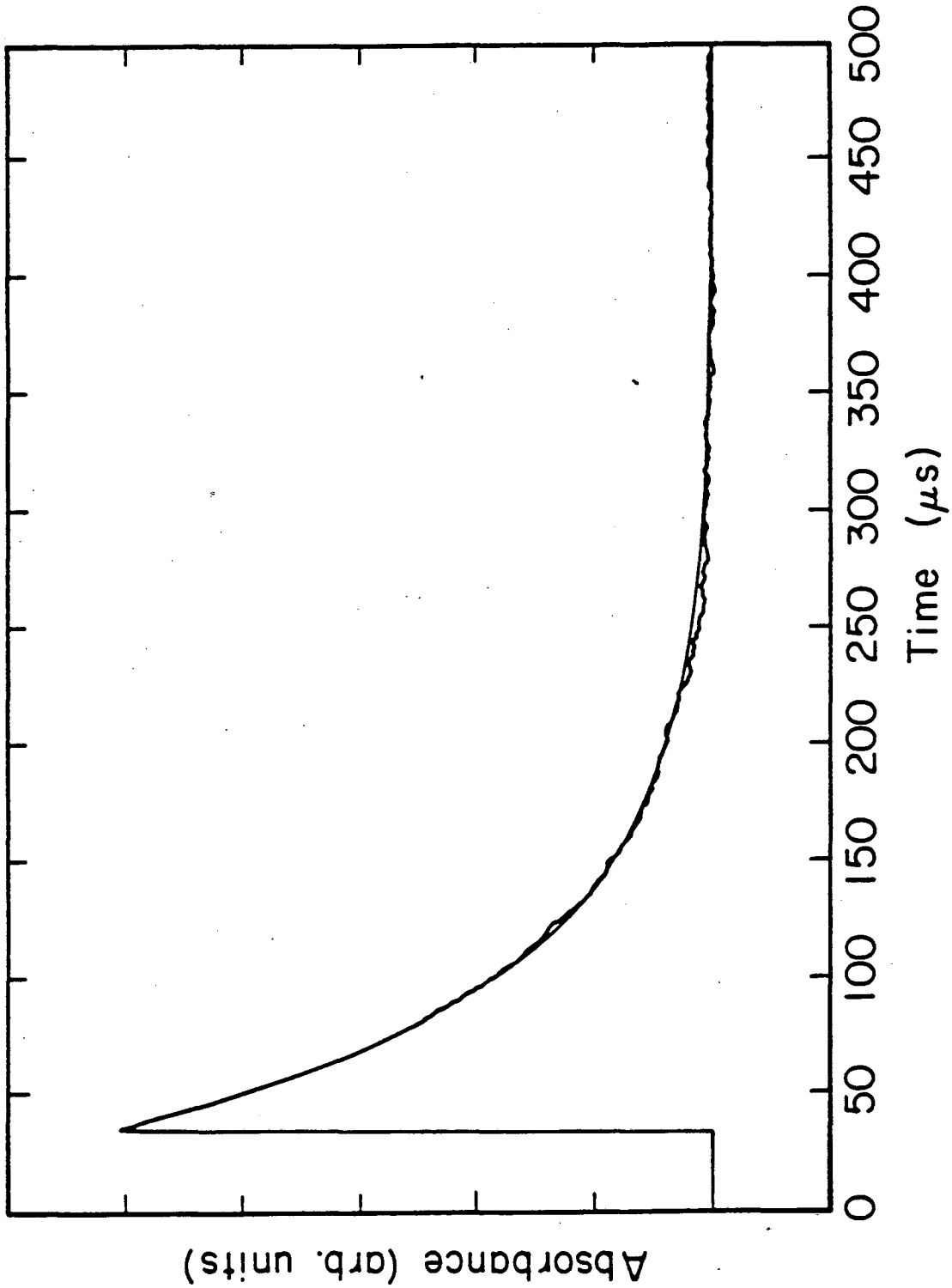
Absorbance (arb. units)
0
50
100
150
200
250
300
350
400
450
500
Time (μs)

Fig. IV-2

FIG. IV-3. Pseudo-first-order rate constants for removal of HCO and DCO by NO. ○ - formaldehyde precursor, 3-5 Torr total pressure; △ -glyoxal precursor, 3-5 Torr total presure; □ -glyoxal precursor, 1000 Torr total pressure. The solid lines correspond to the rate constants given in Table IV-1 and the text. The dashed line in the DCO plot corresponds to the HCO rate constant. Filled symbols correpond to DCO.

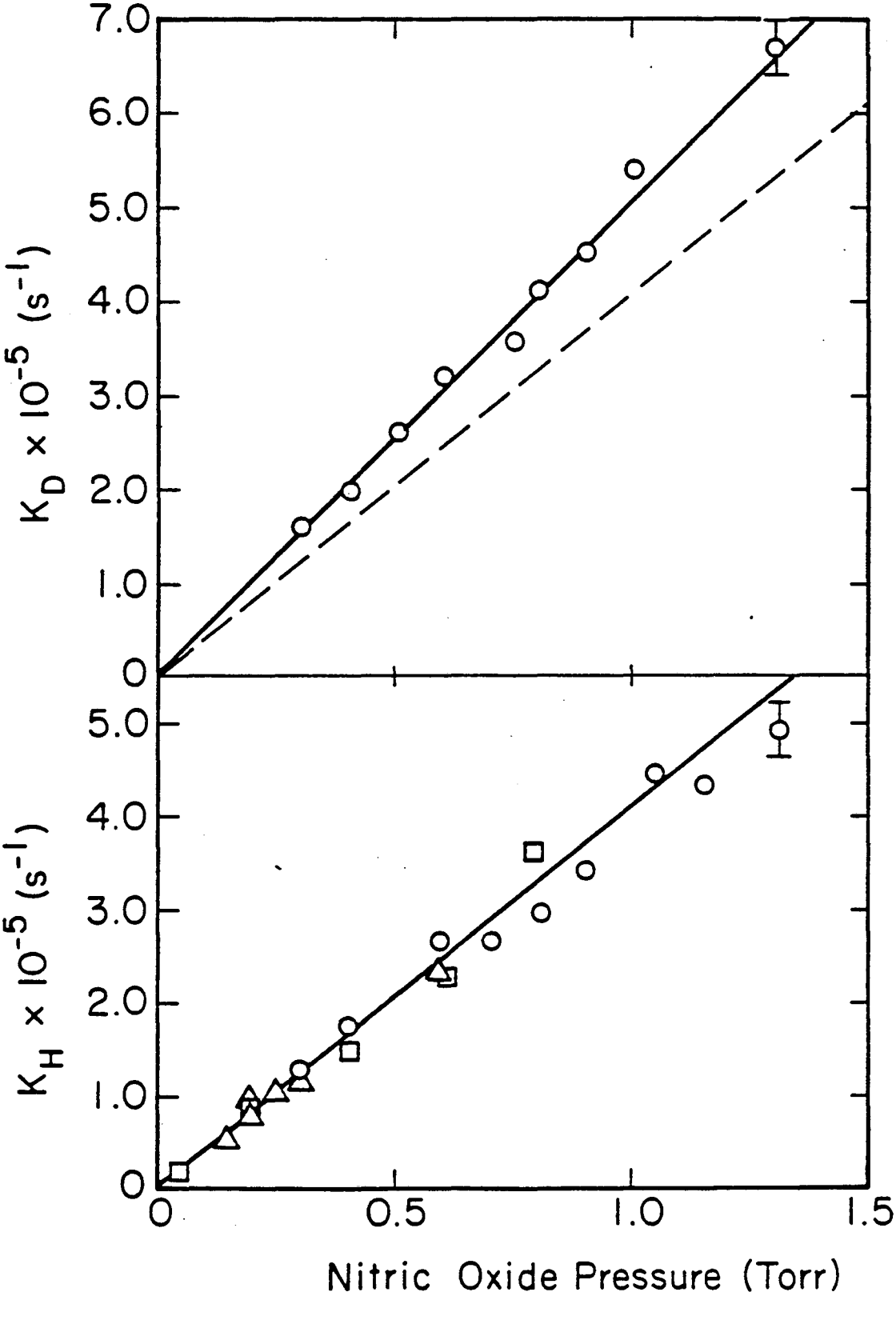
7.0
6.0
5.0
4.0
3.0
2.0
1.0
0
$K_D \times 10^{-5}$ (s^{-1})
5.0
4.0
3.0
2.0
1.0
0
$K_H \times 10^{-5}$ (s^{-1})
0
0.5
1.0
1.5
Nitric Oxide Pressure (Torr)

Fig. IV-3

FIG. IV-4. Pseudo-first-order rate constants for removal of HCO and DCO by O_2. The symbols have the same meaning as in Fig. IV-3.

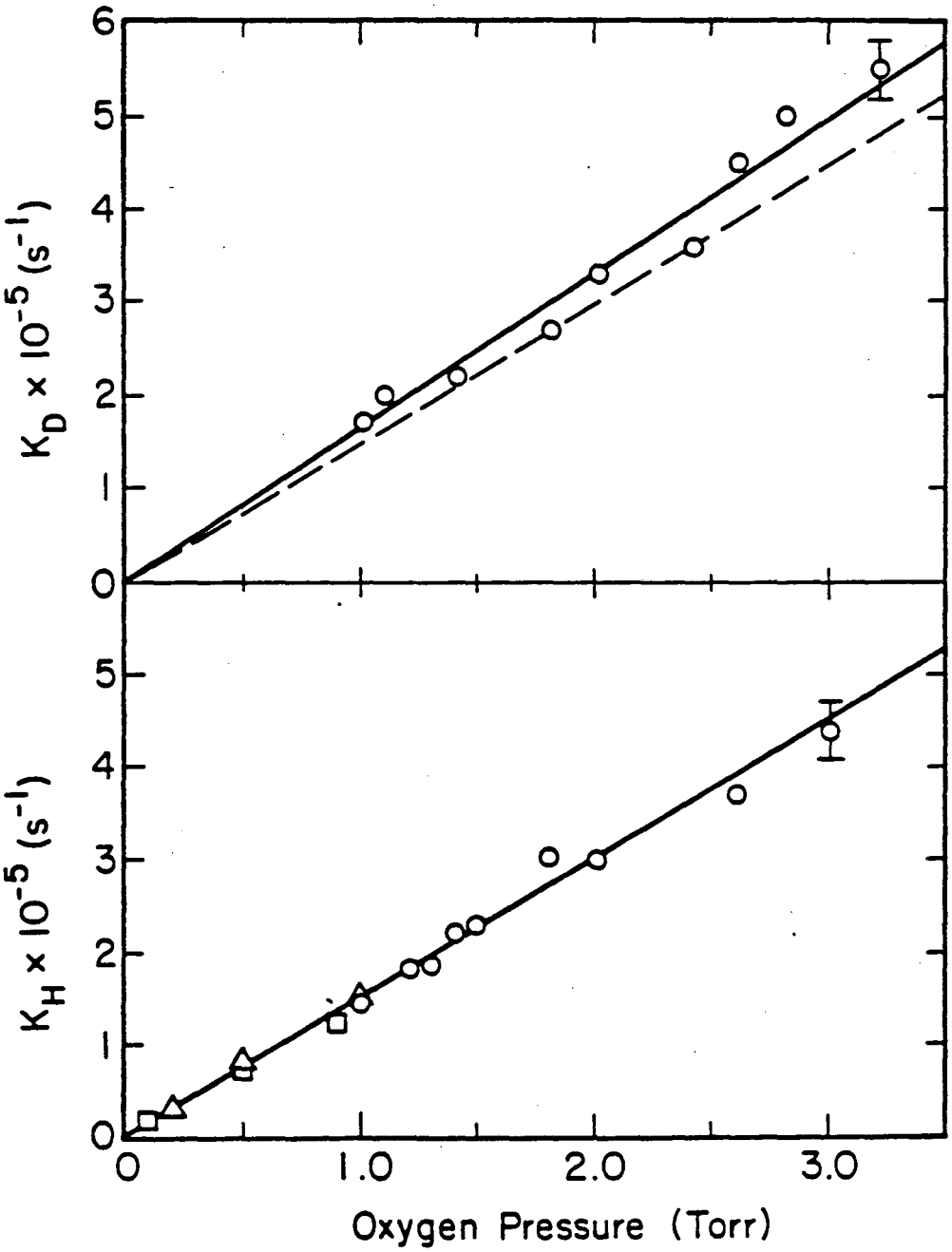
$K_D \times 10^{-5}\ (s^{-1})$
$K_H \times 10^{-5}\ (s^{-1})$
0
1
2
3
4
5
6
0
1.0
2.0
3.0
Oxygen Pressure (Torr)

Fig. IV-4

FIG. IV-5. Absolute rate constants for removal of HCO and DCO by O_2. The symbols have the meaning as in Fig. IV-3.

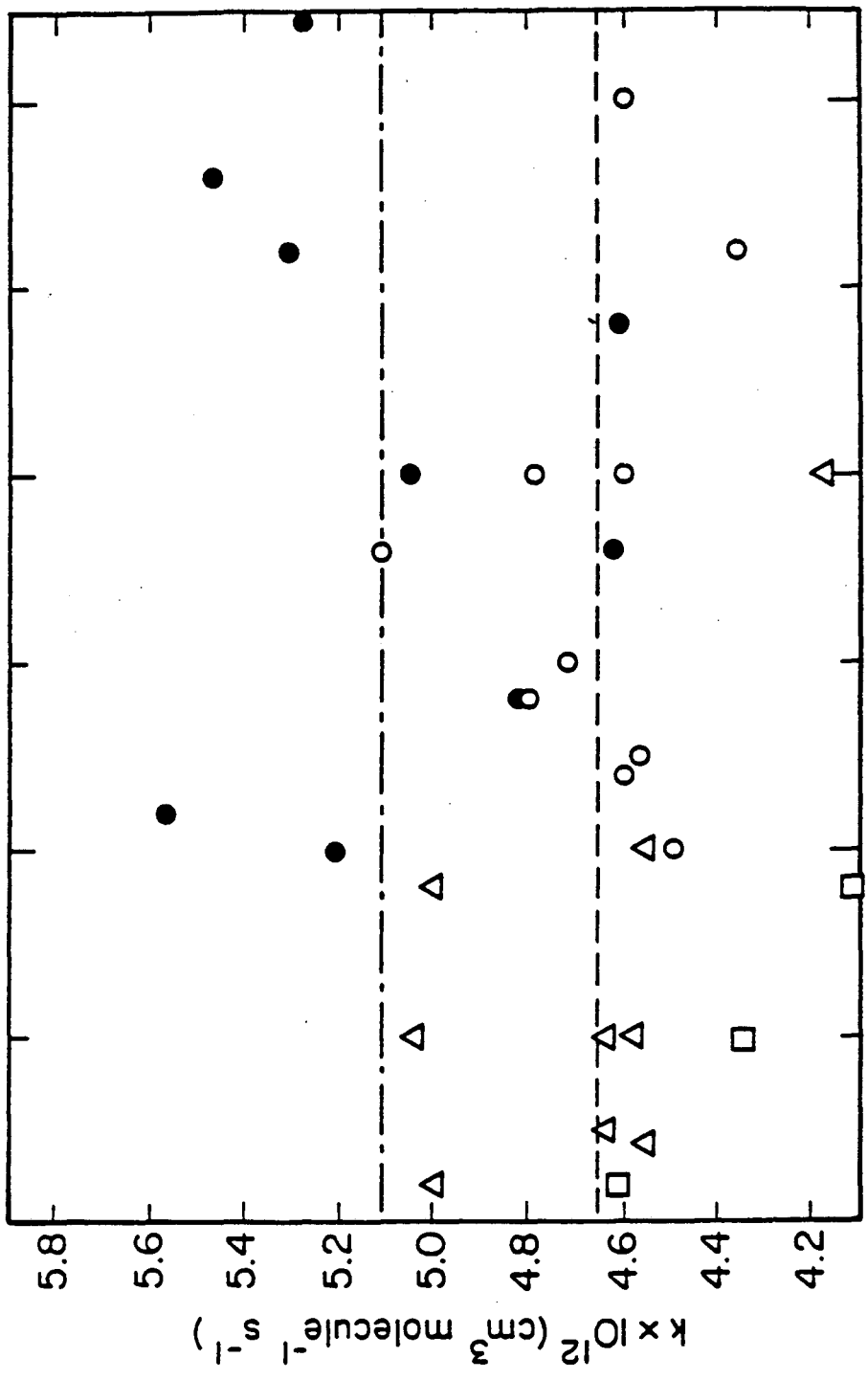
Oxygen Pressure (Torr)
0
1.0
2.0
3.0
4.2
4.4
4.6
4.8
5.0
5.2
5.4
5.6
5.8
k x 10^12 (cm^3 molecule^-1 s^-1)

Fig. IV-5

FIG. IV-6. Absolute rate constants for HCO and DCO removal by NO. The symbols have the same meaning as in Fig. IV-3.

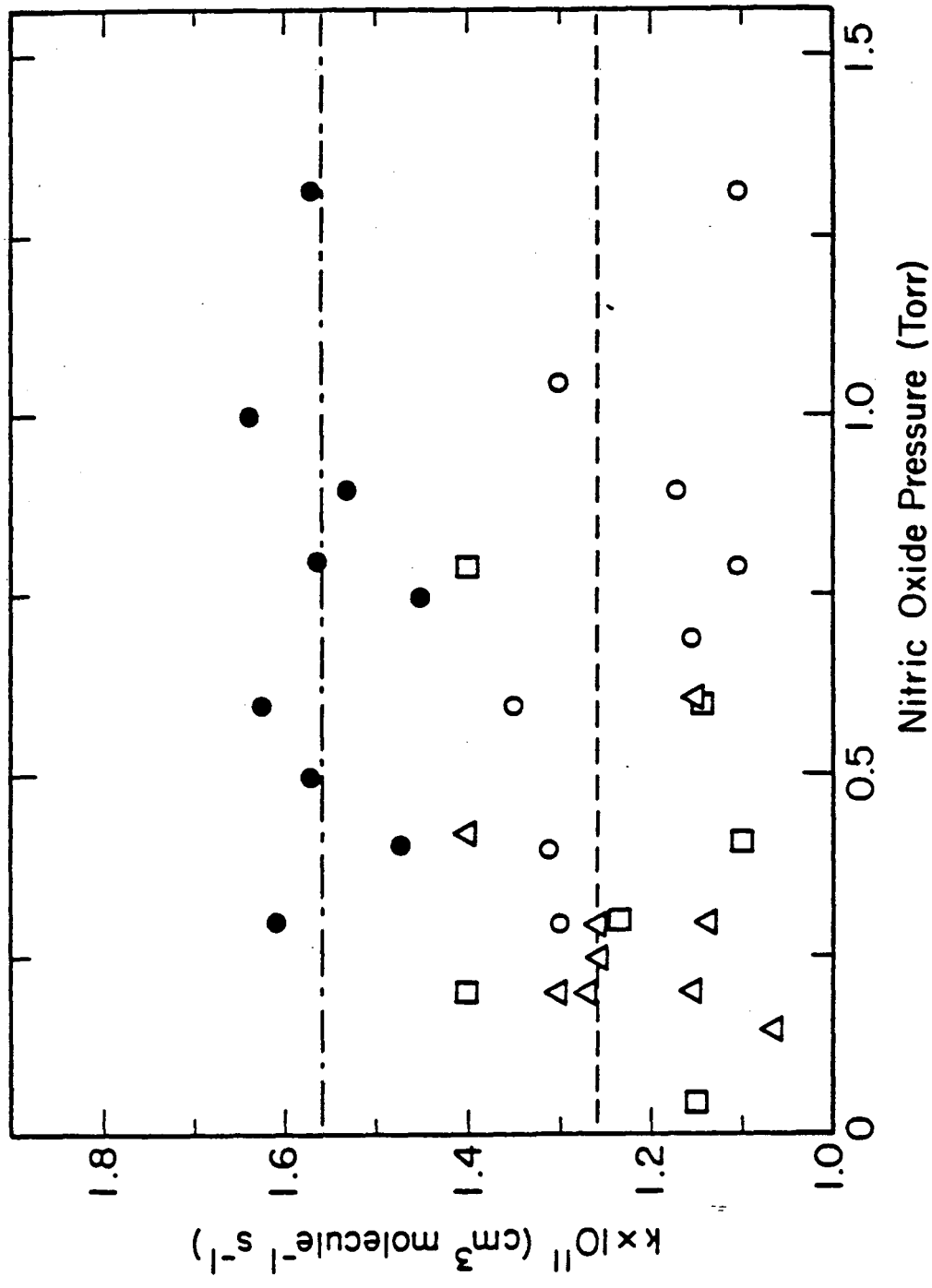
k × 10^11 (cm^3 molecule^-1 s^-1)
1.8
1.6
1.4
1.2
1.0
0
0.5
1.0
1.5
Nitric Oxide Pressure (Torr)

Fig. IV-6

FIG. IV-7. Schematic potential energy diagram for the collision complex mechanism illustrated for reaction (2). The symbols are described in the text.

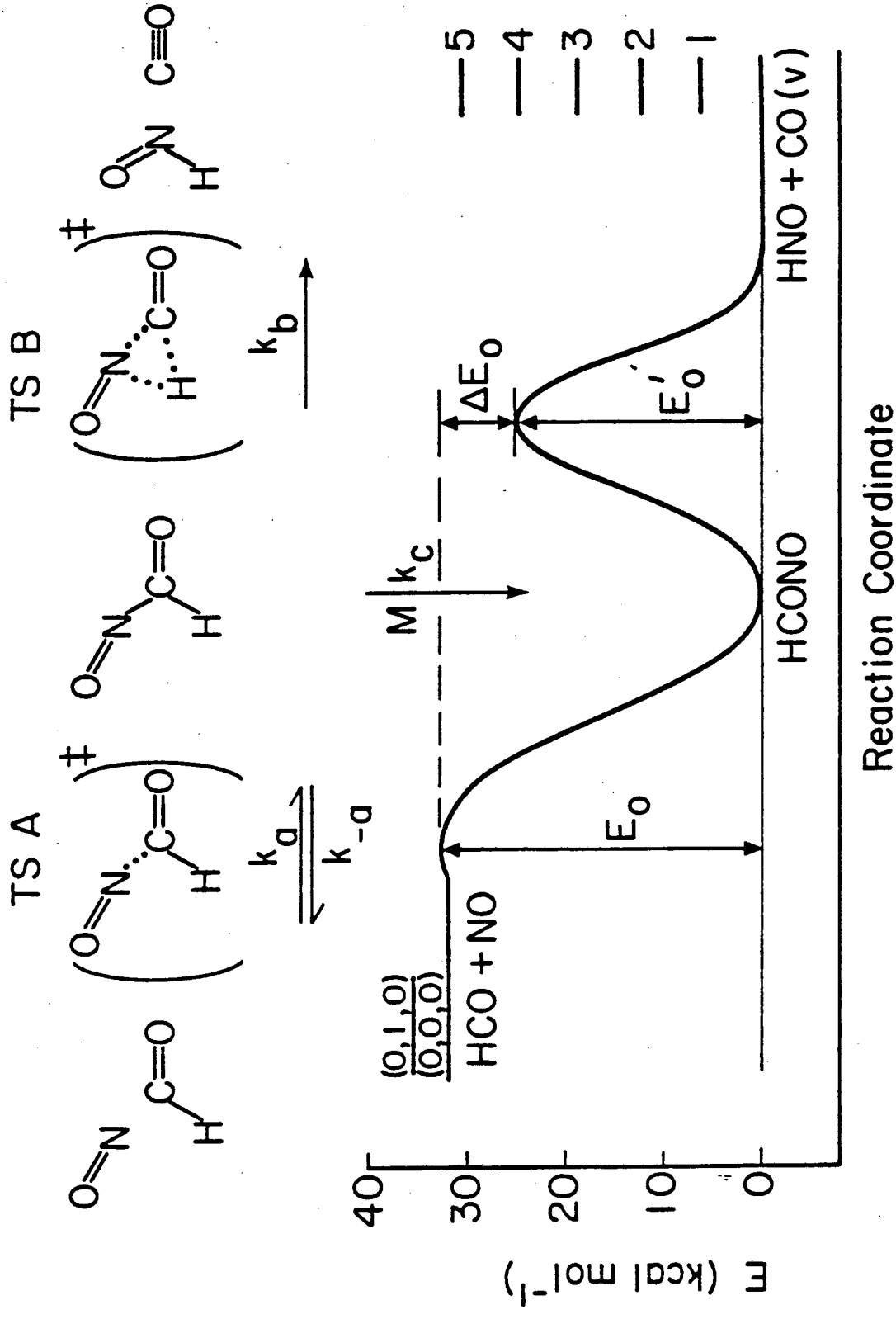
TS A
TS B
k_a
k_{-a}
k_b
M
k_c
ΔE_o
E_o
E_o'
HCO + NO
(0,1,0)
(0,0,0)
HCONO
HNO + CO(v)
5
4
3
2
1
40
30
20
10
0
E (kcal mol^{-1})
Reaction Coordinate

Fig. IV-7

FIG. IV-8. Calculated and experimental temperature dependences of k_1 and k_2. ▲ and △ correspond to rate constants for NO and O_2 determined in this study. ● and ○ are rate constants reported by Veyret and Lesclaux.

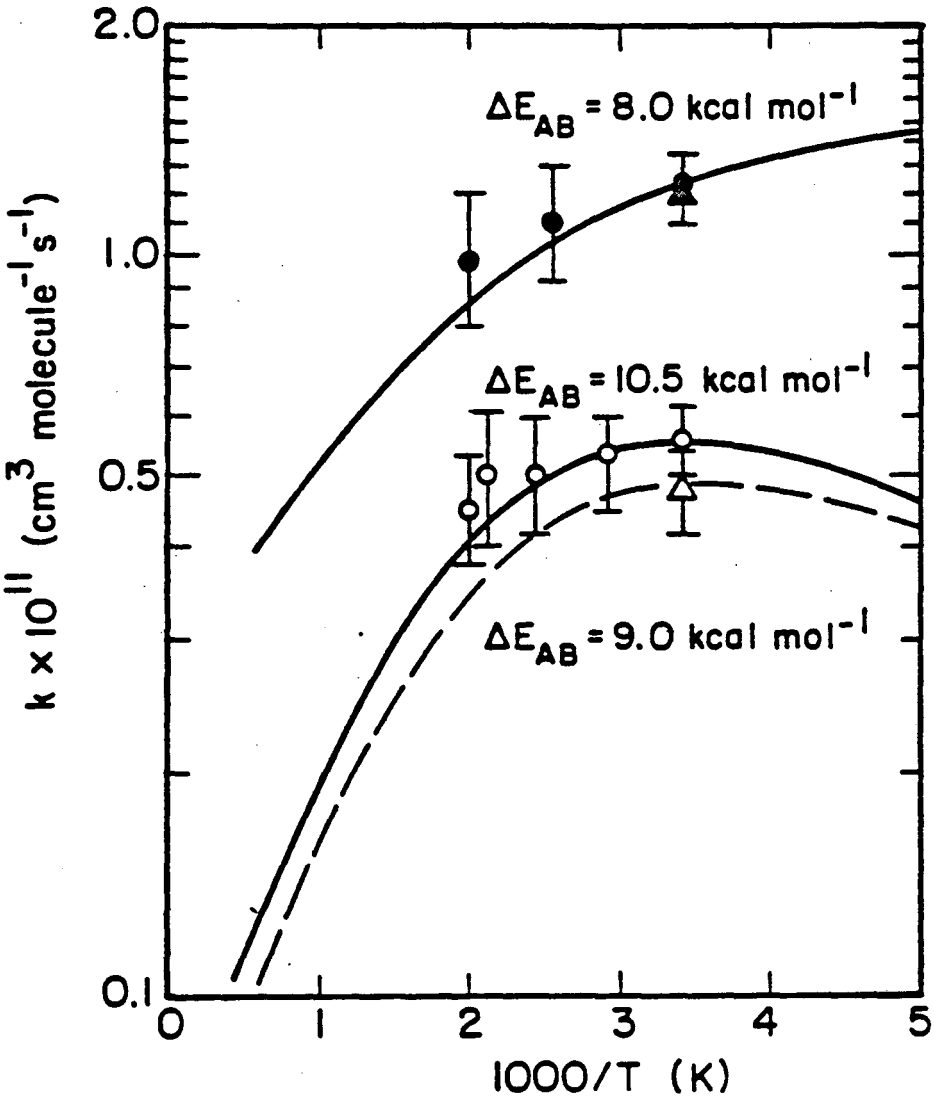
2.0
1.0
0.5
0.1
0
1
2
3
4
5
1000/T (K)
k x 10^11 (cm^3 molecule^-1 s^-1)
ΔE_AB = 8.0 kcal mol^-1
ΔE_AB = 10.5 kcal mol^-1
ΔE_AB = 9.0 kcal mol^-1

Fig. IV-8

CHAPTER V. COLLISIONAL REMOVAL OF SINGLET METHYLENE

A. INTRODUCTION

Despite the fundamental importance of methylene to synthesis, molecular structure, and chemical kinetics, its chemistry is not well established.[1] Many of the problems and much of the interest stem from the existence of two low-lying electronic states which differ significantly in reactivity and structure. The energy difference between the triplet ground state ($^3B_1$) and the singlet first excited state ($^1A_1$) remains a subject of controversy.[2-6]

Although CH_2 ($^1A_1$) absorbs in the visible,[7] kinetic measurements based on spectroscopic detection have been hampered by the short lifetime of this state under collisional conditions. By contrast, electronic transitions from the relatively long-lived ($^3B_1$) state lie in the less accessible vacuum ultraviolet.[7,8] Experimental studies of gas phase methylene reactions have therefore been confined primarily to indirect methods such as end product analysis. Distinguishing the chemistry of singlet and triplet methylene by such methods is complicated by the efficient collision-induced intersystem crossing which converts singlet methylene to the triplet ground state. Indirect studies of singlet chemistry therefore rely on the use of radical scavengers to preferentially remove triplet methylene from the reaction system. Interpretation of such studies is not always straightforward.

The use of pulsed laser-induced fluorescence (LIF) for detecting CH_2 ($^1A_1$) has been successfully demonstrated in several laboratories.[2,3,9-12] The first direct measurements of CH_2 ($^1A_1$) removal rates have

recently been reported by Ashfold et al.[11,12] who used LIF to monitor CH_2 ($^1A_1$) and CD_2 ($^1A_1$) produced in the ir multiphoton dissociation (MPD) of acetic anhydride. These workers reported rate constants for CH_2 ($^1A_1$) removal approximately one order of magnitude larger than previously accepted values inferred primarily from studies of CH_2 ($^3B_1$) kinetics.[8] These new results provide information essential for the further development of theoretical descriptions of collision-induced intersystem crossing in methylene. In conjunction with earlier product analysis studies, these results also imply that CH_2 ($^1A_1$) is removed by many hydrocarbons with near gas-kinetic collision efficiency.[13,14]

In the present study, cw laser resonance absorption (LRA) has been used to monitor individual rotational levels of singlet methylene produced in the near uv photolysis of ketene. This technique offers the advantages of continuous temporal detection with the narrow linewidth of a cw laser and thus permits studies of photodissociation and reaction processes with greater detail than is practical with pulsed probing techniques. Absolute rate constants for CH_2 ($^1A_1$) removal by the following processes have been determined at 295 K:

$$CH_2\ (^1A_1) + CH_2CO \rightarrow C_2H_4 + CO \quad (1)$$

$$CH_2\ (^1A_1) + He \rightarrow CH_2\ (^3B_1) + He \quad (2)$$

$$CH_2\ (^1A_1) + Ar \rightarrow CH_2\ (^3B_1) + Ar \quad (3)$$

$$CH_2\ (^1A_1) + Kr \rightarrow CH_2\ (^3B_1) + Kr \quad (4)$$

$$CH_2\ (^1A_1) + N_2 \rightarrow \text{products} \quad (5)$$

$$CH_2\ (^1A_1) + CO \rightarrow \text{products} \quad (6)$$

$$CH_2\ (^1A_1) + O_2 \rightarrow \text{products} \quad (7)$$

$$CH_2\ (^1A_1) + NO \rightarrow \text{products} \quad (8)$$

$$CH_2\ (^1A_1) + H_2 \rightarrow \text{products} \quad (9)$$

CH_2 ($^1A_1$) + CH_4 → products (10)

CH_2 ($^1A_1$) + C_2H_6 → products (11)

CH_2 ($^1A_1$) + C_3H_8 → products (12)

CH_2 ($^1A_1$) + C_2H_4 → products (13)

CH_2 ($^1A_1$) + i-C_4H_8 → products (14)

The rotational and vibrational level dependence of inert gas removal rates have also been studied. The results are compared with previous experimental and theoretical work.

B. EXPERIMENTAL

1. Apparatus

Singlet methylene ($^1A_1$) was produced by photolysis of ketene at 308 nm with the XeCl excimer laser. The 12 ns FWHM pulse and beam cross section of 7 x 25 mm (in the photolysis cell) resulted in a maximum single pass energy fluence of 10 mJ/cm^2 and a maximum power density of 0.5 MW/cm^2.

The Ar^+-pumped ring dye laser (Spectra-Physics 171-06/380 A) with a linewidth of 20 MHz was used to detect CH_2 ($^1A_1$) through absorption at rotational lines between 590 and 610 nm.[7] The laser wavelength was determined to within 0.02 cm^{-1} with the commercial wavemeter (Burleigh WA-20). The dye laser beam was collimated to a diameter of 2 mm and reflected into the photolysis cell. The multipass arrangement of Fig. II-3 was used in these experiments. Since the cross-sectional area of the photolysis beam was much larger than the probe beam, the loss of CH_2 through diffusion from the reaction volume was negligible on the timescale of collisional removal.

Hrvoje Petek and Peter Ogilby are thanked for the use of the high resolution kinetic absorption spectrum of Fig V-1 which was obtained by integrating the absorption signal with a boxcar integrator (PAR 162/164), and scanning the dye laser.

2. Sample Handling

Ketene was prepared by pyrolysis of acetic anhydride[15] and multiply distilled from 156 K to 77 K before use. The purity of samples stored at 77 K to prevent polymerization was periodically checked by FTIR spectroscopy. Nitric oxide (Matheson 99.0%) was purified by distillation through a silica gel trap kept at 195 K to remove NO_x impurities. Other gases, He (LBL extra pure 99.999%), Ar (Matheson UHP 99.999%), Kr (Baker research grade 99.995%), N_2 (LBL 99.999%), CO (Baker research grade 99.97%), H_2 (Baker research grade 99.9995%), O_2 (Baker research grade 99.995%), CH_4 (Matheson UHP 99.97%), C_2H_6 (Scientific Gas Products C.P. 99.2%, with less than 0.2% each H_2, CH_4, and C_2H_4 and 0.1% N_2 and O_2), C_3H_8 (Matheson research grade 99.99%), C_2H_4 (Matheson C.P. 99.5%), and i-C_4H_8 (Matheson C.P. 99.3%, with less than 0.4% 1-butene, 0.2% n-C_4H_{10}, and 0.1% i-C_4H_{10}) were used without further purification. Gases were transferred to the cell from a standard glass and grease vacuum line with a base pressure of 10^{-6} Torr. Pressures were measured using a 0 - 10 Torr capacitance manometer (Baratron 145AH-10) accurate to within ± 0.1%.

In typical experiments with He, Ar, Kr, and N_2, ketene was first loaded into the cell and the desired partial pressure of the added gas expanded in from a high pressure reservoir. When other gases were used, ketene was frozen into a sidearm of the cell while the reactant gas was added. The ketene was then allowed to thaw and the desired partial

pressure of helium added as before. Mixing times of several minutes were generally adequate for the low pressures ($\lesssim$ 10 Torr) used in these experiments. All experiments were performed at an ambient temperature of 295 ± 2 K.

C. RESULTS AND ANALYSIS

1. Production of CH_2 ($^1A_1$).

At 308 nm, all of the methylene produced through single-photon excitation of ketene is in the $\tilde{a}(^1A_1)$ state.[6,16] Rate constants for the collisional removal of CH_2 ($^1A_1$) were obtained primarily from the analysis of absorption data for the 4_{14} rotational level, monitored via the $4_{04}(0,14,0) \leftarrow 4_{14}(0,0,0)$ transition near 16928.79 cm^{-1}.[7] A high resolution spectrum of the $^{P}Q_{1,J}$ (J) sub-branch containing this transition is shown in Fig. V-1. Although perturbations in the upper state of this transition prohibit the determination of rotational populations,[7,9] the 4_{14} level was found to have the strongest absorbance near 590 nm under rotationally thermalized conditions. The temporal evolution of this level under typical conditions is shown in Fig. V-2.

Even though the 4_{14} level always decayed exponentially due to bimolecular collisions under pseudo-first-order conditions, the decay was preceeded by an exponential rise reaching a maximum several hundred nanoseconds after the 12 ns photolysis pulse. Bi-exponential analysis of the absorbance leads to production and removal rates proportional to collision gas pressure (Figs. V-3 and 4). This indicates that the 4_{14} level is populated primarily through bimolecular relaxation of the initial population rather than direct dissociation. The production rate constants obtained from the data in Figs. V-3 and 4 are consistent with

rotational relaxation. The production of CH_2 $\tilde{a}$ ($^1A_1$) by electronic quenching of CH_2 $\tilde{b}$ ($^1B_1$) formed via two-photon excitation of ketene can be ruled out through the linear fluence dependence of the CH_2 ($^1A_1$) absorbance (Fig. V-5). Vibrational relaxation from the (0,1,0) level also seems to be unimportant (see below). Deconvolution of the exponential decay from this rise should therefore give removal rates for thermalized CH_2 ($^1A_1$).

2. Removal of CH_2 ($^1A_1$).

3. Absolute Rate Constants

Absolute rate constants for CH_2 ($^1A_1$) removal by helium and ketene were derived from a linear least-squares fit of Eq. (15) using decay rates obtained over ketene and helium pressure ranges of 0.05 to 0.50 Torr and 1 to 10 Torr, respectively.

$$K_{exp} = k_1[CH_2CO] + k_2[He]. \qquad (15)$$

Some of these data are shown in Figs. V-3,4, and 6. Figures V-3 and 4 indicate that for ketene pressures below 0.20 Torr and helium pressures above 3 Torr, the rotational relaxation rate is more than an order of magnitude faster than the decay rate. Under these conditions, the rise can be neglected and the data analyzed as a single exponential decay. Whenever possible, the experimental conditions were chosen to permit this simplification.

Rate constants for CH_2 ($^1A_1$) removal by Ar, Kr, and N_2 were determined by a least-squares fit of decay rates covering an inert gas pressure range of 3 to 10 Torr with a constant partial pressure of 0.100 or 0.200 Torr CH_2CO. The value of k_1 was constrained to 2.7×10^{-10} cm^3 $molec^{-1}$ s^{-1} (determined from CH_2CO/He experiments) in these fits. The pressure dependence of CH_2 ($^1A_1$) decay rates in He, Ar, Kr, and N_2 are

shown in Fig. V-6.

The rotational-level independence of these removal rates, illustrated for N_2 in Fig. V-7, probably results from rotational equilibration which is fast on the timescale of collisional removal. The levels shown in Fig. V-7, spanning a rotational energy range of nearly 500 cm^{-1}, were probed via absorptions in the $^{P}Q_{1,J}$ (J) and $^{P}P_{1,J-1}$ (J) branches near 16930 cm^{-1}.[7] Rate constants for the removal of vibrationally excited CH_2 ($^1A_1$) (0,1,0) by He, Ar, and CH_2CO were determined using the $2_{11}(0,15,0) \leftarrow 1_{01}(0,1,0)$ transition at 16405.25 cm^{-1}.[7] The absorbance due to this level was approximately 10% of the $4_{14}(0,0,0)$ absorbance. The (0,1,0) removal rate constants were found to be equal within experimental error to the ground state values (Fig. V-8). For He and Ar, these results imply that vibrational-translational transfer from the (0,1,0) level is probably slow compared to intersystem crossing. This conclusion is consistent with measured rates for deactivation of the bending modes of H_2O, D_2O, D_2S, H_2Se,[17,18] and NH_2[19] by inert gases which are 10-100 times slower than the methylene intersystem crossing rates.

Rate constants for CH_2 removal by reactive species were obtained from a least-squares fit of Eq. (16) using decay rates from mixtures with partial pressures of 0.100 or 0.200 Torr ketene and 4.0 or 6.0 Torr helium. Reactant pressures were varied from 0.05 to 0.50 or 1.00 Torr depending on the reaction rate.

$$K_{exp} = k_1[CH_2CO] + k_2[He] + k_R[R]. \qquad (16)$$

In these fits, k_1 and k_2 were constrained to the values in Table I. Some of these results are shown in Figs. V-9 and 10.

b. Error Estimates

The error limits given in the first column of Table V-1 are estimates of the total uncertainty associated with each rate constant measurement. These limits are in all cases greater than one standard deviation in the result of the least-squares fit. The most important sources of error in these measurements are: i) uncertainty in the data analysis and ii) uncertainty in the reactant pressures.

Uncertainties in the data obtained by single exponential analysis can result from insufficient separation of the rise and decay. In typical mixtures with 0.200 Torr CH_2CO and 6.0 Torr He, rotational relaxation was 95% complete within 200 ns. The single exponential fits were typically initiated at times much longer than 200 ns and the quality of each fit could be checked by increasing or decreasing the delay between t = 0 and the origin of the fit. Uncertainties due to the analysis are therefore less than 10%.

Although the Baratron used for pressure measurements should be accurate to within 0.08%, uncertainties in the partial pressures of various gases could result from depletion of the reactant molecules and the buildup of reaction products over the course of a photolysis run. The ketene absorption cross section of 2.5×10^{-20} cm^2/molecule at 308 nm[20] with a quantum yield of unity for the production of CH_2 ($^1A_1$), implies that irradiation of 0.100 Torr of ketene with the maximum energy fluence of 10 mJ/cm^2 produced approximately 10^{13} molecules/cm^3 CH_2 ($^1A_1$). Since the reaction volume (defined as the volume swept out by the photolysis beam) of 140 cm^3 was less than 10% of the total cell volume, less than 0.03% of the ketene was photolyzed per shot. If only 3 Torr of helium was present in the cell, an additional 0.02% was removed through reaction (1). The net loss of ketene over the course of 64 shots, the

typical number required to obtain signal-to-noise ratios comparable to Fig. V-2 was therefore always less than 4%. Depletion of other reactants was even less. No systematic changes in reaction rates due to reactant depletion or product buildup were observed, even over the course of several hundred laser shots.

D. DISCUSSION

Absolute rate constants for the removal of CH_2 ($^1A_1$) by various gases are shown in Table V-1. The present results, listed in the first column, and the results of Ashfold et al.[12] in the second column, are the only absolute rate constants based on direct measurements of singlet concentrations. These rate constants are approximately one order of magnitude larger than those of Braun, Bass, and Pilling[8] (third column) which are based on the appearance rates of CH_2 ($^3B_1$) produced by intersystem crossing or CH_3 formed through reaction of the singlet with H_2 or CH_4. The source of this discrepancy, noted in Ref. 12, stems from the incorrect assumption that reaction (1) is too slow to compete with intersystem crossing for CH_2 ($^1A_1$) removal. Although this assumption renders the absolute rate constants from Ref. 8 incorrect, a self-consistent set of relative rate constants is obtained. These rate constants, normalized to a value of 1.0 for singlet removal by He, are compared to relative values from the two direct studies in Table V-2.

Relative rate constants from three product analysis studies are included in Table V-2 for comparison. These studies are but a small fraction of an extensive literature recently reviewed by Laufer.[1] Cox and Preston[21] photolyzed ketene at 249 nm and 280 nm in mixtures with O_2

or CO to scavenge triplet CH_2 ($^3B_1$). Relative rates for intersystem crossing induced by the addition of inert gases were determined from the reduced yield of C_2H_4 produced by reaction (1). These rates are therefore normalized to a value of 77 for k_1. With the exception of k_4, the rates shown in Table V-2 are from 280 nm photolyses with CO as a scavenger.

Eder and Carr[22] photolyzed ketene in the presence of propane, oxygen, and various inert gases at 260 nm, 313 nm, 334 nm, and 350 nm. Rate constants were measured relative to the reaction of CH_2 ($^1A_1$) with C_3H_8. The rates listed in Table V-2 are those obtained at 313 nm and are normalized to a value of 69 for singlet reaction with propane.

The experimental method of Bell[23] was similar to that of Ref. 22 except that CH_2 ($^1A_1$) was produced by the 405 nm photolysis of diazomethane. These rates are also normalized to a value of 69 for CH_2 ($^1A_1$) reaction with C_3H_8.

1. CH_2 ($^1A_1$) Removal by Rare Gases

The absolute values of rate constants for CH_2 ($^1A_1$) removal by He, Ar, and Kr reported in Ref. 12 agree with the present results to within 15%. Relative values of k_2 and k_3 from ref. 8, and k_2 and k_4 from ref. 21 are in reasonable agreement with the absolute values. The rare gas rates determined by Bell[23] are significantly faster than the values from other studies.

Although it is clear that inert gases can remove singlet methylene by inducing intersystem crossing to the triplet ground state, the mechanism is not completely understood. The modest heavy atom effect,

Table V-1, shows that intersystem crossing induced by collisions with rare gases depends on the spin-orbit coupling within the methylene molecule itself. Translation of the rare gas interacts with the vibrational and rotational coordinates of the two states of methylene. Transitions may occur during a collision as vibration-rotation energies of singlet levels cross those of triplet levels. Dahler and co-workers[24,25] have treated such resonances involving only the bending levels. Since these are spread by several kT in energy, calculated S-T quenching rates depend strongly on the level spacing in the free molecule and hence on the singlet-triplet energy gap. The inclusion of rotational energies and C-H stretching should decrease this strong dependence on vibrational level position. The small changes in S-T quenching rates with singlet vibrational excitation (Fig. V-6) and with deuteration[12] suggest that accidental vibrational resonances do not change rates by orders of magnitude. Freed, Gelbart, and co-workers[26-28] consider the modest singlet-triplet perturbations which must exist in the free molecule for some rotational levels of the singlet vibrational ground state. The mixing of vibration, rotation, and translation during the collision then gives S-T rates proportional to the product of a vibration-rotation relaxation rate within the triplet manifold and the square of a coefficient for triplet character in singlet levels. The observed rates of a few percent gas kinetic then imply that triplet perturbations with at least a few percent intensity should exist in singlet spectra.

It is probable that collision-induced intersystem crossing rates are strong functions of the singlet vibration-rotation quantum numbers. Experimentally, this cannot be observed since rotational relaxation within the singlet manifold is more than an order of magnitude faster

than intersystem crossing (Figs. V-3 and 4).

2. CH_2 ($^1A_1$) Removal by Inorganic Molecules

When the collision partner is a molecule, reactive processes may also contribute to the removal of CH_2 ($^1A_1$). Since the present experiments did not distinguish products, the relative contributions of reactive channels and intersystem crossing to the measured removal rates were not directly determined. The expected products for many of these reactions are discussed in Ref. 1.

Reactions between CH_2 ($^1A_1$) and diatomic molecules probably form highly excited addition products. Since the lifetimes of such small molecules with 50 - 100 kcal mol^{-1} excess energy are typically less than one nanosecond, stabilization of these adducts or buildup of a steady state concentration is negligible over the pressure range used in the present experiments.

a. CH_2 ($^1A_1$) + N_2

The present rate constant for CH_2 ($^1A_1$) removal by N_2 is approximately 25% greater than the value of Ref. 12. Braun, Bass, and Pilling[8] found that stabilization of half the diazomethane formed in the addition reaction requires nitrogen pressures in excess of 400 Torr. This conclusion is based on a decrease in the CH_2 ($^3B_1$) yield with increasing N_2 pressure. Quantitatively, the rate of adduct formation was found to be approximately 60% greater than the rate of direct interystem crossing. The excellent agreement (< 5%) between the present rate for CH_2 ($^1A_1$) removal by N_2 and the relative rate for direct intersystem crossing from Ref. 8 implies that the adduct dissociates primarily to CH_2 ($1A_1$) rather than CH^2 (3B1).

b. CH_2 ($^1A_1$) + CO

The absolute values of k_6 reported in ref. 12 and the present study differ by less than 15%. In product analysis studies, DeGraff and Kistiakowsky[29] and Cox and Preston[21] found relative efficiencies for the removal of CH_2 ($^1A_1$) by CO and CH_2CO to be 0.14 and 0.12, respectively. The approximations required in analysis of these indirect measurements are larger than the difference from the present result of $k_6/k_1 = 0.18 \pm 0.02$. The production of ^{14}CO in the reaction of $^{14}CH_2$ ($^1A_1$) with CO led Montague and Rowland[30] to conclude that an oxirene adduct forms in collisions of $^1CH_2$ with CO. They reported that a CO pressure of ~ 840 Torr was necessary to stabilize 50% of the excited oxirene complexes. A complex dissociation rate of 3×10^9 s^{-1} was inferred. Their indirectly measured complex formation rate was 0.1 k_1. However, to the extent that oxirene decomposes to CH_2 ($^1A_1$) + CO, the oxirene formation rate is not included in the value of k_6 reported here.

C. CH_2 ($^1A_1$) + O_2

The only significant disagreement between this study and ref. 12 is the factor of 2.5 difference between values of k_7. Indirect values of this rate constant also vary considerably. Eder and Carr[22] found that a value of k_7/k_{12} which decreased at longer photolysis wavelengths (0.44 at 260 nm, 0.46 at 313 nm, 0.20 at 334 nm, and 0.095 at 350 nm) provided the best fit to their data. This decrease was attributed to a small activation barrier to reaction, surmountable by internal excitation of CH_2. This interpretation was favored by Ashfold et al. since the MPD value of k_7/k_2 was consistent with Eder and Carr's values of k_7/k_{12} and k_2/k_{12} when the former was determined at 350 nm. This comparison may not be valid, however, since more recent experiments indicate that CH_2 ($^1A_1$)

is not produced in the 350 nm photolysis of ketene.[6] In addition, k_2/k_{12} was determined only at 313 nm in Ref. 22 and relative rate constants for singlet removal by other species (including Ar and Xe) were found to be wavelength dependent in that study.

Since both direct measurements of k_7 are representative of thermalized CH_2 ($^1A_1$), the discrepancy may be related to the method of CH_2 production. In a preliminary account,[11] Ashfold et al. described the production of substantial visible luminescence following the multiphoton dissociation of $(CH_3CO)_2O$ in the presence of O_2. This luminescence (and the discrepancy in rate constants) may perhaps be due to reaction between vibrationally excited acetic anhydride or ketene with oxygen.

d. CH_2 ($^1A_1$) + NO

The only reported rate constant for singlet CH_2 removal by NO is $k_8/k_1 = 1.25$ determined through product analysis by Laufer and Bass.[31] This ratio is more than double the present value ($k_8/k_1 = 0.55$) and possibly includes contributions from CH_2 ($^1B_1$) produced in the vacuum ultraviolet photolysis of ketene. The relative efficiencies of reaction and intersystem crossing are unknown.

e. CH_2 ($^1A_1$) + H_2

The absolute values for k_9 differ by approximately 20%. A relative value of k_9/k_2 determined by Braun, Bass, and Pilling[8] is 10% lower than the present ratio. These workers spectroscopically observed the production of CH_3 in the reaction of CH_2 ($^1A_1$) with H_2 and by isotopic substitution determined that the reaction proceeds through an excited methane adduct. Product analysis in that study indicated that the intersystem crossing rate was approximately 20% of the reaction rate.

3. CH_2 ($^1A_1$) Removal by Organic Molecules

a. Alkanes

In reactions with alkanes, CH_2 ($^1A_1$) inserts into the C-H bonds to form excited alkane adducts.[32] Relative rates for insertion into the various C-H bonds of several alkanes have been reported by Halberstadt and Crump[13] who produced singlet methylene by 313 nm photolysis of ketene. These rates are in good agreement with the relative insertion rates determined by Hase and Simons,[14] and the relative CH_2 ($^1A_1$) removal rates determined in this study (Table V-3). The absolute rate constant for CH_2 ($^1A_1$) removal by CH_4 reported in Ref. 12 differs from the present result by less than 5%.

The good agreement between relative rates derived from insertion product yields and the relative CH_2 ($^1A_1$) removal rate implies that intersystem crossing is probably unimportant in these collisions. The generally good agreement between the relative rates from this study and the rates of Eder and Carr[22] measured relative to CH_2 ($^1A_1$) reaction with propane lends support to this conclusion. Carr and co-workers[22,33] have also indicated that the correlation of intersystem crossing rates with collision partner polarizability (derived from inert gas removal rates) implies intersystem crossing rates which are only 4 - 6% of the insertion rate for collisions with CH_4, C_2H_6, and C_3H_8.

These conclusions are seemingly at odds with other studies including that of Braun, Bass, and Pilling[8] which found comparable efficiencies for intersystem crossing and insertion in collisions between CH_2 ($^1A_1$) and CH_4. This result is based both on product analysis and spectroscopic observation of the CH_3 (from $C_2H_6^*$ dissociation) and CH_2 ($^3B_1$) products. In addition, Bell[23] found CH_2 ($^1A_1$) removal rates (relative to

reaction with propane) significantly greater than the present rates indicating that intersystem crossing is very important in collisions with C_3H_8.

These differences may be linked to the method of CH_2 ($^1A_1$) production. In studies based on competition with insertion reactions, it must be assumed that the fate of the insertion products is known. If the degree of stabilization of these products is overestimated, the resulting removal rates will be too large relative to the insertion reaction since the apparent yield of insertion products is too small. Since the probability of stabilizing these products depends on the degree of internal excitation, the amount of energy available for internal excitation (determined by the excess energy available for CH_2 ($^1A_1$) excitation in the photodissociation process) can affect the results. This may explain why the relative rates determined by Bell,[23] with ~ 45 kcal mol^{-1} available for CH_2 ($^1A_1$) excitation in the 405 nm photolysis of CH_2N_2,[8] are significantly greater than both the present rates and the rates of Eder and Carr[22] and Halberstadt and Crump[13] (~ 8 kcal mol^{-1} available for CH_2 ($^1A_1$) excitation.[6]) This hypothesis is consistent with the results of Braun, Bass, and Pilling from CH_2 ($^1A_1$) produced in the vacuum ultraviolet photolysis of ketene and diazomethane ($\gtrsim$ 70 kcal mol^{-1} available for CH_2 ($^1A_1$) excitation) which indicate that intersystem crossing is important under those conditions.

b. Alkenes

Singlet methylene reacts with olefins primarily through addition to the double bonds.[32,34] Although absolute rate constants for CH_2 ($^1A_1$) removal by olefins have not been reported previously, Krzyzanowski and Cvetanovic have measured rate constants for the addition of CH_2 ($^1A_1$) to

ethylene, propylene, 1-butene, cis-2-butene, trans-2-butene, trimethylethylene, tetramethylethylene, and 1,3-butadiene relative to isobutene addition.[34] These rates range from 0.54 (ethylene) to 1.73 (1,3-butadiene) times as fast as the isobutene rate. The present ratio of $k_{13}/k_{14} = 0.67$ is in reasonable agreement with these results. The relative rates for trans-2-butene and isobutene from ref. 34, together with the present values of k_1 and k_{14}, imply relative rates for trans-2-butene and ketene in good agreement with the ratio reported by Carr and Kistiakowsky.[35]

Taylor and Simons have reported the relative efficiencies for neopentane/isobutene and n-butane/cis-2-butene pairs to be 0.87 and 1.09 respectively.[36] The relative efficiencies for isobutene and cis-2-butene implied from these results and the work of Hase and Simons (Table V-3) are also in good agreement with the results of Krzyanowski et al. The absolute rate constant for isobutene implied from the work of Taylor and Simons and the data in Tables V-1 and 3 is approximately 50% greater than the present value of k_{14}.

c. Ketene

Ketene removes singlet methylene with virtually every collision, the most efficient of fourteen collision partners used in the present study. This occurs primarily through reaction (1), with possible contributions (< 10%) from intersystem crossing.[23] There is no evidence that singlet methylene reacts with ketene by other channels.[1]

An estimate of $k_1 = 4 \times 10^{-10}$ cm^3 molec^{-1} s^{-1} reported by Lengel and Zare[2] compares favorably to the present value of 2.7×10^{-10} cm^3 molec^{-1} s^{-1}. Ths result is based on LIF detection of the ketene photoproduct. Earlier rate constants obtained by indirect methods are one to two orders

of magnitude lower than these values.[31,37]

E. CONCLUSIONS

Absolute rate constants for the removal of CH_2 ($^1A_1$) by NO, C_2H_6, C_3H_8, C_2H_4, i-C_4H_8, and CH_2CO have been directly measured for the first time, using the technique of laser resonance absorption. Absolute rate constants for He, Ar, Kr, N_2, CO, and H_2 obtained by this method are in excellent agreement with those obtained by laser-induced fluorescence. Comparisons between these results and those of product analysis studies indicate that carefully interpreted indirect studies can provide accurate relative rate constants. These may prove particularly valuable for measurements of CH_2 ($^1A_1$) removal rates at pressures significantly greater than 10 Torr where direct measurements will be hampered by the rapid rate of collision-induced intersystem crossing.

The intersystem crossing rate appears to be independent of CH_2 ($^1A_1$) bending vibrational excitation. Thus a strong dependence of rate on the $^1A_1$ - $^3B_1$ vibronic level gaps appears unlikely. Since the rotational state dependence of intersystem crossing rates is obscured by rapid rotational equilibration, the ability of kinetic measurements to test theories of collision-induced intersystem crossing is reduced. A better understanding of collision-induced intersystem crossing in methylene may be provided by spectroscopic studies. In particular, it has been suggested that interactions between ($^1A_1$) and ($^3B_1$) levels may lead to perturbations in the ($^1B_1$) ← ($^1A_1$) absorption spectrum.[38,39]

References

1. A.H. Laufer, Rev. Chem. Int. 4, 225 (1981).
2. R.K. Lengel and R.N. Zare, J. Am. Chem. Soc. 100, 7495 (1978).
3. D. Feldmann, K. Meier, H. Zacharias, and K.H. Welge, Chem. Phys.Lett. 59, 171 (1978).
4. J.W. Simons and R. Curry, Chem. Phys. Lett. 38, 171 (1976).
5. P.C. Engelking, P.R. Corderman, J.J. Wendoloski, G.B. Ellison, S.V. O'Neill, and W.C. Lineberger, J. Chem. Phys. 74, 5460 (1981).
6. C.C. Hayden, D.M. Neumark, K. Shobatake, R.K. Sparks, and Y.T. Lee, J. Chem. Phys. 76, 3607 (1982).
7. G. Herzberg and J.W.C. Johns, Proc. Roy. Soc. 295A, 107 (1966).
8. W. Braun , A.M. Bass, and M.J. Pilling, J. Chem. Phys. 52, 5131 (1970).
9. A.J. Grimley and J.C. Stephenson, J. Chem. Phys. 74, 447 (1981).
10. D.L. Monts, J.G. Dietz, M.A. Duncan and R.E. Smalley, Chem. Phys. 45, 133 (1980).
11. M.N.R. Ashfold, G. Hancock, G.W. Ketley, and J.P. Minshull-Beech, J. Photochem. 12, 75 (1980).
12. M.N.R. Ashfold, M.A. Fullstone, G. Hancock, G.W. Ketley, Chem. Phys. 55, 245 (1981).
13. M.L. Halberstadt and J. Crump, J. Photochem. 1, 295 (1972/73).
14. W.L. Hase and J.W. Simons, J. Chem. Phys. 54, 1277 (1971).
15. R.L. Nutall, A.H. Laufer, and M.V. Kilday, J. Chem. Thermodyn. 4, 167 (1971).
16. P.M. Kelley and W.L. Hase, Chem. Phys. Lett. 35, 57 (1975).
17. F.E. Hovis and C.B. Moore, J. Chem. Phys. 69, 4947 (1978); ibid 72, 2397 (1980).

18. S.S. Miljanic, E. Specht, and C.B. Moore, J. Chem. Phys. 77, 4949 (1982).

19. V.A. Nadtochenko, O.M. Sarkisov, M.P. Frolov, R.A. Tsanava, and S.G. Cheskis, Kinet. Catal. USSR 22, 670 (1981).

20. A.H. Laufer and R.A. Keller, J. Am. Chem. Soc. 93, 61 (1971).

21. R.A. Cox and K.R. Preston, Can. J. Chem. 47, 3345 (1969).

22. T.W. Eder and R.W. Carr, J. Chem. Phys. 53, 2258 (1970).

23. J.A. Bell, J. Phys. Chem. 75, 1537 (1971).

24. M.Y. Chu and J.S. Dahler, Mol. Phys. 27, 1045 (1974).

25. K.C. Kulander and J.S. Dahler, J. Phys. Chem. 80, 2881 (1976).

26. W.M. Gelbart and D. Cazes, Chem. Phys. Let. 15, 37 (1972).

27. W.M. Gelbart and K.F. Freed, Chem. Phys. Lett. 18, 470 (1973).

28. K.F. Freed and C. Tric, Chem. Phys. 33, 249 (1978).

29. B.A. DeGraff and G.B. Kistiakowsky, J. Phys. Chem. 71, 3984 (1967)

30. D.C. Montague and F.S. Rowland, J. Am. Chem. Soc. 93, 5381 (1971).

31. A.H. Laufer and A.M. Bass, J. Phys. Chem. 78, 1344 (1974).

32. W. Kirmse, "Carbene Chemistry," 2nd Ed., (Academic Press, New York, 1971).

33. V. Zabransky and R.W. Carr, Jr., J. Phys. Chem. 79, 1618 (1975).

34. S. Krzyzanowski and R.J. Cvetanovic, Can J. Chem. 45, 665 (1967).

35. R.W. Carr and G.B. Kistiakowsky, J. Phys. Chem. 70, 118 (1966)

36. G.W. Taylor and J.W. Simons, Int. J. Chem. Kin. 3, 25, 453 (1971).

37. M.J. Pilling and J.A. Robertson, J. Chem. Soc. Faraday Trans I. 73, 968 (1977).

38. G. Duxbury, J. Mol. Spectrosc. 25, 1 (1968).

39. T.J. Sears, P.R. Bunker, and A.R.W. McKellar, J. Chem. Phys. 77, 5363 (1982).

TABLE V-1: Absolute rate constants x 10^{12} (cm^3 $molec^{-1}$ s^{-1}) and average cross sections ($Å^2$) for CH_2 ($^1A_1$) removal

	σ^a	k	k^b	k^c
He	0.25	3.5 ± 0.3	3.1 ± 0.3	0.30 ± 0.07
Ne	0.50[b]	-----	4.2 ± 0.6	-----
Ar	0.75	5.8 ± 0.5	6.0 ± 0.5	0.67 ± 0.13
Kr	1.1	7.9 ± 0.6	7.0 ± 0.6	-----
Xe	2.3[b]	-----	16 ± 2	-----
N_2	1.3	11 ± 1	8.8 ± 0.3	0.90 ± 0.2
CO	6.0	49 ± 4	56 ± 6	-----
O_2	9.2	74 ± 5	30 ± 4	-----
NO	20.	160 ± 15	-----	-----
H_2	5.6	105 ± 5	130 ± 10	7.0 ± 1.5
CH_4	7.6	70 ± 4	73 ± 6	3.5 ± 1.0
C_2H_6	23	190 ± 20	-----	-----
C_3H_8	31	240 ± 20	-----	-----
C_2H_4	18	150 ± 60	-----	-----
i-C_4H_8	30	225 ± 20	-----	-----
CH_2CO	35	270 ± 20	-----	-----

[a] $\sigma = k(8\ KT/\pi\mu)^{-1/2}$

[b] From Ref. 12.

[c] From Ref. 8

TABLE V-2: Relative rate constants for CH_2 ($^1A_1$) removal

	this work	Ref. 12	Ref. 8	Ref. 21	Ref. 22	Ref. 23
He	1.0	1.0	1.0	1.3	0.7	---
Ne	---	1.4	---	---	---	---
Ar	1.7	1.9	2.2	1.1	2.1	8.3
Kr	2.3	2.3	---	2.5	---	---
Xe	---	5.2	---	6.0	3.2	20
N_2	3.1	2.8	3.0	4.1	3.4	5.5
CO	14	18	---	9	---	---
O_2	21	9.7	---	---	32	43
NO	46	---	---	---	---	---
H_2	30	42	28	---	---	---
CH_4	20	24	12	---	---	33
C_2H_6	54	---	---	---	---	---
C_3H_8	69	---	---	---	69	69
C_2H_4	43	---	---	---	---	---
i-C_4H_8	64	---	---	---	---	---
CH_2CO	77	---	---	77	---	---

TABLE V-3: Relative rate constants for CH_2 ($^1A_1$) collisions with alkanes

	This work[a]	Ref. 13[b]	Ref. 14[b]
CH_4	1.0	1.0	---
C_2H_6	2.7	2.52	---
C_3H_8	3.4	3.32	3.3
$n\text{-}C_4H_{10}$	---	4.28	4.1
$i\text{-}C_4H_{10}$	---	3.89	3.5
$n\text{-}C_5H_{12}$	---	---	3.9

[a]Relative rates based on singlet methylene removal.

[b]Relative rates based on insertion product yields.

Figure V-1. Absorption spectrum of several rotational lines in the $^{P}Q_{1,J}(J)$ sub-branch near 16,929 cm^{-1} obtained from the photolysis of 0.50 Torr CH_2CO with 4.0 Torr He. The 500 ns boxcar gate was opened at the same time as the photolysis pulse. The assignments are from Ref. 7.

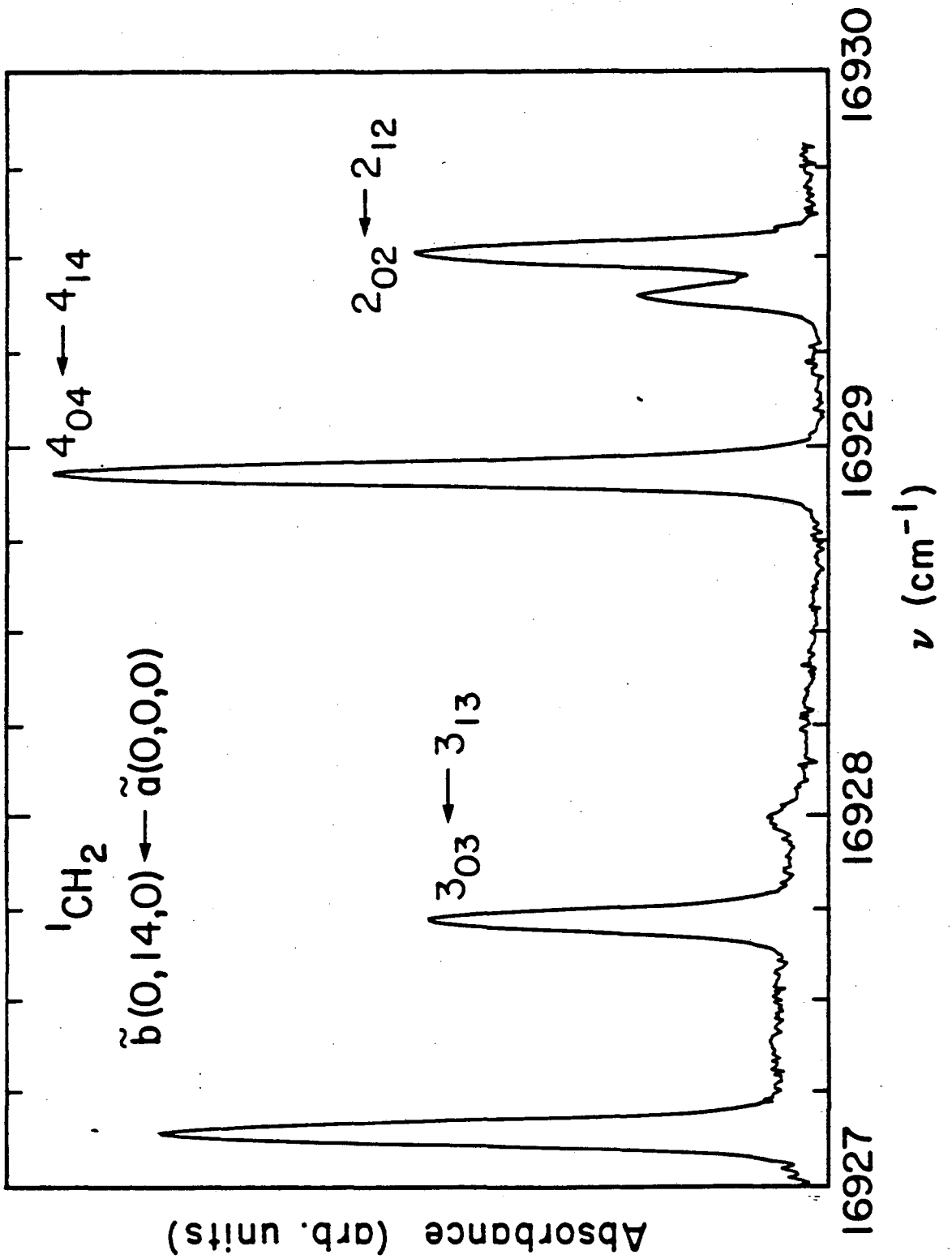
Absorbance (arb. units)
16927
16928
16929
16930
ν (cm⁻¹)
$^1CH_2$
$\tilde{b}(0,14,0) \leftarrow \tilde{a}(0,0,0)$
$4_{04} \leftarrow 4_{14}$
$2_{02} \leftarrow 2_{12}$
$3_{03} \leftarrow 3_{13}$

Fig. V-1

Figure V-2. Temporal evolution of the 4_{14} rotational level of CH_2 ($^1A_1$) in 0.200 Torr CH_2CO with 3.00 Torr He after 64 laser shots. The solid line corresponds to the rates given in Fig. V-3.

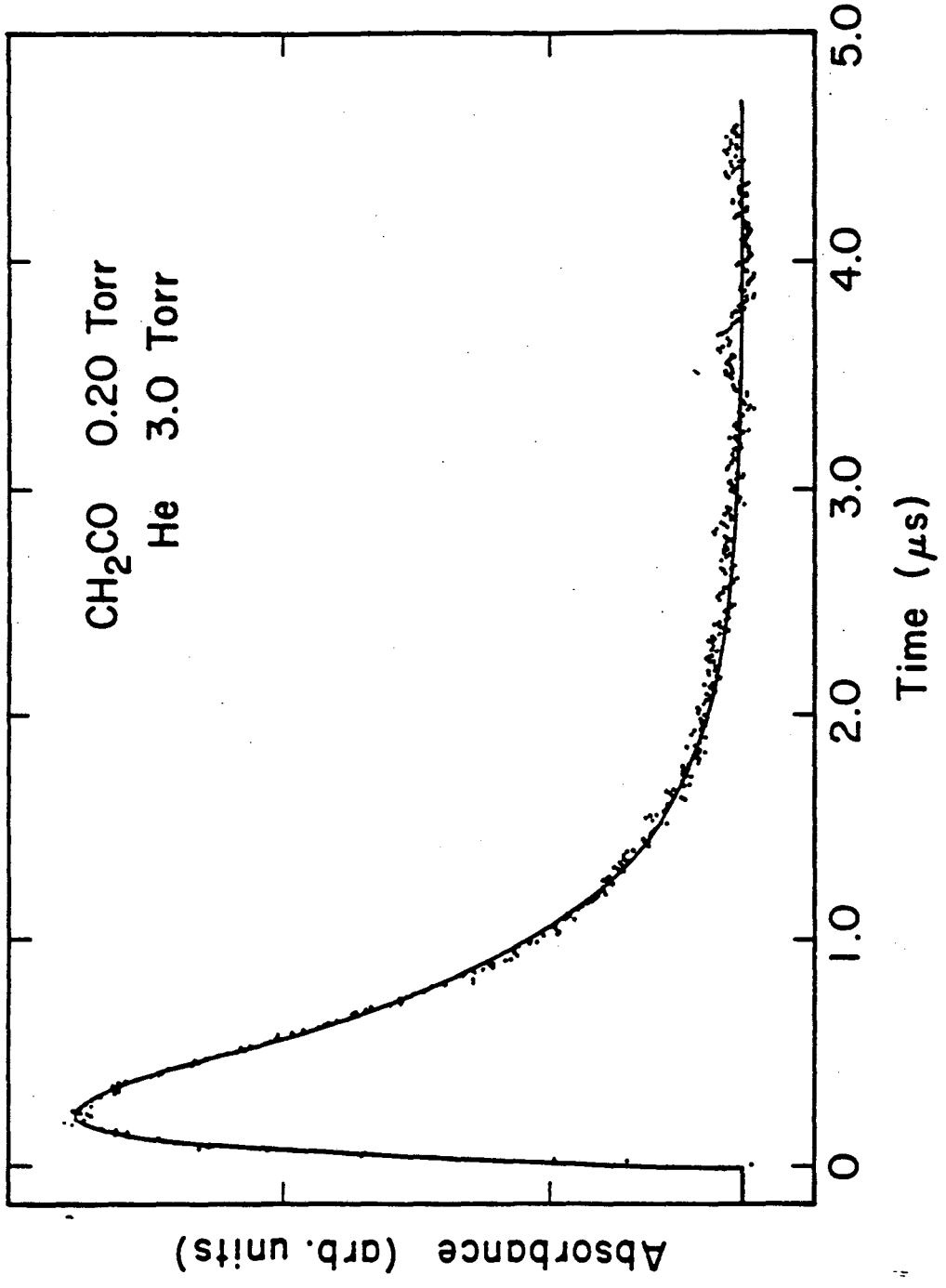
CH_2CO 0.20 Torr
He 3.0 Torr
0
1.0
2.0
3.0
4.0
5.0
Time (μs)
Absorbance (arb. units)

Fig. V-2

Figure V-3. Production (○) and decay (●) rates for CH_2 ($^1A_1$) in 3.00 Torr He and 0.050 to 0.500 Torr CH_2CO. The solid lines correspond to production rate constants of 7.3×10^{-10} and 5.9×10^{-11} cm^3 $molec^{-1}$ s^{-1} and removal rate constants of 2.7×10^{-10} and 3.5×10^{-12} cm^3 $molec^{-1}$ s^{-1} for CH_2CO and He respectively. Uncertainties for the production rate constants are ~ 10%.

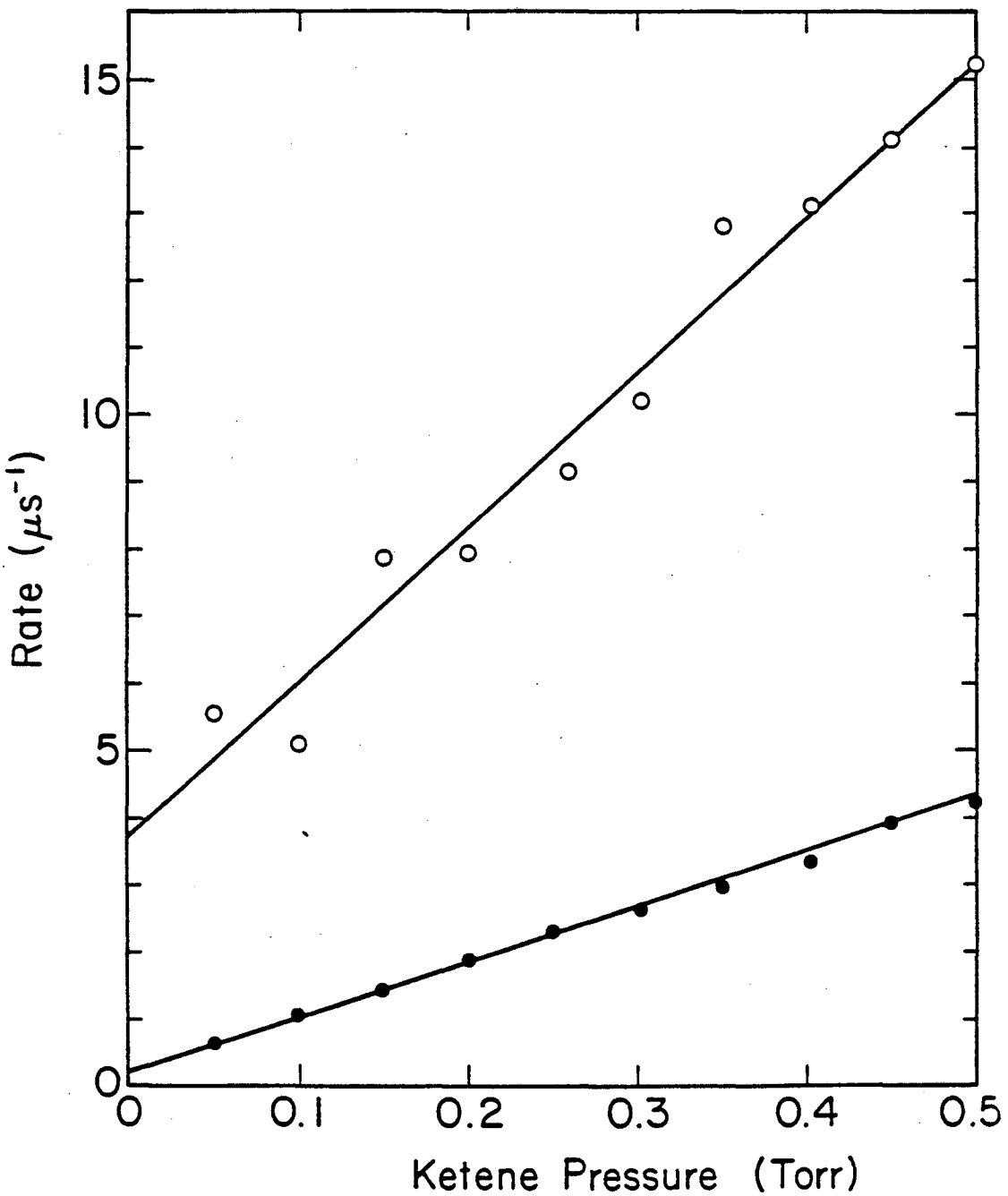

Fig. V-3

Figure V-4. Production (△) and decay (▲) rates for CH_2 ($^1A_1$) in 0.200 Torr CH_2CO and 1.25 to 9.00 Torr He. The solid lines correspond to the rate constants from Fig. V-3.

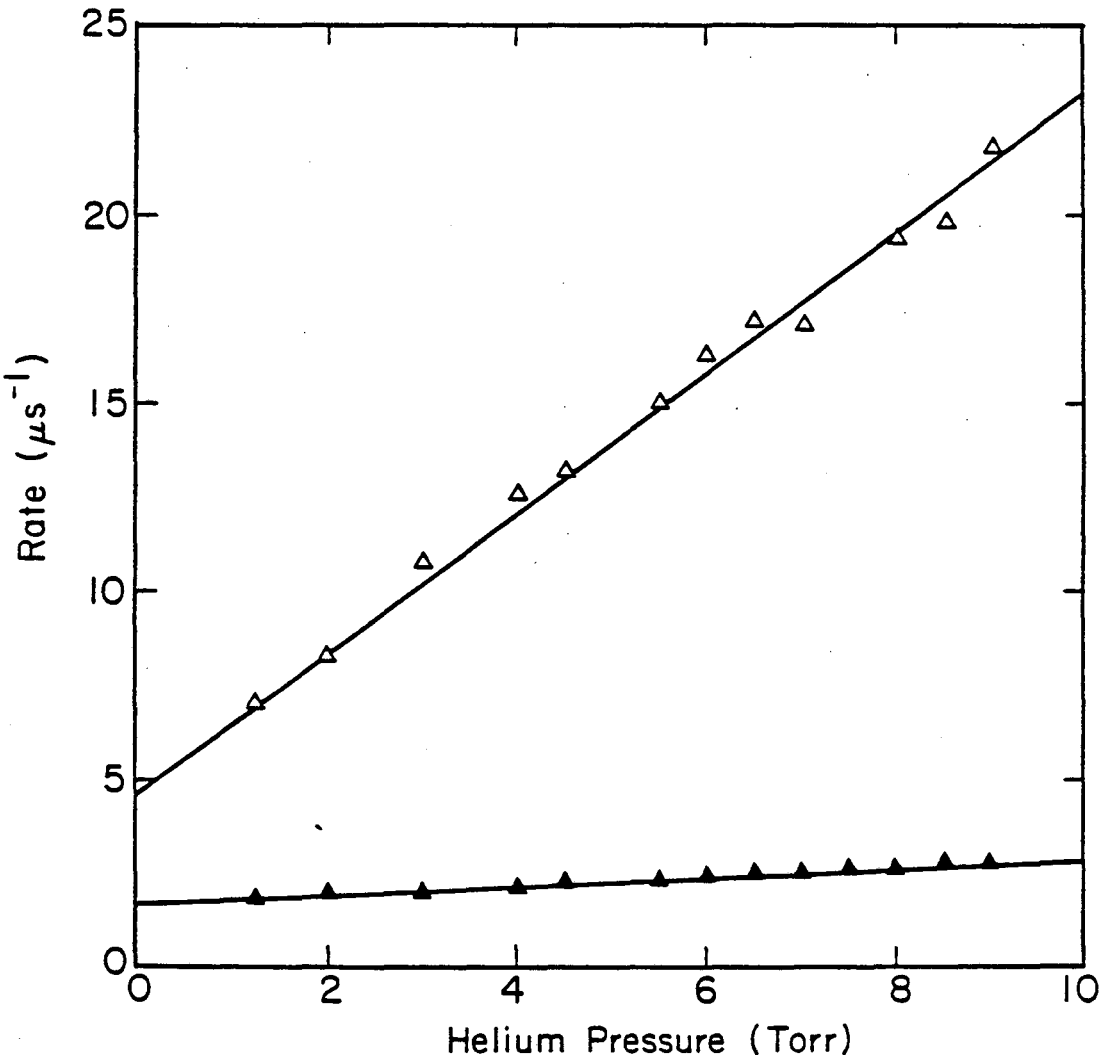

Fig. V-4

Figure V-5. Fluence dependence of CH_2 ($^1A_1$) production in 0.500 Torr CH_2CO and 6.00 Torr He. The triangles correspond to the difference between the peak absorbance and the baseline.

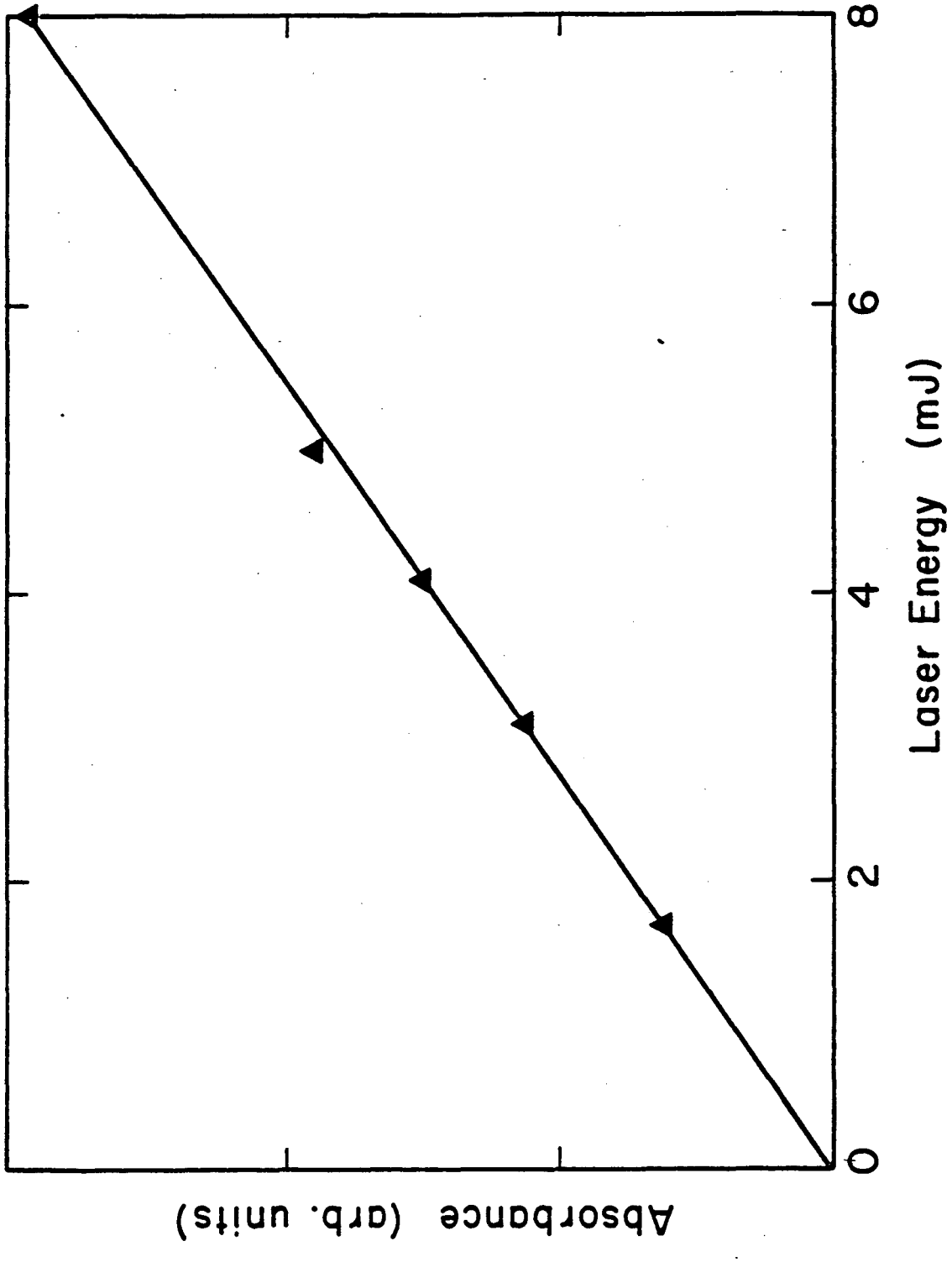

Fig. V-5

Figure V-6. Pseudo-first-order decay rates for CH_2 ($^1A_1$) in 0.200 Torr CH_2CO and He, Ar, Kr, and N_2. The solid lines correspond to rate constants given in Table V-1.

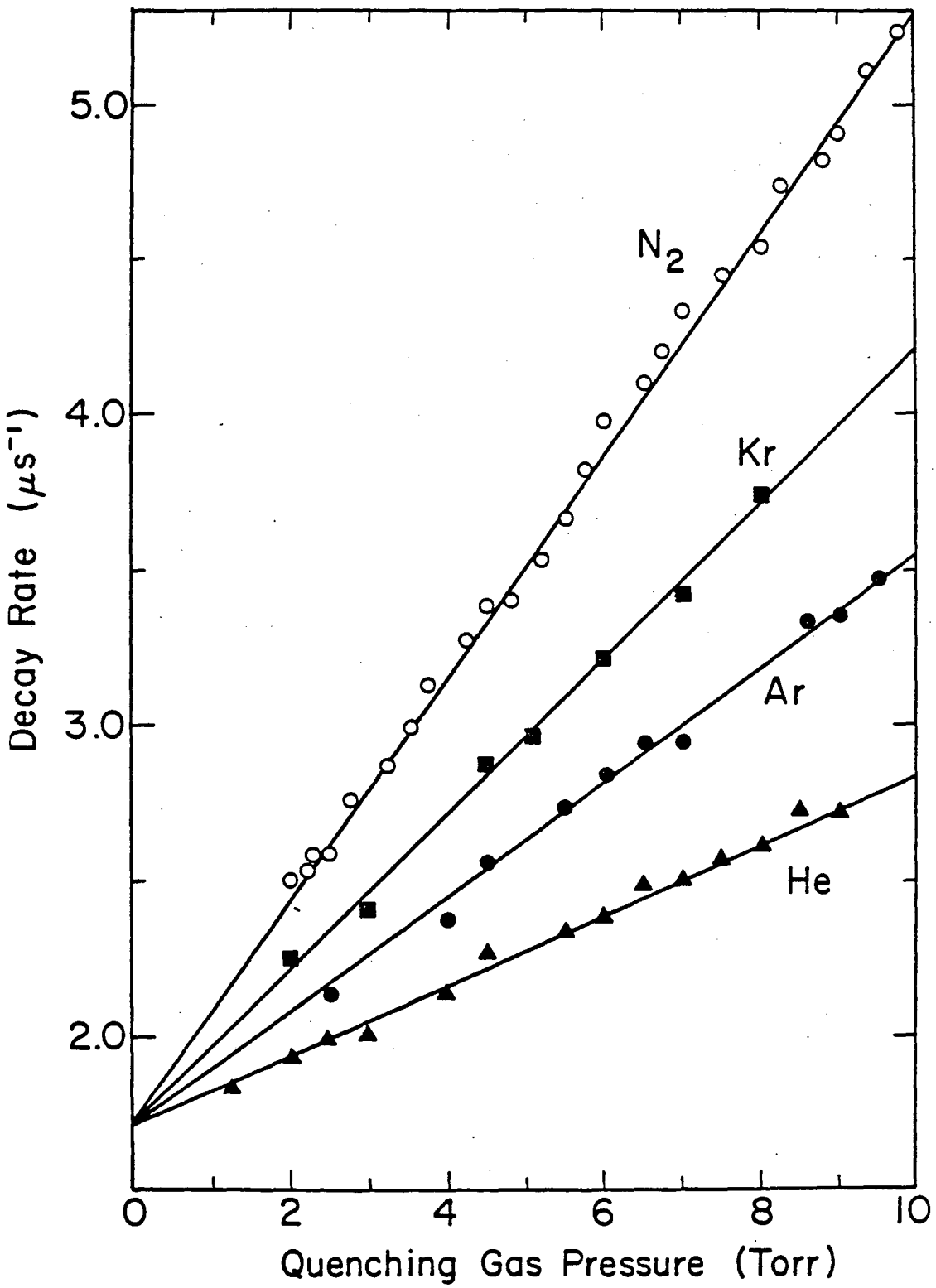
5.0
4.0
3.0
2.0
Decay Rate (μs^{-1})
N_2
Kr
Ar
He
0
2
4
6
8
10
Quenching Gas Pressure (Torr)

Fig. V-6

Figure V-7. Pseudo-first-order decay rates for the 1_{10}, 3_{13}, 4_{14}, and 7_{16} rotational levels of CH_2 ($^1A_1$) in 0.200 Torr CH_2 and added N_2. The rotational energies are 31, 108, 170, and 533 cm^{-1} respectively. The solid line corresponds to the rate constant from Table V-1.

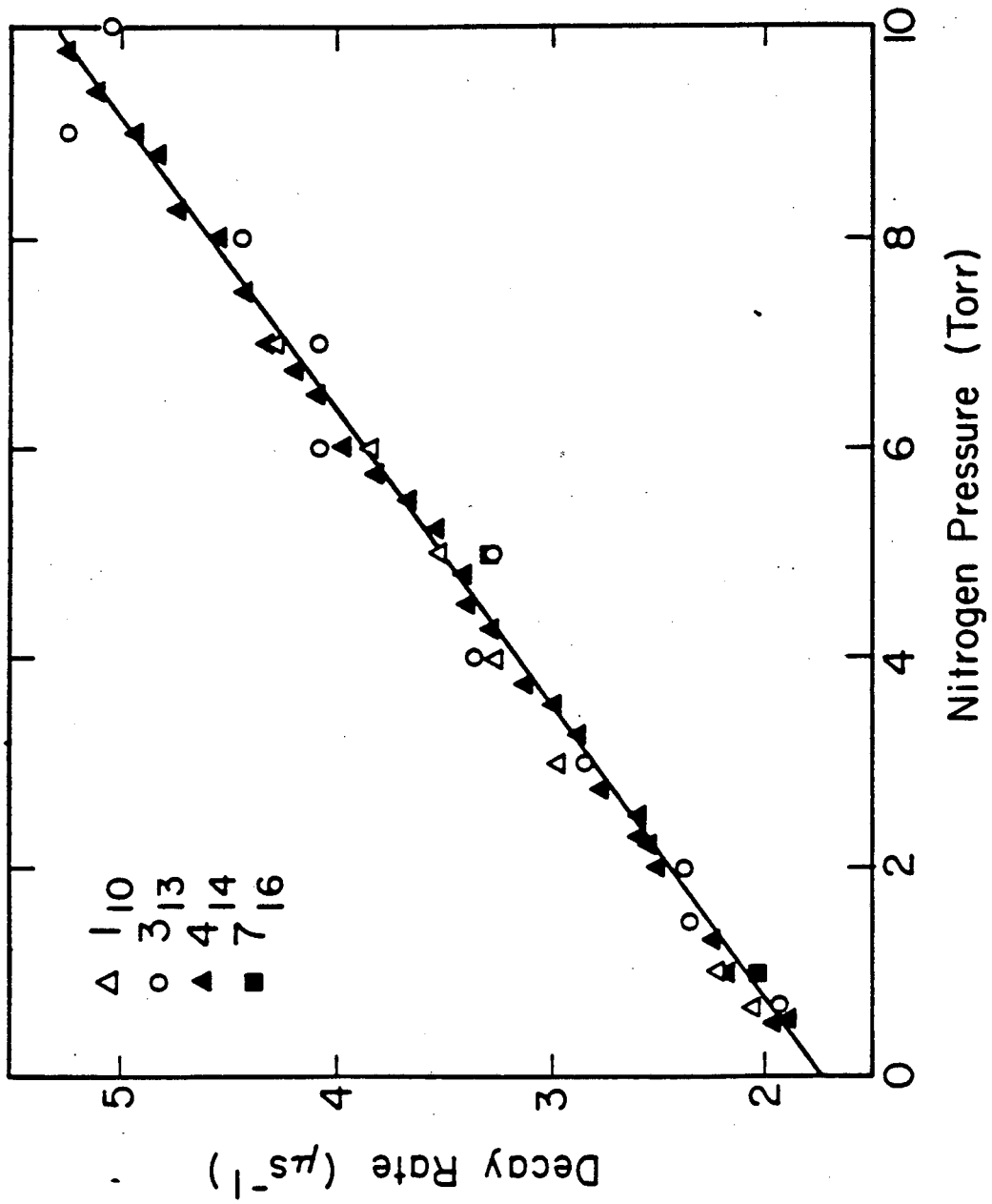
Decay Rate (μs^{-1})
Nitrogen Pressure (Torr)
0
2
4
6
8
10
2
3
4
5
I
10
13
14
16

Fig. V-7

Figure V-8. Pseudo-first-order decay rates for the (0,1,0) and (0,0,0) vibrational levels of CH_2 ($^1A_1$) as a function of added He (△,▲) and Ar (○,●). The CH_2CO pressures are 0.300 Torr for the (0,1,0) decays and 0.200 for the (0,0,0) decays. The solid lines correspond to the (0,0,0) rate constants from Table V-1.

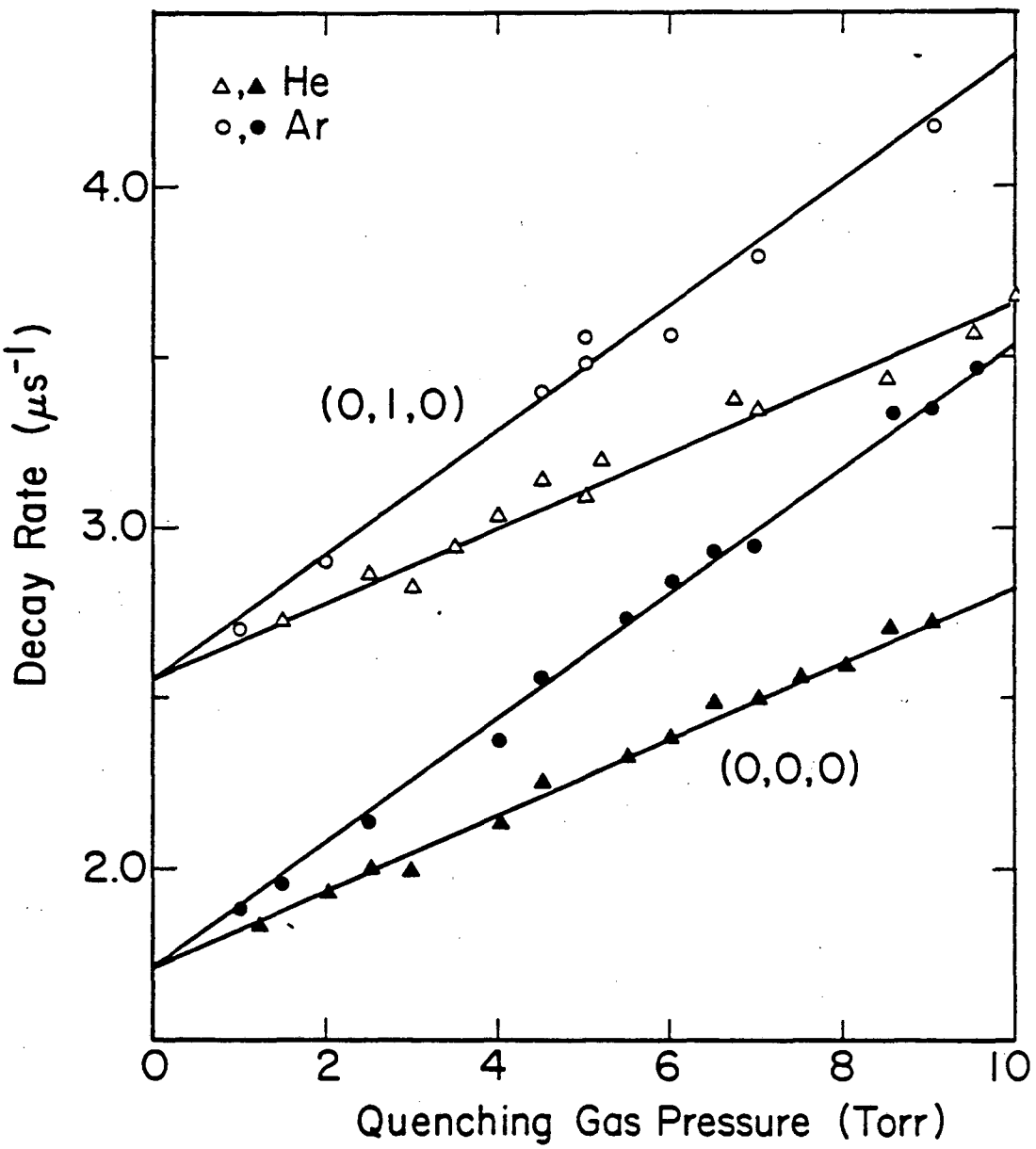
△,▲ He
○,● Ar
(0,1,0)
(0,0,0)
Decay Rate (μs^{-1})
4.0
3.0
2.0
0
2
4
6
8
10
Quenching Gas Pressure (Torr)

Fig. V-8

Figure V-9. Pseudo-first-order decay rates for CH_2 ($^1A_1$) in 0.100 Torr CH_2CO, 6.00 Torr He, and added CO, O_2, H_2, and NO. The solid lines correspond to the rate constants given in Table V-1.

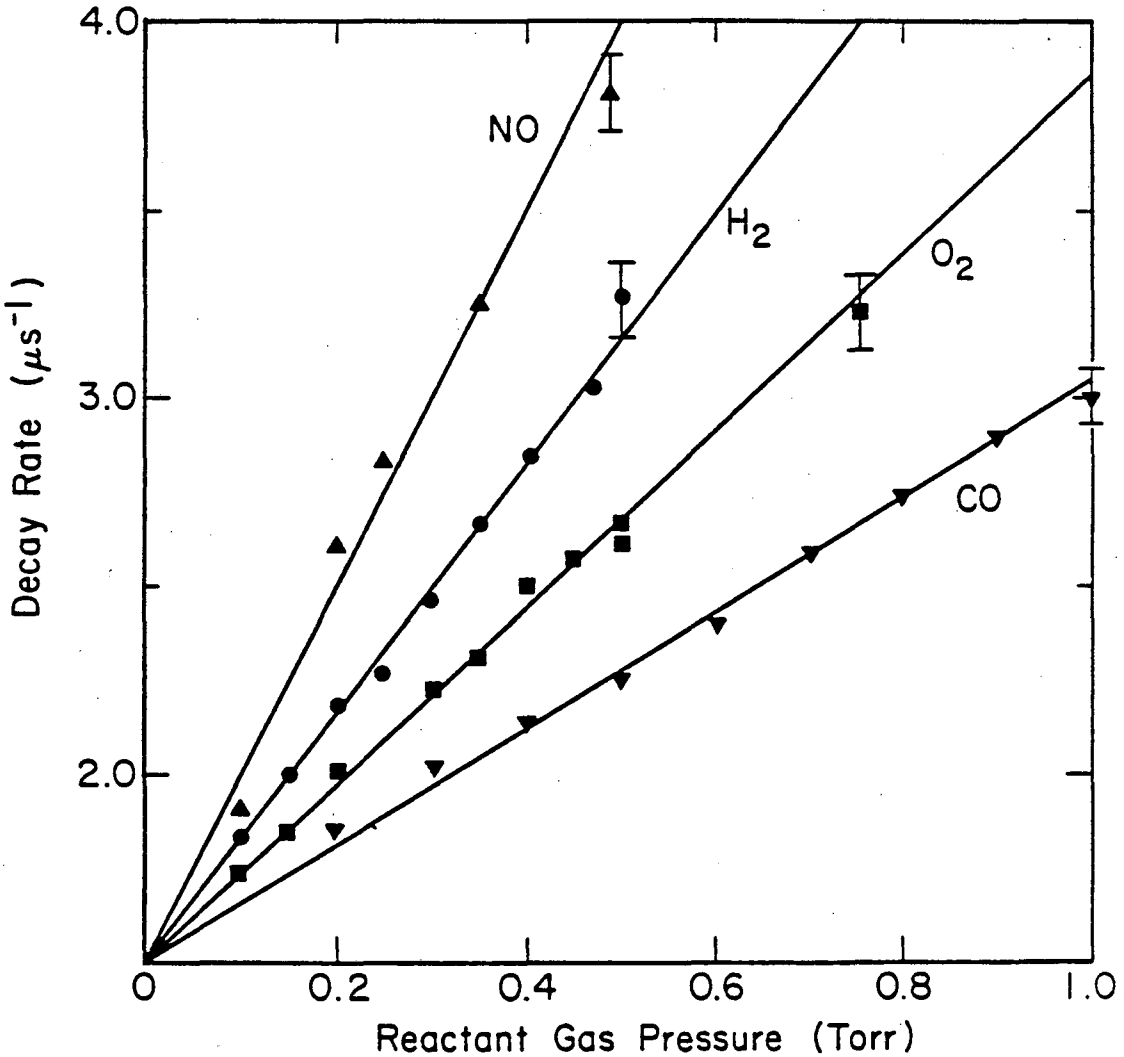
4.0
3.0
2.0
Decay Rate (μs^{-1})
NO
H_2
O_2
CO
0
0.2
0.4
0.6
0.8
1.0
Reactant Gas Pressure (Torr)

Fig. V-9

Figure V-10. Pseudo-first-order decay rates for CH_2 ($^1A_1$) in 0.100 Torr CH_2CO, 6.00 Torr He, and added CH_4, C_2H_6, and C_3H_8. The solid lines correspond to the rate constants given in Table V-1.

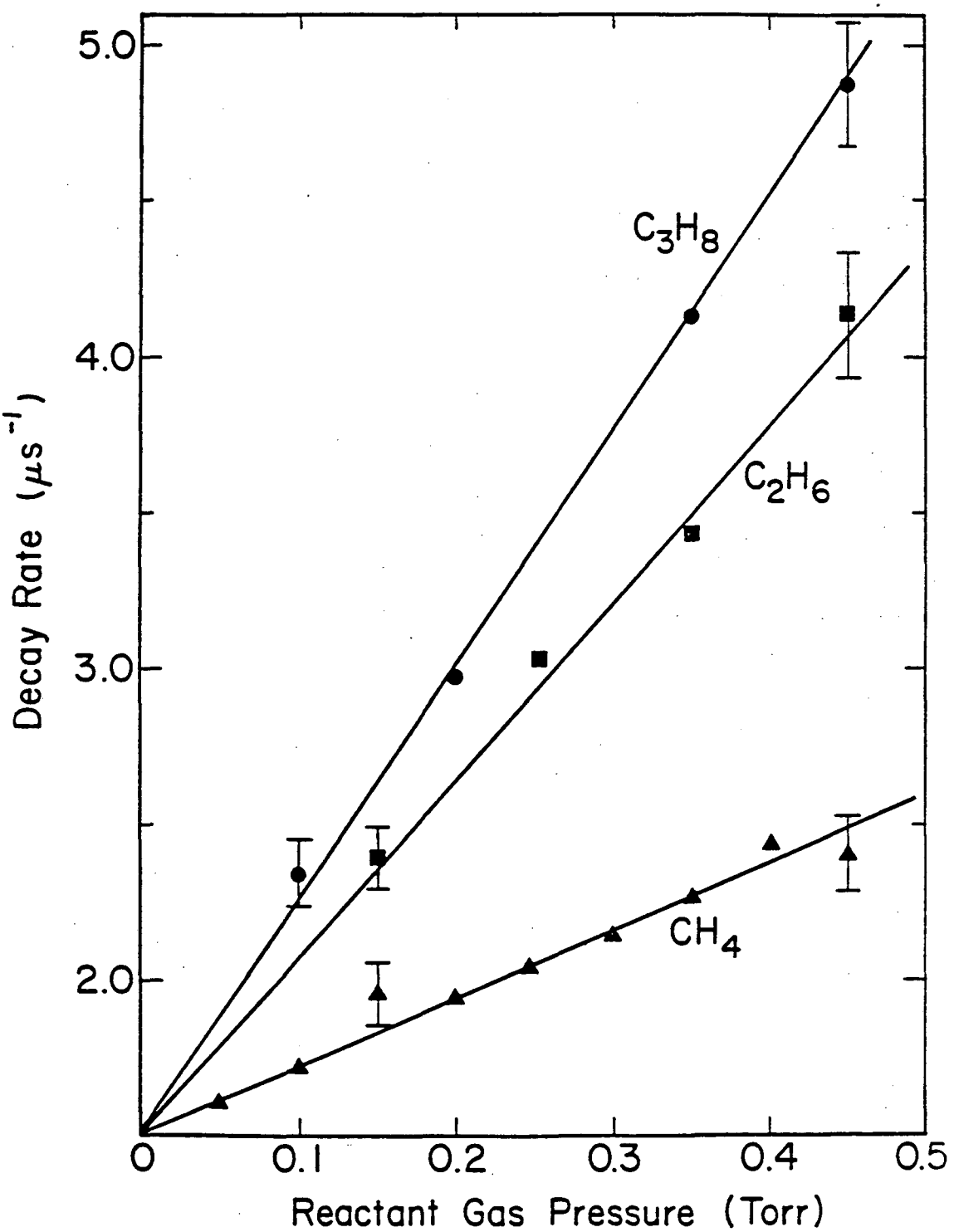
5.0
4.0
3.0
2.0
Decay Rate (μs^{-1})
C_3H_8
C_2H_6
CH_4
0
0.1
0.2
0.3
0.4
0.5
Reactant Gas Pressure (Torr)

Fig. V-10

```
10 REM THIS PROGRAM CALCULATES THE OVERALL REACTION EFFICIENCY FOR
20 REM A REACTION WHICH PROCEEDS THROUGH AN INTERMEDIATE WHICH CAN
30 REM DECOMPOSE TO GIVE REACTANTS (VIA TRANSITION STATE A) OR
40 REM PRODUCTS (VIA TRANSITION STATE B)
50 DELETE WM,WC,WD
60 DELETE TM,TC,TD
70 DELETE TA,TB,TN,TD,NN
80 NO=0
90 NI=0
110 PAGE
120 WAIT 1000
130 PRINT "NO. OF OSCILLATORS IN TRANSITION STATE A?"
140 INPUT OS
150 PRINT "INPUT THE";OS;"VIBRATIONAL FREQUENCIES OF TS A (CM-1)"
160 DIM WM(OS-1),TM(2),TD(2),TC(2),TA(5),TB(5)
170 FOR I=0 TO OS-1
180 PRINT I+1;\INPUT WM(I)\NEXT I
190 PRINT "DOES TRANSITION STATE A CONTAIN ANY FREE ROTATIONS?"
200 INPUT A$
210 IF A$="Y" THEN 2100
220 IF TM(0)=0 THEN 300
230 PRINT "DO YOU WISH TO CHANGE THE FREQUENCIES OF TS B?"
240 INPUT A$
250 IF A$="Y" THEN 360
260 PRINT "DO YOU WISH TO CHANGE THE ENERGY PARAMETERS?"
270 INPUT A$
280 IF A$="Y" THEN 480
290 GOTO 840
300 PRINT "INPUT THE PRINCIPAL MOMENTS OF INERTIA FOR TS A"
310 PRINT "IN UNITS OF AMU-ANGSTROM^2"
320 FOR I=0 TO 2\PRINT I+1;\INPUT TM(I)\NEXT I
330 GOTO 2260
340 PRINT "NO. OF OSCILLATORS IN TRANSITION STATE B?"
350 INPUT NS
355 DIM WC(NS-1)
360 PRINT "INPUT THE";NS;"VIBRATIONAL FREQUENCIES OF TS B (CM-1)"
370 FOR I=0 TO NS-1\PRINT I+1;\INPUT WC(I)\NEXT I
380 IF TC(0)=0 THEN 430
390 PRINT "DO YOU WISH TO CHANGE THE ENERGY PARAMETERS?"
400 INPUT B$
410 IF B$="Y" THEN 550
420 GOTO 840
430 PRINT "INPUT THE PRINCIPAL MOMENTS OF INERTIA FOR TS B"
440 PRINT "IN THE SAME ORDER AS BEFORE"
450 FOR I=0 TO 2\PRINT I+1;\INPUT TC(I)\NEXT I
460 PAGE
470 WAIT 1000
480 DELETE SN,SB,SD,NN
490 DELETE E,EP,SA,SM
500 DELETE TN,SC,TD,TF
550 PRINT "INPUT THE FOLLOWING QUANTITIES IN UNITS OF KCAL/MOLE"
610 DELETE EI
620 DELETE BL
630 PRINT "MINIMUM EXCITATION ENERGY?"
640 INPUT LE
650 PRINT "ENERGY INCREMENT?"
660 INPUT EI
670 PRINT "TOTAL NUMBER OF INCREMENTS?"
680 INPUT NN
```

APPENDIX. RRKM Computer Program for Calculating Reaction Efficiencies.

```
690 PRINT "BARRIER ENERGY?"
700 INPUT BE
710 ME=LE+NN*EI
720 PRINT "MAXIMUM EXCITATION ENERGY IS";ME,"TEMPERATURE?"
730 INPUT T
740 EO=LE*350
750 EM=ME*350
760 EB=BE*350
770 IN=EI*350
780 DIM E(NN-1),EP(NN-1),SA(NN-1),SB(NN-1)
790 DIM SN(NN-1),SD(NN-1),DS(NN-1)
800 REM CORRECTION TO ENERGIES FOR ADIABATIC ROTATIONS
810 DJ=-(1.987E-03*T)*(1-((TC(0)*TC(1)*TC(2))/(TM(0)*TM(1)*TM(2)))^.5)
820 ED=EO-EB+(DJ*350)
830 REM WHITTEN-RABINOWITCH  CALCULATION OF SUMS OF STATES
840 PF=1
850 PRINT "I'M THINKING-I'M THINKING!!!"
860 NR=NO+2*NI
870 IF NR=0 THEN 970
880 REM CALCULATION OF PART. FCNS. FOR INT. RTRS.
890 IF NO=0 THEN 930
900 FOR I=0 TO NO-1\PT=.4316*(TA(I))^.5
910 PF=PT*PF
920 NEXT I
930 IF NI=0 THEN 970
940 FOR I=0 TO NI-1\PT=.05931*TB(I)
950 PF=PT*PF
960 NEXT I
970 SW=0
980 WS=0
990 FOR I=0 TO OS-1
1000 WS=WS+WM(I)*WM(I)
1010 SW=SW+WM(I)
1020 NEXT I
1030 SS=SW*SW
1040 BT=(OS-1)*(OS+NR/2)/OS*WS/SS
1050 REM CALCULATION OF ZERO POINT ENERGY FOR TS A
1060 ZE=0
1070 FOR I=0 TO OS-1\ZE=ZE+WM(I)/2\NEXT I
1080 NT=(NR/2)*2
1090 IF (NR-NT)>0 THEN 1140
1100 ND=OS+NR/2
1110 GM=0
1120 FOR I=0 TO ND-1\GM=GM+LOG(I+1)/LOG(10)\NEXT I
1130 GOTO 1190
1140 NZ=OS+NR/2+1
1150 GM=0
1160 MX=2*NZ-1
1170 FOR I=0 TO MX-1\GM=GM+LOG(I+1)/LOG(10)\NEXT I
1180 GM=GM+LOG(1.7725/2^NZ)/LOG(10)
1190 PR=0
1200 FOR I=0 TO OS-1\PR=PR+LOG(WM(I))/LOG(10)\NEXT I
1210 REM CALCULATION OF THE SUM OF STATES FOR TS A
1220 XP=OS+NR/2
1230 FOR J=0 TO NN-1
1240 E(J)=J*IN
1250 EP(J)=E(J)/ZE
1260 IF (EP(J)-1)>=0 THEN 1290
1270 WW=1/(5*EP(J)+2.73*SQR(EP(J))+3.51)
1280 GOTO 1300
1290 X3=-1.0506*EP(J)^.25*2.3026
1300 AA=1-BT*WW
1310 ONERR NOWARN
1320 AU=LOG(PF)/LOG(10)-GM-PR+(XP*LOG(E(J)+AA*ZE)/LOG(10))
1330 SA(J)=10^AU
1340 NEXT J
```

```
1345 GOTO 2340
1350 PF=1
1360 SW=0
1370 WS=0
1380 FOR I=0 TO NS-1
1390 WS=WS+WC(I)*WC(I)
1400 SW=SW+WC(I)
1410 NEXT I
1420 SS=SW*SW
1430 BT=(NS-1)*WS/SS
1440 REM CALCULATION OF ZERO POINT ENERGY FOR TS B
1450 ZE=0
1460 FOR I=0 TO NS-1\ZE=ZE+WC(I)/2\NEXT I
1470 PR=0
1480 FOR I=0 TO NS-1\PR=PR+LOG(WC(I))/LOG(10)\NEXT I
1490 REM CALCULATION OF THE SUMS OF STATES FOR TS B
1500 XP=NS
1510 FOR J=0 TO NN-1\E(J)=ED+J*IN
1520 EP(J)=E(J)/ZE
1530 IF (EP(J)-1)>=0 THEN 1560
1540 WW=1/(5*EP(J)+2.73*SQR(EP(J))+3.51)
1550 GOTO 1570
1560 X3=-1.0506*EP(J)^.25*2.3026
1570 AA=1-BT*WW
1580 AU=LOG(PF)/LOG(10)-GM-PR+(XP*LOG(E(J)+AA*ZE)/LOG(10))
1590 SB(J)=10^AU
1600 NEXT J
1605 Q=0
1610 ES=IN
1620 ED=ED+IN
1625 TF=0
1630 REM TRAPEZOIDAL INTEGRATION FOR OVERALL REACTION EFFICIENCY
1635 ONERR NOWARN
1640 RT=1.987E-03*350*T
1650 FOR J=0 TO NN-1
1655 IF Q=1 THEN 1670
1660 SN(J)=(SB(J)*SA(J))/(SA(J)+SB(J))
1665 GOTO 1680
1670 SN(J)=(SB(J)*SA(J))/(DS(J)*3.336E-11)
1680 EF=SN(J)/SA(J)
1690 ES=ES+IN
1700 ED=ED+IN
1710 NEXT J
1720 E=IN
1730 TN=.5*(SN(0)*EXP(-E/RT)+SN(NN-1)*EXP(-EM/RT))
1740 TD=.5*(SA(0)*EXP(-E/RT)+SA(NN-1)*EXP(-EM/RT))
1750 E=2*IN
1760 FOR J=1 TO NN-1
1770 BL=EXP(-E/RT)
1780 SM=SN(J)*BL
1790 TN=TN+SM
1800 SC=SA(J)*BL
1810 TD=TD+SC
1820 E=E+IN
1830 NEXT J
1840 TF=TN/TD
1843 IF Q=0 THEN 1860
1845 Q=Q+1
1850 IF Q=2 THEN 1965
1855 GOTO 1610
1860 PAGE\WAIT 1000
1870 PRINT "THE OVERALL REACTION EFFICIENCY FOR:"
1880 PRINT "WM(I)="
1890 FOR I=0 TO OS-1\PRINT WM(I)\NEXT I
1900 PRINT "WC(I)="
1910 FOR I=0 TO NS-1\PRINT WC(I)\NEXT I
```

```
1920 PRINT "MINIMUM ENERGY IS";LE,
1930 PRINT "MAXIMUM ENERGY IS";ME,
1940 PRINT "ENERGY INCR.=";EI,
1950 PRINT "NO. OF INCR. IS ";NN,"BARRIER HT. IS";BE,,,
1960 PRINT "THE REACTION EFFICIENCY IS ";TF(NN-1)
1963 GOTO 1845
1965 PRINT "THE FORWARD RATE CONSTANT (KB) IS";TF(NN-1)
1970 PRINT "DO YOU WISH TO CHANGE THE FREQUENCIES OF TS A?"
1980 INPUT A$
1990 IF A$="Y" THEN 1995
1993 GOTO 2000
1995 DELETE WM
1997 GOTO 150
2000 PRINT "DO YOU WISH TO CHANGE THE FREQUENCIES OF TS B?"
2010 INPUT B$
2020 IF B$="Y" THEN 360
2030 PRINT "DO YOU WISH TO CHANGE THE ENERGY PARAMETERS?"
2040 INPUT C$
2050 IF C$="Y" THEN 480
2060 PRINT "TRY ANOTHER PROBLEM?"
2070 INPUT B$
2080 IF B$="Y" THEN 10
2090 END
2100 IF NO+NI=0 THEN 2140
2110 PRINT "DO YOU WISH TO CHANGE THE FREE ROTOR PARAMETERS?"
2120 INPUT A$
2130 IF A$="N" THEN 220
2140 PRINT "NO. OF ONE-DIMENSIONAL FREE ROTORS IN TS A?"
2150 INPUT NO
2160 IF NO=0 THEN 2190
2170 PRINT "INPUT THE MOMENTS OF INERTIA FOR THE";NO;" 1-D FREE ROTORS"
2180 FOR I=0 TO NO-1\PRINT I+1;\INPUT TA(I)\NEXT I
2190 PRINT "NO. OF TWO-DIMENSIONAL FREE ROTORS IN TS A?"
2200 INPUT MI
2210 NI=MI
2220 IF NI=0 THEN 220
2230 PRINT "INPUT THE ";NI;"MOMENTS OF INERTIA FOR THE";MI;" 2-D FREE ROTORS"
2240 FOR I=0 TO NI-1\PRINT I+1;\INPUT TB(I)\NEXT I
2250 GOTO 220
2260 PRINT "NO. OF OSCILLATORS IN COLLISION COMPLEX?"
2270 INPUT MS
2280 DIM WD(MS-1)
2290 PRINT "INPUT THE";MS;"VIBRATIONAL FREQUENCIES OF THE COMPLX (CM-1)"
2300 FOR I=0 TO MS-1\PRINT I+1;\INPUT WD(I)\NEXT I
2310 PRINT "INPUT THE PRINCIPAL MOMENTS OF INERTIA FOR THE COMPLEX"
2320 FOR I=0 TO 2\PRINT I+1;\INPUT TD(I)\NEXT I
2330 GOTO 340
2340 PF=1
2343 SW=0
2345 WS=0
2350 FOR I=0 TO MS-1
2360 WS=WS+WD(I)*WD(I)
2370 SW=SW+WD(I)
2380 NEXT I
2390 SS=SW*SW
2400 B1=(MS-1)*WS/SS
2410 REM CALCULATION OF ZERO POINT ENERGY FOR THE COMPLEX
2420 ZE=0
2430 FOR I=0 TO MS-1\ZE=ZE+WD(I)/2\NEXT I
2440 REM CALCULATION OF GAMMA FUNCTION
2450 GM=0
2460 FOR I=0 TO MS-2
2470 GM=GM+LOG(I+1)/LOG(10)
2480 NEXT I
2490 PR=0
2500 FOR I=0 TO MS-1\PR=PR+LOG(WD(I))/LOG(10)\NEXT I
```

```
2510 REM CALCULATION OF THE DENSITY OF STATES FOR THE COMPLEX
2520 XP=MS-1
2530 FOR J=0 TO NN-1\E(J)=EO+(DJ*350)+J*IN
2540 EP(J)=E(J)/ZE
2550 IF EP(J)>1 THEN 2610
2560 NM=-1*(5/ZE+.5*2.73/SQR(E(J))/SQR(ZE))
2570 DM=(5*EP(J)+2.73*SQR(EP(J))+3.51)^2
2580 DW=NM/DM
2590 WW=1/(5*EP(J)+2.73*SQR(EP(J))+3.51)
2600 GOTO 2640
2610 NM=-1.0506*.25/E(J)^.75*2.3026
2620 DM=ZE^.25
2630 WW=EXP(X3)
2640 AA=1-BT*WW
2650 AM=LOG(PF)/LOG(10)-GM-PR
2660 AD=AM+(XP*LOG(E(J)+AA*ZE)/LOG(10))+LOG(1-ZE*BT*DW)/LOG(10)
2670 DS(J)=10^AD
2680 NEXT J
2700 GOTO 1350

READY
*
```

This report was done with support from the Department of Energy. Any conclusions or opinions expressed in this report represent solely those of the author(s) and not necessarily those of The Regents of the University of California, the Lawrence Berkeley Laboratory or the Department of Energy.

Reference to a company or product name does not imply approval or recommendation of the product by the University of California or the U.S. Department of Energy to the exclusion of others that may be suitable.

TECHNICAL INFORMATION DEPARTMENT
LAWRENCE BERKELEY LABORATORY
UNIVERSITY OF CALIFORNIA
BERKELEY, CALIFORNIA 94720